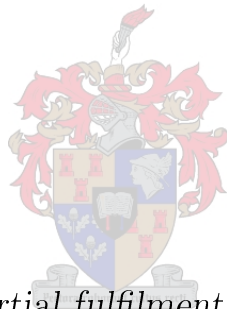


# The development of a hand-held, self-powering bio-sensing device for the early detection of *Mycobacterium tuberculosis*.

by

Sihle Christopher Tom



*Thesis presented in partial fulfilment of the requirements for  
the degree of Master of Engineering in Electronic Engineering  
in the Faculty of Engineering at Stellenbosch University*

Supervisor: Prof. Willem Jacobus Perold

Co-supervisor: Prof. Rob Warren

April 2019

The financial assistance from the Council for Scientific and Industrial Research(CSIR) towards this research is hereby acknowledged. Opinions expressed and conclusions arrived at are however those of the author and are not necessarily to be attributed to the CSIR.

# Declaration

By submitting this thesis electronically, I declare that the entirety of the work contained therein is my own, original work, that I am the sole author thereof (save to the extent explicitly otherwise stated), that reproduction and publication thereof by Stellenbosch University will not infringe any third party rights and that I have not previously in its entirety or in part submitted it for obtaining any qualification.

Date: .....

Copyright © 2019 Stellenbosch University  
All rights reserved.

# Abstract

Tuberculosis (TB) has been described as one of the top 10 leading infectious and deadliest diseases in the world and millions of people still contract and die from TB each year. TB diagnosis serves as one of the most important aspects towards controlling and ending TB. The current methods of testing for TB infection are very expensive and non-portable, laboratory-based, require experienced personnel, sometimes with poor accuracy and lack the ability to generate same-day results at point-of-care. Hence, the time from diagnosis to treatment is unnecessarily prolonged.

This project presents the fabrication of a low-cost, portable, electronic biosensor for the early detection of Tuberculosis. A biotin-modified probe was linked using the non-covalent interaction of streptavidin-biotin and immobilised on Zinc Oxide (ZnO) nanosensor. Streptavidin and biotin immobilisation was studied and confirmed using a Fourier Transform Infrared (FTIR). The ZnO nanowires were grown and optimized using the electrochemical deposition technique, which helped to improve the c-axis alignment of the nanowires. The ZnO nanowires were characterized using a scanning electron microscopy (SEM). Probe immobilisation was studied and confirmed using an atomic force microscopy (AFM) and the piezoelectric response of the nanosensor itself. The high affinity of the biotinylated-probe, immobilised on the nanosensor surface, to the target molecule, resulted in a direct piezoelectric effect, meaning the increase in the concentration and binding of the target molecule caused the measured output piezoelectric voltage of the nanowires due to the high degree of bending of the nanowires. Electronic circuits were simulated and built for an easy and inexpensive way to measure the piezoelectric voltage from the nanosensor, without having to use expensive equipment. The electronic circuit was successfully used to measure the piezoelectric voltage from the nanosensor. The biosensor was successfully fabricated and tested as a proof of concept, the chosen biotin-probe was the anti-luteinizing hormone- $\beta$  to detect the luteinizing hormone present in our bloodstream. An increase in piezoelectric potential were due to an increase in antibodies concentration bound to the sensor surface, and this evidence shows that the ZnO nanosensor may be used to record changes in antibody concentrations. The recorded concentrations of the anti-luteinizing hormone- $\beta$  were ranging from 25 to 10 ng/ $\mu$ l.



# Opsomming

Tuberkulose (TB) word beskryf as een van die top 10 dodelike infeksiesiektes in die wêreld en miljoene mense kontrakteer en sterf van TB elke jaar. TB diagnose is een van die belangrikste aspekte om TB te beheer en te beëindig. Die huidige toetsmetodes vir TB-infeksie is baie duur, nie-draagbaar en laboratoriumgebaseerd. Dit vereis ervare personeel, is nie baie akkuraat nie, en het nie die vermoë om op dieselfde dag resultate by versorging te genereer nie. Dit verleng dus die tyd van diagnose tot behandeling onnodig.

In hierdie projek word gepoog om 'n laekoste, draagbare, elektroniese biosensor vir die vroeë opsporing van Tuberkulose te ontwerp en te implementeer. 'n Biotien-gewysigde probe word gekoppel deur middel van die nie-kovalente interaksie van streptavidien-biotien en geïmmobiliseer op 'n sinkoksied (ZnO) nanosensor. Streptavidien- en biotien-immobilisering is bestudeer en bevestig met behulp van 'n Fourier Transform Infrared (FTIR) metode. Die ZnO nanodrade is gegroei en geïmplementeër met behulp van 'n elektrochemiese deposisie-tegniek, wat gehelp het om die c-as-belyning van die nanodrade te verbeter. Die ZnO nanodrade is gekarakteriseer deur 'n skandering-elektronmikroskopie (SEM). Probe-immobilisering is bestudeer en bevestig met behulp van atoomkrag-mikroskopie (AFM) asook die piësoëlektriese respons van die nanosensor self. Die hoë affiniteit van die gebiotinileerde probe, geïmmobiliseer op die nanosensor oppervlak, met die teikengroep, het 'n direkte piësoëlektriese effek tot gevolg gehad, wat beteken dat die toename in die konsentrasie en binding van die teikenmolekule veroorsaak het dat die gemete uitset piësoëlektriese spanning van die sensor veroorsaak was as gevolg van die hoë mate van buiging van die nanodrade. Elektroniese stroombane is gesimuleer en gebou as 'n maklike en goedkoop manier om die piësoëlektriese spanning van die nanosensor te meet, sonder om duur toerusting te gebruik. Die elektroniese stroombaan is suksesvol gebruik om die piësoëlektriese spanning van die nanosensor te meet.

Die biosensor is suksesvol vervaardig en getoets as 'n bewys van konsep. Die gekose biotien probe was die anti-luteïniserende hormoon -  $\beta$  om die luteïniserende hormoon teenwoordig in ons bloedstroom op te spoor. Die toename in piësoëlektriese potensiaal was te wyte aan 'n toename in teenliggaamkonsentrasie gebonde aan die sensor oppervlak, en dit bewys dat die ZnO nanosensor

gebruik kan word om veranderinge in antiliggam konsentrasies te registreer. Die gemete konsentrasies van die anti-luteïniserende hormoon -  $\beta$  het gewissel van 25 tot 10 ng /  $\mu$  l.

# Acknowledgements

The author, Sihle Tom, would like to thank the following people for their contribution towards the completion of this project.

- Prof W.J Perold, my supervisor, for giving me an opportunity to part of the SAND research group. Secondly, for his enthusiasm and encouragement about the work done during the project, as well as all the advice given regarding designs, report writing and editing.
- Prof H. Jacobsen, my external-co-supervisor, for his enthusiasm, advices and encouragement during the project, as well as all the techniques given regarding ZnO nanowire fabrication and thin film sputtering procedures.
- Dr S. Kamlich, for his overall contribution during the project and advices on nanowire growth .
- Prof R. Warren and Prof T. Grant, my co-supervisors, for their enthusiasm, advices and contribution during the project, as well as providing their well detailed insight on the biomedical side of the project.
- Dr Melanie Grobelaar, for all the she spent on calculating and designing the DNA and RNA bioanalyzer experiments. Your contribution during the project is truly appreciated.
- Dr. Frederick Isingizwe for all time he put to organise the lab the time spent fixing and replacing materials and equipment needed in the lab.
- To Mrs Jenny Martin, for her hard work, support and making sure the orders placed correctly and on time.
- To all my colleagues in room E210, Whelan Sergio Mohale, Daniel Retief, Alexander Lloyd, Stephan Schoeman and Moremogolo Tsatsi, thank you for your suggestions, encouragement and support during the hard times. A special thanks goes to Whelan Mohali for his help and contribution to the project.
- To my family, thank you for supporting and loving me.

*ACKNOWLEDGEMENTS*

vii

- Last but not least, to my girlfriend, thank you for your support and love through those stressful and hard times.

# Contents

<b>Declaration</b>	<b>ii</b>
<b>Abstract</b>	<b>iii</b>
<b>Opsomming</b>	<b>iv</b>
<b>Acknowledgements</b>	<b>vi</b>
<b>Contents</b>	<b>viii</b>
<b>Abbreviations</b>	<b>xii</b>
<b>List of Figures</b>	<b>xiv</b>
<b>1 Introduction</b>	<b>1</b>
1.1 Motivation for Early Detection . . . . .	1
1.2 Aims and Objectives . . . . .	2
1.3 Research Topic . . . . .	4
1.4 Scope . . . . .	4
1.5 Significance . . . . .	5
1.6 Thesis Structure . . . . .	6
<b>Abbreviations</b>	<b>1</b>
<b>2 Literature Study</b>	<b>8</b>
2.1 Nanotechnology for Early Tuberculosis Detection . . . . .	8
2.1.1 Nanostructures . . . . .	11
2.1.2 Piezoelectricity . . . . .	13
2.1.3 Piezoelectricity in a single ZnO NW . . . . .	17
2.1.4 Governing Equations . . . . .	19
2.1.5 ZnO Nanowires Synthesis Methods . . . . .	22
2.1.6 Piezoelectric Devices . . . . .	27
2.2 Nucleic Acid Probe Immobilisation Techniques . . . . .	28
2.2.1 Physical Adsorption . . . . .	29
2.2.2 Covalent Immobilization . . . . .	30

2.2.3	Bio-affinity Immobilization . . . . .	31
2.3	Self-Assembled Monolayers of Thiolates on Metals as a part of Nanotechnology . . . . .	32
2.4	Factors affecting SAMs . . . . .	34
2.5	Biosensors . . . . .	35
2.5.1	Types Of Biosensors . . . . .	36
2.5.2	Bio-receptor Categorization . . . . .	37
2.5.3	Transducer Categorization . . . . .	43
2.6	Conclusions . . . . .	50
<b>3</b>	<b>Design and Simulation Of 3D ZnO Nanowire Based Mass Sensor</b>	<b>51</b>
3.1	Introduction . . . . .	51
3.2	Comsol Modeling . . . . .	52
3.3	Comsol Simulation . . . . .	55
3.4	Comsol Simulation Results And Discussions . . . . .	57
<b>4</b>	<b>ZnO Transducer Design And Fabrication</b>	<b>59</b>
4.1	Introduction . . . . .	59
4.2	Materials and Methods . . . . .	59
4.2.1	Preparation of silicon wafers . . . . .	59
4.2.2	Deposition of the Aluminum layer . . . . .	60
4.2.3	Deposition of the Gold layer . . . . .	60
4.2.4	Deposition of the ZnO seed layer . . . . .	60
4.2.5	Synthesis of ZnO nanowires And Insulation . . . . .	60
4.2.6	Results And Discussions . . . . .	61
4.3	Conclusion . . . . .	68
<b>5</b>	<b>Probe Design And Manufacturing</b>	<b>69</b>
5.1	Introduction . . . . .	69
5.2	Chemical And Biological Materials . . . . .	69
5.3	Methodology . . . . .	69
5.3.1	Mycobacterium Cell Lysis And RNA Extraction. . . . .	71
5.3.2	Hybridisation Through Electrophoresis. . . . .	73
5.4	Results And Discussions . . . . .	74
5.5	Conclusion . . . . .	81
<b>6</b>	<b>Data Capturing and Refining Electronics</b>	<b>82</b>
6.1	Introduction . . . . .	82
6.2	Simulation of Data Refining Circuitry . . . . .	82
6.2.1	Ideal Piezoelectric Nanogenerator Equivalent Circuit . . . . .	83
6.2.2	Simulation of a Rectifying Circuit . . . . .	84
6.3	Practical Circuitry . . . . .	87
6.3.1	Rectifying Circuit . . . . .	88

6.3.2	Microcontroller-Driving Circuit . . . . .	89
6.3.3	Conclusion . . . . .	90
<b>7</b>	<b>ZnO nanowire-array biosensor construction for the detection and quantification of tuberculosis</b>	<b>91</b>
7.1	Introduction . . . . .	91
7.2	Materials And Methods . . . . .	91
7.2.1	immobilization of Biotin-SAMs on Nanosensor Surface . . . . .	91
7.2.2	Immobilisation of Streptavidin on Biotin-SAMs . . . . .	95
7.2.3	Immobilisation of Biotinylated Probe on Biotin-Streptavidin Layer . . . . .	96
7.3	Biosensor Testing as a Proof Of Concept . . . . .	99
7.4	Results and Discussions . . . . .	102
<b>8</b>	<b>Conclusions</b>	<b>104</b>
	<b>List of References</b>	<b>106</b>
	<b>Appendices</b>	<b>113</b>
	<b>RNA extraction protocol</b>	<b>114</b>
	Total RNA isolation . . . . .	115
	Total RNA isolation . . . . .	116
	Total RNA isolation . . . . .	117
	Total RNA isolation . . . . .	118
	Total RNA isolation . . . . .	119
	<b>Flow chart for spin coating Zinc Oxide thin films</b>	<b>120</b>
	ZnO seed layer flow diagram . . . . .	121
	<b>Piezoelectric voltage curves from nanosensors</b>	<b>122</b>
	Piezoelectric voltages generated by the nanosensors . . . . .	123
	Piezoelectric voltages generated by the nanosensors . . . . .	124
	Piezoelectric voltages generated by the nanosensors . . . . .	125
	Piezoelectric voltages generated by the nanosensors . . . . .	126
	<b>Schematic and PCB board</b>	<b>127</b>
	<b>Bioanalyzer Experiments</b>	<b>131</b>
	Bioanalyzer Experiments . . . . .	132
	Bioanalyzer Experiments . . . . .	133
	Bioanalyzer Experiments . . . . .	134
	Bioanalyzer Experiments . . . . .	135
	Bioanalyzer Experiments . . . . .	136

<i>CONTENTS</i>	<b>xi</b>
<b>Final representation of the biosensor</b>	<b>137</b>
<b>FTIR Chart</b>	<b>139</b>
Fourier Transform Infrared Chart . . . . .	140
<b>Biosensor Testing Setup</b>	<b>141</b>
<b>Arduino code</b>	<b>143</b>



# Abbreviations

- Au - Gold
- AFM - Atomic Force Microscopy
- BW - Bulk wave
- DC - Direct Current
- div-division
- DNA -Deoxyribonucleic Acid
- eV - electron Volts
- FTIR - Fourier Transform Infrared
- g- gram
- IBM - International Business Machines
- ISE - Ion - Selective Electrode
- LED - Light Emitting Diode
- LH - Luteinizing Hormone
- LOD -limit of detection
- min(s) - minute(s)
- mm - mili ( $10^{-3}$ ) meter
- mol - mole
- MTB - Mycobacterium Tuberculosis
- MTBC - Mycobacterium Tuberculosis Complex
- N - Newton
- nm - nano ( $10^{-9}$ ) meter

- NW(s)- Nanowire(s)
- PBS - Phosphate buffered saline
- PC - Personal Computer
- PCB - Printed Circuit Board
- PE-FET piezoelectric field effect transistor
- PMMA - Poly(methyl methacrylate)
- PNA - Peptide Nucleic Acid
- QCM - Quartz Crystal Microbalance
- RIN - RNA Integrity Number
- RNA - Ribonucleic Acid
- rpm - rotations per minute
- SAMs - Self-Assembled Monolayers
- SAW - Surface Acoustic Wave
- SEM - Scanning Electron Microscope
- Si -Silicon
- TB - Tuberculosis
- TE - Tris- Ethylene-Diamine-Tetra-Acetic acid
- $\mu\text{m}$  -micro ( $10^{-6}$ ) meter
- V - volts
- WHO - World Health Organization
- XRD - X-Ray Diffraction
- ZnO - Zinc Oxide
- 0D - zero dimensional
- 1D - one dimensional
- 2D - two dimensional
- 3D - three dimensional

# List of Figures

2.1	Size comparison of objects at the nanoscale level. . . . .	8
2.2	The Lycurgus Cup at the British Museum, lit from the outside (A) and from the inside (B). . . . .	9
2.3	IBM acronym spelled with atoms at nanoscale. . . . .	10
2.4	Nanotechnology market growth between the years 2005 and 2015. .	10
2.5	A schematic diagram of the types of nanocrystalline materials categorized by the dimensions of their structural elements: (A) zero-dimensional clusters; (B) one-dimensional tubes; (C) two-dimensional films ; (D) three-dimensional polycrystals. . . . .	11
2.6	A schematic diagram showing both direct(a-b) and inverse piezoelectric effects(c-d) respectively. Direct piezoelectric effect:(a) at applied compressive force, (b) at applied tensile force. Inverse piezoelectric effect:(c) at applied positive voltage and (d) at applied negative voltage. Both (c) and (d) are the same in terms of length change due to internal polarization as well as the reversed external voltage. . . . .	14
2.7	A schematic diagram of (a) a ZnO wurtzite structure, (b) tetrahedral organization between Zn and O atoms, (c) an applied force which displaces the positive charge with respect to the negative charge, resulting a potential difference in the structure. . . . .	15
2.8	(A) schematic diagram of a NW governed by a set of axis, (B) longitudinal strain( $\epsilon_z$ ) distribution in the NW after deflected by an AFM tip, (C) induced electric field( $E_z$ ) in the NW due to deflection, (D) voltage distribution due to the piezoelectric effect, (E and F) the contact between the AFM tip and the NW with the I-V insert showing the forward and reverse Schottky diode. . . . .	18
2.9	A schematic diagram of a cross section of a NW deflected by a force $f_y$ producing a typical voltage demonstrated by the insert (b). . . .	21
2.10	Schematic representation of the growth of ZnO nanowires by VLS mechanism. . . . .	23
2.11	Schematic representation of the VLS setup mechanism. Showing the Argon gas flow direction, the position of the source material and the substrate. . . . .	24

2.12	Schematic representation of the (a)formation of nucleation sites and (b) the growth of ZnO nanostructures(top view) from the nucleation sites in aqueous solutions. . . . .	25
2.13	Schematic representation showing the zinc metals in the solution and oxygen from the water being attracted to the nucleation sites and form layers, which stack up to form the ZnO nanowires in an aqueous solution. . . . .	26
2.14	Schematic drawing to explain the hydrothermal method used to grow ZnO NWs. Schematic representation showing the zinc metals in the solution and oxygen from the water being attracted to the nucleation sites and form layers, which stack up to form the ZnO nanowires in an aqueous solution. . . . .	26
2.15	Schematic diagram of a typical PE-FET nanodevice based on a single nanowire. When an external nanoforce(F) is applied on the single nanowire connected between two electrodes, a proportional voltage( $V_p$ ) can be measured. . . . .	27
2.16	Schematic diagram of a typical PE-diode nanodevice based on a single nanowire. The single nanowire is held stationary by one probe and while the other is exerting force (F) to end the NW to produce a voltage ( $V_p$ ) which can be measured. . . . .	28
2.17	Schematic diagram showing the immobilisation techniques: (a) Physical adsorption (b) Covalent binding and (c)Streptavidin-Biotin Immobilization. . . . .	29
2.18	Schematic diagram showing the Streptavidin-Biotin immobilisation technique with a nucleic acid probe at the affine layer. . . . .	31
2.19	A typical building blocks of SAMs. Showing the terminal functional group, alkane chain, functional headgroup and the gold substrate. the formation of SAMs starts from the functional headgroup on the substrate to the terminal functional group. . . . .	32
2.20	The building blocks of a typical biosensor. Showing the bioreceptor, transducer and the signal processing electronics.The signal processing electronics consist of the amplifying, the signal processing and the display stages. . . . .	36
2.21	Categories of biosensors based on bioreceptors and transducers. . .	37
2.22	A schematic of a cell-based biosensor. Showing the living cells as the bioreceptors immobilized on a gold electrode interacting with an analyte. . . . .	38
2.23	A schematic diagram of an Enzyme-based biosensor. Showing the enzyme as the bioreceptors immobilized onto a transducer and interacting with a target analyte. . . . .	39
2.24	A diagram of an antibody. The antibody is 'Y' shaped immunoglobulin with two heavy chains and two light chains. The diagram also shows the antigen binding sites . . . . .	40

2.25	A schematic diagram of an Antibody-based biosensor. Showing the antibody used as the bioreceptors immobilized onto a transducer and interacting with a target analyte (specific antigens with markers).	41
2.26	A schematic diagram of an ideal Nucleic acid-based biosensor. Showing (A) the biosensor and the probe used as the bioreceptors immobilized onto a transducer, (B) the target analyte, which is nucleic acids as well and (C-D) The hybridization process, which is the binding of target to the complementary probe. . . . .	42
2.27	A schematic diagram of a chemical model of peptide nucleic acid and deoxyribonucleic acid. Showing (a) the hybridized PNA-DNA duplex in terms of the Watson-Crick base pairing rule and (b) the difference in the backbone chemical structures of PNA and DNA. .	43
2.28	A basic electrochemical biosensor setup consisting of an electrochemical cell which is composed of working electrode (WE), reference electrode (RE), counter electrode (CE) in a solution and an electrochemical analyser. . . . .	45
2.29	A basic (A) thermistor and its (B) schematic diagram showing vital components of the thermistor . . . . .	46
2.30	A basic calorimetric biosensor (also known as Enzyme thermistor) setup consisting of a thermistor as the transducer, heat exchanger, enzyme column. . . . .	46
2.31	An optical biosensor architecture showing the scattering of light from the laser source to the detection device (antenna), optoelectronic setup and the immobilised probe. . . . .	47
2.32	(A) Schematic setup of a typical QCM biosensing technique. Showing an oscillator and a frequency counter which will record the changes in frequency from the QCM. (B) Schematic of a typical piezoelectric crystal. . . . .	48
2.33	Schematic diagram of a typical piezoresistive cantilever beam sensing technique. When the biomolecules attach to the cantilever beam, the cantilever bends and causes a change in the resistance of the resistor placed inside the cantilever. . . . .	49
3.1	A Comsol model of a 3D Silicon wafer (p-type Si<100>). The Silicon wafer is modeled such that it has a thickness of 0.1 $\mu\text{m}$ and an area of 10x10 mm <sup>2</sup> . . . . .	53
3.2	A meshed model of a 3D Silicon wafer with 9242 elements. . . . .	53
3.3	A Comsol model of a 3D ZnO nanowire sensor. A Comsol model of a 3D ZnO nanowire sensor. Showing the Zinc oxide nanowires (green colour) which are supported by a silicon wafer (Si(100)) substrate. .	54
3.4	A meshed model of a 3D ZnO nanowire sensor. Showing the Zinc oxide nanowires (blue colour) which are supported by a silicon wafer (Si<100>) substrate (grey colour). The meshed sensor consists of complete meshed of 61070 elements. . . . .	54

3.5	A 3D simulated nanosensor. The nanosensor consist of 5 activated ZnO nanowires. Only 5 nanowires were chose to represent the nanosensor due to computational time and memory space. . . .	55
3.6	A displaced 3D simulated ZnO nanowire with an applied force of 10 nN in the y-direction. . . . .	56
3.7	Simulated graphs showing the (a) generated Electric Potential Energy as function of an applied force on the simulated nanowire. Note that the Electric Potential Energy is directly proportional to the applied force. (b) Calculated Electric Potential Energy as function of an applied force using equation 2.1.11. Note the graph has the same trend as the simulated graph from (a) and also that the Electric Potential Energy is directly proportional to the applied force. (c) Generated Electric Potential Energy as function of the length of the simulated nanowire. Note that the graph sarturates at length more 1000 nm. (d) Generated Electric Potential Energy as function of the radii of the simulated nanowire. Note that the Electric Potential Energy is indirectly proportional to the nanowire radii. . . . .	58
4.1	SEM images obtained via the FIE-SEM of non-optimised nanowires grown via the Hydrothermal method. Images (a) and (b) show the top view of the randomly grown nanowires. Image (c) shows the side view of the nanowires of the randomly clustered nanowires. Image (d) shows the nanowire growth branched at different directions other than the c-axis which is a huge problem. . . . .	62
4.2	SEM images obtained via the ZIESS SEM of optimised nanowires grown via the Electrodeposition method. Figures 4.2(a)-(d) show the top view of the nanowires. Figure. 4.2(b) shows the zoomed version (at $2\mu\text{m}$ ) of Figure. 4.2(a). Figures 4.2(c) and (d) show the nanowires at scale of $1\mu\text{m}$ . The nanowires successfully grew perperndicular to the substrate via the electrodeposistion method just under an hour. . . . .	63
4.3	ZnO nanowires grown via the Electrodeposition method characterised using an ZEISS-SEM at Stellenbosch University, shown in Figure. 4.3 (a) and (b), zoomed at $1\mu\text{m}$ and 200 nm, is an array of ZnO nanowires with a thin layer of gold on top of the nanowires to form a Schottky contact. . . . .	64

4.4	ZnO nanowires grown via the Electrodeposition method characterised using an AFM in our nanolaboratory at Stellenbosch University, shown in Figure 4.3 (a) and (a1). Figures 4.3 (b) and (c) show the output voltage of a nanosensor under the tapping mode of the AFM. The tapping mode of an AFM is when the AFM tip is in contact with a defined number of nanowires causing them, through the applied force, to bend and generate potential energy of about 295 mV. Figure 4.3 (c) shows a zoomed-in version voltage response of Figure 4.3 (b). . . . .	65
4.5	A generated voltage of a ZnO nanosensor obtained by a digital multimeter (Agilent, 34401A Digital Multimeter) which uses the BenchVue software. When the pressure is applied on the nanosensor the nanowires bend to generate a specific voltage which depicts the "on" state and when no pressure is applied there is no voltage which depicts the "off" state of the sensor. The first nanosensor, shown in Fig. 4.5(a), generated an average voltage of 0.032 mV. On the other hand, a different nanosensor, shown in Fig. 4.5(b), generated an average voltage of 0.05 mV. . . . .	66
4.6	X-ray diffraction pattern of ZnO Nws synthesized on a glass substrate via the electrodeposition method. The major diffraction planes, such as (100), (101) and (102), could be easily indexed. . . .	67
5.1	The blast results of 16 rRNA Mycobacterium Tuberculosis obtained from an online NCBI BLAST. The highlighted region shows the region of interest in complete genome of the bacterium. . . . .	71
5.2	A base bioanalyzer electropherogram of the extracted total RNA showing the RNA area,contamination, concentration, RNA ratio and the RNA Integrity Number(RIN). The electropherogram also shows 3 peaks which depict the marker, 16S rRNA and the 23S rRNA. . . . .	75
5.3	Bioanalyzer electropherogram results of the extracted Mycobacterium tuberculosis total RNA incubated in TE buffer at room temperature. The incubation was carried out in different RNA concentrations of 31 ng and 21 ng as shown in Figures.5.3(a) and (c) , respectively. The electropherograms show the RNA area,contamination, concentration, RNA ratio and the RNA Integrity Number(RIN) for each concentration. The inset in Figure5.3(b) electropherogram also shows 2 peaks which depict the 16S and the 23S rRNA concentrations. . . . .	76

5.4	Bioanalyzer electropherogram results of the extracted different concentrations of the <i>Mycobacterium tuberculosis</i> total RNA incubated in RNase free-water buffer at room temperature. The incubation was carried out in different RNA concentrations of 17 ng, 17 ng and 14 ng as shown in Figures.5.4(a)-(c) , respectively. The electropherograms show the RNA area,contamination, concentration, RNA ratio and the RNA Intergrity Number(RIN) for each concentration. The inset in Figure5.4(a) electropherogram also shows 2 peaks which depict the 16S and the 23S rRNA concentrations. . . . .	77
5.5	Bioanalyzer electropherogram results of the the cDNA probe incubated with the total RNA at different concentration ratios. the dilution ratio was 500:1 and 1000:1 as shown in Figures 5.5(a) and (b), respectively. The incubation was carried out in different RNA concentrations of 22 ng and 127 ng as shown in Figures.5.5(a) and (b) , respectively. The electropherograms show the RNA area,contamination, concentration, RNA ratio and the RNA Intergrity Number(RIN) for each concentration. . . . .	78
5.6	Bioanalyzer electropherogram results of the the cDNA probe incubated with the total RNA at different concentration ratios. the dilution ratio was 500:1 and 100:1 as shown in Figures 5.6(a) and (b), respectively. The incubation was carried out in different RNA concentrations of 79 ng/ul and 66 ng/ul as shown in Figures.5.6(a) and (b) , respectively. The electropherograms show the RNA area,contamination, concentration, RNA ratio and the RNA Intergrity Number(RIN) for each concentration. . . . .	79
5.7	Bioanalyzer electropherogram results of the the cDNA probe incubated with the total RNA at a concentration of 203 ng/ul. The dilution ratio was 500:1 as shown in Figures 5.7. The incubation was carried out in different RNA concentrations of 203 ng/ul and . The electropherogram shows the RNA area,contamination, concentration, RNA ratio and the RNA Intergrity Number(RIN) for each concentration. . . . .	80
6.1	An equivalent circuit diagram of the nanosensor modeled with a voltage source in series with an input resistance and an input capacitor.The equivalent circuit is modeled to resemble a nanosensor on a rigid susbtrate. . . . .	83
6.2	A simulated output voltage of the equavalent nanosensor circuit.The inset shows the magnified voltage of the nanosensor and also shows the "On" and "Off" states. . . . .	84
6.3	A circuit diagram of a full bridge rectifying circuit with the nanosensor circuit diagram connected as an input source of voltage. The Purpose of the rectifying circuit is to scavenge power form the nanosensor and convert it to a DC voltage. . . . .	85



6.4	A simulated voltage output of the full bridge rectifying circuit with the nanosensor circuit diagram connected as an input source of voltage. The output capacitor charges and it reaches a steady state of 3.33 mV DC after 25 seconds and the ripple voltage is about 81.6 $\mu$ V as shown by the inset. . . . .	85
6.5	A circuit diagram of a driving circuit with a microcontroller. This circuit is used to interpret and make sense the processed data from the rectifying circuit and provides easy end-user interface. . . . .	86
6.6	A full circuit diagram for data capturing and refining used for the biosensor. . . . .	87
6.7	A built practical circuit for data capturing and refining used for the biosensor. . . . .	88
6.8	A measured output voltage of the full bridge rectifying circuit. Figure 6.8 (i) shows that the input signal can be rectified by the scavenging circuit using a sinusoidal input voltage. Figure 6.8(ii) shows the charging capacitor (curve: a-b), the fully charged capacitor (curve: b-c) and the discharging capacitor through the load resistance (curve: c-d) due to change in input piezoelectric voltage. . . . .	89
6.9	A measured output voltage across the LED when switching "on" and "off" as shown by the insets. . . . .	90
7.1	An FTIR spectrometer for biotin-SAMs solution. The SAMs solution is not yet immobilised onto the nanosensor gold surface. Since the biotin-SAMs were prepared with ethanol as a solvent, the spectrometer also shows the OH group (blue) and the biotin (orange). . . . .	93
7.2	An FTIR spectrophotometer for a gold thin layer. This is included just for reference. The gold layer has not yet been immersed into the SAM solution for biotin immobilization. . . . .	94
7.3	An FTIR spectrometer showing the immobilization of Biotin-SAMs on the gold surface of the nanosensor. The major spectrometer peaks can be easily identified and verified. The major spectrometer peaks for NH, OH, H-C=O and C-H are 1646.16 cm <sup>-1</sup> , 3326.79 cm <sup>-1</sup> , 2323.82 cm <sup>-1</sup> and 821.84 cm <sup>-1</sup> , respectively. . . . .	95
7.4	A measured piezoelectric voltage responses during the immobilization of streptavidin and biotinylated-probe. The increase in mass bends the nanowires and induce a piezoelectric voltage. During the immobilization step, PBS was first introduced as a control(a), then a solution of streptavidin was introduced (b) and lastly the biotinylated probe(c) was introduced. The voltage spikes before the incubation of PBS are due to the immobilised Biotin-SAMs. . . . .	97

7.5	A measured output DC voltage of the full-bridge rectifier during the immobilization of streptavidin and biotinylated-probe. The increase in mass bends the nanowires and induce a piezoelectric voltage. During the immobilization step, PBS was first introduced as a control(a), then a solution of streptavidin was introduced (b) and lastly the biotinylated probe(c) was introduced. The small DC voltage spikes before the incubation of PBS are due to the immobilised Biotin-SAMs. . . . .	98
7.6	A schematic setup used for the testing of the piezelectric biosensor. The schematic shows the 3 probe sensor holder, a digital multimeter and a PC for displaying and logging data. . . . .	99
7.7	Measured output voltage of the biosensor before and after incubation of PBS as a control buffer. Figures 7.7(a) and (b) show the measured piezoelectric voltage before and after the addition of the control buffer, respectively. . . . .	100
7.8	Measured output voltage of the biosensors before and after incubation of LH hormone. Figures 7.8(a) and (b) show the measured piezoelectric voltage before and after the addition of 10 ng/ $\mu$ l of LH hormone, respectively. . . . .	101
7.9	Measured output voltage of the biosensors before and after incubation of LH hormone. Figures 7.8(a) and (b) show the measured piezoelectric voltage before and after the addition of 25 ng/ $\mu$ l of LH hormone, respectively. . . . .	101
1	PCB board designed with Altium. . . . .	128
2	PCB board designed with Altium. . . . .	129
3	A manufactured GeneTB PCB board designed with Altium designer. . . . .	130
4	A schematic representation of the final working biosensor. . . . .	138
5	The setup of the equipment used to test the biosensor. . . . .	142
6	The code used to test the LED driving circuit. . . . .	144

# Chapter 1

## Introduction

### 1.1 Motivation for Early Detection

TB has existed over a period of thousands of years and still remains a global health problem[1]. Roughly about 95% of TB cases and deaths in low to medium income countries are caused by the lack of proper and effective diagnostic methods for infectious diseases with the highest burden in Africa(24%) and Asia[2][3]. Even in developed countries, most life threatening infectious disease diagnosis is performed by culturing methods, in which the time to treatment is unnecessarily prolonged[4]. TB and human immunodeficiency virus (HIV) are one of the major infectious diseases that remain a global health problem[5][6]. Alone, TB claims millions of lives annually[7]. TB is a common life threatening disease caused by the *bacillus mycobacterium tuberculosis* that commonly affects the lungs, and could be fatal if left untreated. Globally, TB remains the second leading fatal disease, after the HIV[8]. In 2015, the World Health Organization (WHO) estimated that about 10.4 million people were infected with TB and about 1.8 million died from the disease. Moreover, 1.71 million TB deaths occurred in countries with low to middle income[9]. India, with leading count, tailed by Indonesia, China, Nigeria, Pakistan and South Africa accounted for nearly over 1.03 million deaths combined[1]. These countries prove to fall under the developing countries category with very limited resources to fight against the spread of TB.

WHO has significantly claimed that implementations for controlling, monitoring and ending the global TB epidemic is of utmost importance[1][2]. Controlling and monitoring TB has many facets. Diagnosis serves as one of the most vital facets in controlling and monitoring TB[10]. In simple words, before the treatment stage of a patient a rapid, efficient and accurate diagnosis has to be performed. Conventional TB detection strategies mostly rely on microbiological and biochemical analysis. Conventional diagnostic methods of active TB include sputum smear microscopy and *M. tuberculosis* chest radiog-

raphy. Smear microscopy is easy, fast and inexpensive, however it lacks specificity to differentiate between the *M. tuberculosis* and other non-photogenic *Mycobacterium*[9]. Similarly, chest radiography is not always specific or sensitive enough to conclude a diagnosis[11]. Even though these methods are globally employed, they are overly time consuming, fail to accurately classify the disease with high specificity and sensitivity, they are also cost-ineffective, require special personnel training and they have no integration room for an on-site diagnosis. Furthermore, these conventional methods are laboratory based and they require extensive training and experience. The major disadvantage of these conventional methods is the delay of diagnosis-results-treatment process, which may take weeks. This causes an unnecessary delay in time from diagnosis to treatment[7][12]. In this regard, rapid TB screening remains a pressing issue. Alternate tools for accurate, specific and highly sensitive detection of TB has hence been a field of interest across the world[10][12].

Biosensors have attracted tremendous attention as the new alternative tools for pathogen detection[13]. Biosensors are analytical devices which translate a specific bio-recognition event into a measurable electric signal[14][15]. Biosensors offer several advantages such as high specificity, high degree of sensitivity, cost effectiveness, and portability[15]. Moreover, they are ideal for near patient point-of-care (POC) diagnosis. In countries with limited resources and developing health care systems, like South Africa, biosensors can be employed in aiding with rapidly screening groups of people who have been exposed to Tuberculosis in order to significantly stop the spread of TB.

This project will investigate the fabrication and development of a portable self-powering Nucleic Acid biosensor. This device will employ the use of a piezoelectric nanogenerator as the transducer for the sensor. The piezoelectric nanogenerator convert mechanical nanoforce to an electrical signal through the piezoelectric effect[16][17]. Zinc oxide (ZnO) nanowires will be used as the piezoelectric material, accordingly, when an external force is applied to the nanowires an electrical signal will be generated and Peptide Nucleic Acid (PNA) will be used as a bioreceptor for the sensor. The completed device, consisting of ZnO piezoelectric nanogenerator as the transducer and a PNA probe immobilized on the tips of the ZnO nanowires.

## 1.2 Aims and Objectives

The project is divided into nine main objectives: first, a thorough literature study; secondly, to identify and manufacture an optimum transducer element. Thirdly, extracting the single stranded amplicons of the MTBC genomic target 16S rRNA. Fourth, the designing and synthesis of a complementary probe, which can be immobilized onto the transducer. Fifth, develop a method to link

probe to biosensor material. Sixth, the optimization of the binding process of the bio-recognition elements onto the transducer. Seventh, optimization of the hybridization conditions to limit non-specific binding and efficient hybridization. Eighth, design a data capturing electronics and the communication to the handheld sensing device. Ninth, testing the sensor for sensitivity, specificity and repeatability.

The first objective is to do a complete literature study, which will provide a better understanding of nanostructures, piezoelectricity & piezoelectric devices, immobilisation techniques, and biosensors. The literature study will cover different aspects of the biosensors, such as its building blocks. After literature study, an optimum transducer element will be identified and manufactured; transducers play a major role in energy conversion. In general, the transducer transforms the chemical interaction between the target analyte and the biological receptor into a measurable electric signal. The aim is to get a signal that can be more easily measured and quantified. A method to extract the target 16S rRNA is developed, the main objective is to obtain and analyze selected copies of the genomic target 16S rRNA without PCR amplification. The selected genomic target will be analyzed and used to obtain its base sequences, specific to TB, to manufacture the probe.

After the base sequence is known, a complementary single sided probe can be manufactured. The aim is to design the complementary nucleotide bases of the single sided 16S rRNA target. This is very important because the target has to hybridize with the probe and this event is known as hybridization. The probe, target and the transducer are very crucial to the success of this project. Covalent bonding technique and Self-Assembled Monolayers(SAMs) will be employed to cross-link the probe to the transducer. This step is very important because the probe has to bind successfully to the transducer in order to obtain proper measurements. After that, the binding process of the bio-recognition elements onto the transducer has to be optimized, the aim here is to optimally and successfully link the probe with the piezoelectric transducer.

The second last objective is to design a data capturing electronics and the communication to the hand-held sensing device. The main objective is to process the raw data coming from the biosensor into a more user-friendly data. This means that users will be able to use the device with ease and be able to interpret the end-results. Lastly, the biosensor will be tested for limit of detection, sensitivity, specificity and repeatability. The aim here is to use different analyte concentration and/or different specimen and record the changes in the measured results under the same conditions.

The main overarching aim of the project is to produce a proof of concept point-of-care sensing device that is ready to be tested in the field (i.e. in rural areas, etc.) and that will be able to be used for an on-the-spot diagnosis of TB infections.

### 1.3 Research Topic

The research topic for this project is: The development and optimization of a hand-held bio-sensing device for the early detection of *Mycobacterium tuberculosis*, which will be used for near-patient point-of-care diagnosis.

The topic of this study is broken down into three different main aspects. The first section of this study consist of the growth of the ZnO nanowires, which consequently entails the manufacturing of the ZnO transducer. There are various methods which can be used to grow the Zinc Oxide nanowires. However, due to time constraints, material and equipment, only two growth methods are thoroughly explored: aqueous solution and electrochemical deposition method. Both these method operate at temperatures less than 100 degrees celsius. As mentioned, the grown nanowires will be used to fabricate a piezoelectric transducer. The nanowires will be optimised with respect to the output voltage they can generate due to piezoelectricity. This mean that the nanowires will be aoptimised to be more sensitive and produce high potential energy. After the nanowires are optimised, the piezoelectric transducer will be fabricated. The optimization of the transducer or nanowires will be done through Comsol simulations, mathematical models, building physical models and literature study. Secondly, this study consist of biological materials. The biological material will be immobilised onto the piezoelectric transducer(previously mentioned) for the application in the biosensor field. A number of biological material will be immobilised onto the transducer surface: Biotin-SAMs, Streptavidin and biotinylated DNA to make-up a working DNA biosensor. These biological materials are essential part of the biosensor.

Lastly, the biosensor will be tested as a proof-of-concept. The biosensor will be used to for different samples (control, positive and false positive sputum samples). Test limit of detection using different inputs of cultured MTBC bacilli.

### 1.4 Scope

This project focuses on the field of biosensors and nanotechnology. It combines electronic and electrical engineering (E&E), biomedical sciences and nanotechnology to produce a viable solution, as a proof of concept, for the detection of TB.

Firstly, the project focuses on nanotechnology, nanotechnology constitute of various fields and applications such as sensors, textile, defense and biotechnology, to name a few. This is where the ZnO nanowires are investigated and grown as piezoelectric material. ZnO crystal has a high-energy bandgap as compared to other piezoelectric material. The ZnO nanowires can be fabricated using different type of method, such as hydrothermal, electrospinning,

electrochemical deposition, to name a few. However, only two methods are used to grow and fabricate the nanowires due to availability of equipment. Other methods required specialised equipment, which was not available during the course of this project. The chosen methods are easily versatile, meaning they were easily changeable to adapt and work in our nanolaboratory. Eventually, the ZnO nanowires were used to manufacture a piezoelectric transducer for the biosensor. There are different types of transducers, such as optical, electrochemical and colorimetric. However the piezoelectric transducer is chosen because it is cheaper to manufacture and environmentally friendly.

Secondly, the project focuses on the molecular biology & human genetics field. This is where immobilisation of biomarkers / bioreceptors on the piezoelectric transducer and chemistry behind it are investigated. There are different types of biomarkers which can be used as bioreceptors for a biosensor. These include: nucleic acids, enzymes, antibodies and cells, to name a few. Nucleic acids were chosen due to easy base pair manufacturing hence higher target specificity. Firstly, the design and manufacturing of the single-stranded DNA specific to the 16s rRNA mycobacterium tuberculosis. Secondly, the immobilization of surface modifiers are investigated. The biotin-streptavidin noncovalent interactions are investigated due to the high affinity to each other and to gold thin films. This interface serves a great purpose in the manufacturing of biosensors as it protects probes from interaction with the metal surface. Hence, they lose their functionality and start to denature. Thirdly, the immobilisation of DNA probes are investigated. The probes are immobilised through non-covalent bonding, on top of the biotin-streptavidin interface layer. There are different types of biosensors such as The successful immobilisation of biomarkers onto the transducer concludes the manufacturing of the biosensor.

The final part of the project focuses on the design and manufacturing of electronics that will make it possible to acquire and capture raw data and process it to meaning data. The intergration of the biosensor and the electronics makes it possible to test whether the biosensor is works or not, as proof of concept.

## 1.5 Significance

The main overarching objective of this project, as mentioned before, is to produce a proof of concept point-of-care sensing device that is ready to be tested in the field (i.e. in rural areas, etc.) and that will be able to be used for an "on-the-spot" diagnosis of TB infections.

It has been stated before that South Africa has an unnecessarily high incidence of a number of life threatening diseases. TB continues to be the leading cause of death in South Africa[18]. In 2015, South Africa had a TB incident

rate of about 520 per 100,000. A main contributing factor is that early diagnostics are very often not available (rural areas) and are generally prohibitively expensive, to such an extent that testing (even when available) can be done very irregularly. This project will focus on the development of a handheld device, with connectivity to medical facilities, which will be capable of diagnosing TB infections. It is believed that the availability of such versatile biosensors (in remote areas and cities) may have a large impact on the general health of the population through early and cheap diagnostics. The availability of such a sensor has the potential for significant commercial impact. It is not farfetched that Government may be interested in such a device, due to the large potential to help manage and enhance the health of all people in South Africa. This project combines electronic engineering, biomedical sciences and nanotechnology to produce a viable solution, as a proof-of concept, for the detection of TB.

## 1.6 Thesis Structure

This section discusses the flow of this thesis. Literature study is presented in Chapter 2. The chapter begins by discussing nanotechnology and its history, from ancient Greek to present times. A brief description of nanotechnology is given. Furthermore, it reviews the types of nanostructures available and how they would be used for Tuberculosis detection. Piezoelectricity definition, piezoelectricity in a single nanowire and piezoelectric mathematical model for the output voltage of the nanowire are also discussed. This is followed by an in-depth review of ZnO nanowires is also presented. The section highlights the types of methods that can be used to grow ZnO nanowires. Hence, the manufacturing of a nanosensor is also presented. This is followed by a discussion on piezoelectric devices.

This chapter also reviews some of the immobilization techniques that can be used for the success of the project. This is followed by the discussion on Self-Assembled Monolayers (SAMs) and the factors that influence them. Furthermore, the chapter concludes with a review of biosensors that can be used to detect TB.

Chapter 3 focuses on the simulation of the ZnO nanowires. The chapter introduces the reader to the design and simulation of ZnO nanowires. This chapter highlights the modeling and simulation of the ZnO nanowires using Comsol Multiphysics. This chapter concludes by discussing the simulation results.

Chapter 4 discusses the ZnO nanosensor design and fabrication. This chapter highlights the preparation of silicon wafers (substrate). Followed by the discussion on the deposition of conductive thin films such as Aluminium and



Gold layers, respectively. This is followed by the deposition of ZnO seed layers using a Sol-gel coat spinning method. The seed layer can be used to initiate the growth of ZnO nanowires if spun correctly. After that, this section discusses two methods, Hydrothermal and electrodeposition technique, that were used to manufacture the ZnO nanowires. The nanowires are then characterised using methods such as scanning electron microscopy (SEM) and atomic force microscopy (AFM). this chapter also touches on the manufacturing of a nanosensor through PMMA insulation and top electrode gold deposition. The top electrode is used to form a Schottky contact for a continuous conduction.

Chapter 5 discusses the design and fabrication of the DNA probe. This chapter discusses the design of a single stranded DNA that is specific to the mycobacterium tuberculosis 16S rRNA. An online software, NCBI BLAST, was used to search and design the DNA probe. After that, the chapter discusses a protocol that was used for mycobacterium lysis and total RNA extraction. After obtaining the manufactured DNA probe, the chapter carried to discuss RNA and DNA probe hybridisation through electrophoresis. The chapter highlights the experimental procedures used on a Nanodrop<sup>TM</sup> and Bioanalyzer to confirm hybridisation. This chapter concludes by discussing the Bioanalyzer results.

Chapter 6 discusses the electronics used for data capturing and refining. The electronics are designed, modeled, simulated and built. Firstly, the chapter, discusses the design and simulation of the electronics and their results. This is followed by the manufacturing of the electronics and their results.

Chapter 7 discusses the ZnO nanowire-array biosensor for the quantification and detection of tuberculosis. This chapter starts with the discussion on the surface modification using biotinylated-SAMs (Self Assemble Monolayres). This is followed by a discussion on streptavidin biological material immobilised on the biotinylated-SAMs. Then the chapter discusses the immobilisation of biotinylated DNA probe on the Biotin-Streptavidin interface layer. This chapter concludes by discussing the results obtained from the biosensor using the built circuit with an oscilloscope and a digital multimeter .

Chapter 8 concludes the thesis. This chapter highlights the main findings of the project regarding the biosensor as a proof of concepts.

## Chapter 2

# Literature Study

## 2.1 Nanotechnology for Early Tuberculosis Detection

**Whats is Nanotechnology?** The word "*nano*" is defined as one thousand-millionth of a unit or  $10^{-9}$  metre. The word originates from the ancient greek word *nânos* which means "*dwarf*" [17][19][20]. Figure 2.1 shows a number of objects with thier respective size in nanoscale. To put everything in nanoscale perspective, a tennis ball and a typical full stop are about 1 billion and 1 million nanometres respectively.

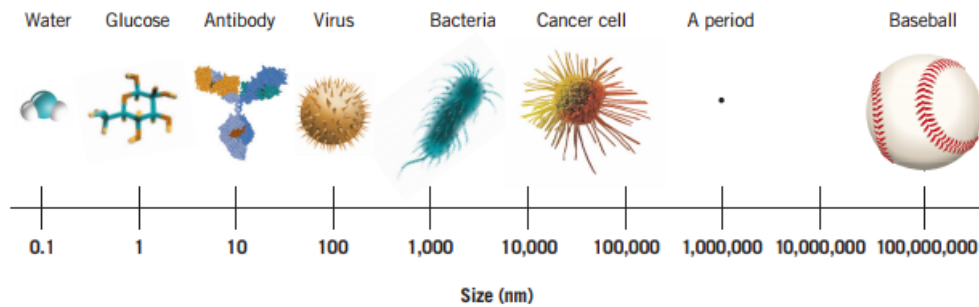


Figure 2.1: Size comparison of objects at the nanoscale level[19].

Nanotechnology can be defined in many different ways, searching for the definition in Google about 729 000 results appear in 0,56 seconds. However, all definitions have a common component, which is "*the art of manipulating materials smaller than 100 nanometres*". So there is no proper definition for nanotechnology. The National Nanotechnology Initiative(NNI) defines nanotechnology as follows [21]:

- Research and technology development at the atomic, molecular, or macromolecular levels, at a length scale of approximately 1 to 100 nanometers (a nanometer is one-billionth of a meter, too small to be seen with a conventional laboratory microscope);
- Creation and use of structures, devices, and systems that have novel properties and functions because of their small and/or intermediate size, at the level of atoms and molecules;
- Ability for atomic-scale control or manipulation

historically speaking, the idea of manipulating very small-scale building blocks and using their properties to construct working structures dates back as far as the 4th century when colloidal gold and silver nanoparticles were used to construct the Lycurgus Cup, shown in Figure 2.2, to make it look opaque green when lit from outside but translucent red when light shines through the inside [22][23].



Figure 2.2: The Lycurgus Cup at the British Museum, lit from the outside (A) and from the inside (B) [23].

However, many of these ideas were set for the first time during Dr. Richard Feynman's classic lecture, "*There's plenty of room at the bottom*", which was given on December 29 in 1959 at the annual meeting of the American Physical Society at Caltech [22]. This lecture has been attributed with triggering the nanotechnology revolution.

The term "*nanotechnology*" was later invented by Professor Norio Taniguchi at the Tokyo Science University in which he introduced the word in a paper in 1974 [17]. Eric Drexler theoretically worked on molecular nanotechnology at Massachusetts Institute of Technology in the year 1977, practical work was not possible as he could not probe and see down to the nanometre scale [24]. In 1981 Gerd Binnig and Heinrich Rohrer overcame the difficulty experienced by Eric Drexler. They developed the Scanning Tunelling Microscope (STM) for

the first time at IBM which made it possible for the scientists to see nanoscale particles. In 1989 the IBM Computer manufacturing company spelled I-B-M as seen on Figure 2.3.

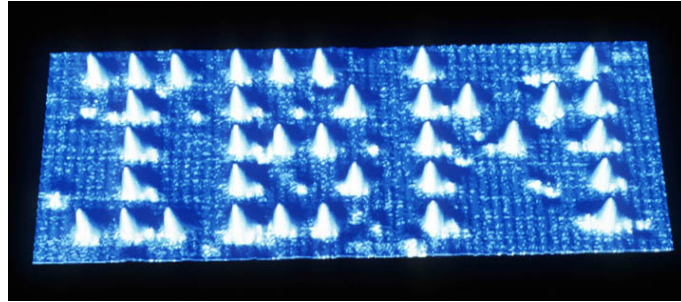


Figure 2.3: IBM acronym spelled with atoms at nanoscale[17].

Nanotechnology based research had major breakthroughs occurred over the years, including the synthesis of carbon nanotubes (CNT) and the appearing of consumer products in the marketplace, which employ nanotechnology.

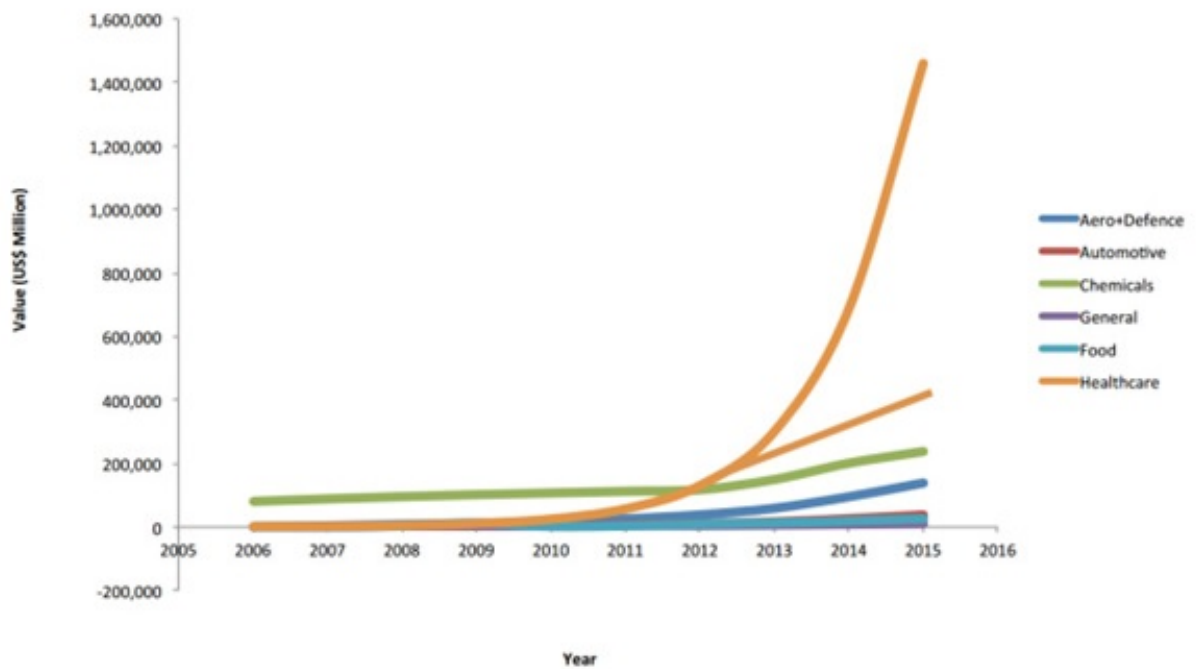


Figure 2.4: Nanotechnology market growth between the years 2005 and 2015[25].

The use of nanotechnology in the health care field has attracted tremendous attention in the past few years[25] as shown in Figure 2.4. Employing nanotechnology has allowed us to make use of novel nanomaterials for use in point of care bioassay applications, which represent a rapidly evolving field. Various nanostructures have been investigated to determine their properties and possible applications in biosensors. Employing nanomaterials in biosensors allows the use of new signal transduction techniques [26]. Nanostructures are the fundamental building blocks and are discussed next.

### 2.1.1 Nanostructures

**What are nanostructures?** The interest in nanotechnology research has increased rapidly over the past few years. Nanotechnology has made it possible to probe and arrange atoms in nanoscale to manufacture nanostructures. Nanostructures are defined as any structures having at least one of its dimension smaller than 100 nm[27][20]. Thus, the material need to be so tiny such that it is not visible to the naked eye. Nanostructures can be classified into four categories based on their dimensions; zero-dimensional(0D), one-dimensional(1D), two-dimensional(2D) and three-dimensional(3D) nanostructures[28]. Figure 2.5 shows the schematic the types of nanocrystalline material.

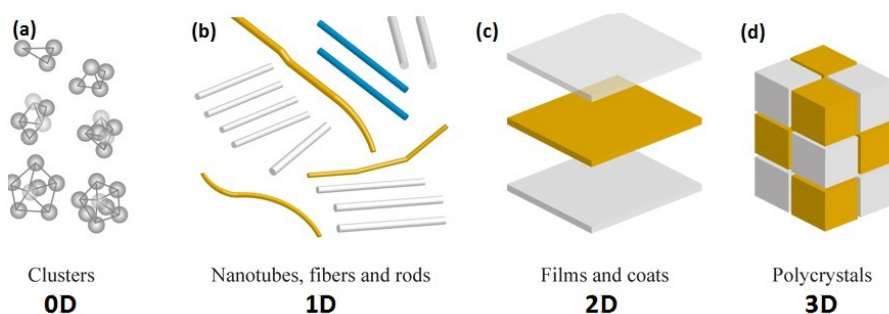


Figure 2.5: A schematic diagram of the types of nanocrystalline materials categorized by the dimensions of their structural elements: (A) zero-dimensional clusters; (B) one-dimensional tubes; (C) two-dimensional films; (D) three-dimensional polycrystals[28].

Zero dimensional(0D) nanostructures are materials where all the dimensions are within the nanoscale range. Examples of such material include the quantum dots, isolated nanoparticles etc. 1D nanostructures refers to materials that have one of their dimensions outside the nanoscale. These types of material are usually wool or needle like structures, such as nanowires, nanorods, nanobelts etc.

In the 2D nanostructure material, two of the dimensions are not in the range of nanoscale. This means that, the two dimensions are basically bigger(macro scale)

than the nanoscale (e.g. films with nanometer thickness). Moreover, 2D nanostructures have not attracted tremendous interest only for their basic understanding of the mechanism of nanostructure growth, but also for investigation and developing novel sensors devices[20]. 3D nanostructures refer to the bulk materials that are outside of the nanoscale in any dimension. Meaning, these materials have all their dimensions above the 100 nm scale.

Nanostructures are sensitive to different environmental or biological parameters. They offer great potential for numerous biomedical applications such as monitoring, diagnoses, repair and treatment of human biological systems[29]. These nanostructures can be fabricated using various methods and functionalized using biomolecules to detect or monitor a specific disease. For instance, nanoparticles can be employed for drug-delivery to treat TB, where drug molecules can be incorporated on the nanoparticle surface[30]. The nanoparticle performance can be tuned to control the rate of drug release and particle decomposition by altering the size and surface functionalization of such nanoparticle[31].

Zinc Oxide nanomaterial have many advantages concerning its optical, physical and chemical properties, which make it suitable for novel nanodevice and biosensor fabrication[31]. These 1D nanostructures have been widely studied due to their high performance in electronic, photonic, optoelectronic, electrochemical and electromechanical devices. Moreover, they are very useful nanostructures for investigating the dependence of electrical and mechanical properties. ZnO nanostructures have attracted tremendous interest in the biosensor field due to advantages such as nontoxicity, biocompatibility, biosafety, high electron transfer rates and easy binding with biomaterial/ligands. ZnO nanostructures are good for immobilizing proteins or DNA with high stability[32]. Deon et al.[16] have constructed biosensor, to detect lysozyme, based on aligned vertical ZnO nanowire arrays grown on a Silicon substrate. The working principle of the biosensor was the molecular weight detection. On the other hand, Choi et al[33] have successfully demonstrated the fabrication of ZnO nanowire field effect transistor (FET) based biosensor for the detection of biomolecular interaction. This project presents the application of nanostructures ( i.e ZnO nanowires). The ZnO nanowires will be fabricated and functionalized with streptavidin-biotin molecules on which the capture probe will be immobilized. Nanotechnology plays a huge role in this project. The project employs the use of ZnO nanowires that are fabricated to manufacture a nanosensors (i.e 2D nanostructure). ZnO nanomaterials is chosen due to its crystal structural properties which allows the nanomaterials to exhibit the piezoelectric effect. Without much effort, ZnONW can be grown in many different nanoscale forms, therefore allowing different devices to be developed. Moreover, ZnONWs are one of the most important semiconductor nanomaterials for fabricating sensors owing to their 1D nanostructure, high thermal and mechanical stability[34]. The principle of piezoelectricity is discussed next.

### 2.1.2 Piezoelectricity

The term "*piezoelectricity*" refers to the electric charge that accumulates in certain solid materials due to an applied mechanical stress or force. There are two piezoelectric effects: direct effect and converse effect. Piezoelectricity is generated through the direct piezoelectric effect. The direct piezoelectric effect can be defined as the generation of electric charge by the bending of certain crystal and ceramic materials. The inverse piezoelectric effect involves the deformation of these material due to an applied voltage. In simple words, when a voltage is applied to apiezoelectric material, the material undergoes deformation. Both the direct and inverse piezoelectric effects are shown in Figure 2.6. Table 2.1 shows piezoelectric materials which can be natural or man-made.

Natural	Synthetic
Quartz	Lead Zirconate Titanate(PZT)
Rochelle Salts	Zinc Oxide(ZnO)
Topaz	Barium Titanate( $\text{BaTiO}_3$ )
Silk	Aluminium Nitride (AlN)
Dentin	Silicon Oxide ( $\text{SiO}_2$ )
Tendon	Lithium Niobate( $\text{LiNbO}_3$ )

Table 2.1: List of man made and naturally occuring piezoelectric material.

Historically, piezoelectric ceramic materials were first discovered by the French physicists Pierre and Jacques Curie in the year 1880. A year after, more than 20 natural crystals which exhibit the piezoelectric effect were found. During the period of WWI, a book by Viogt, titled "*LerbuchderKristallphysik*", was published and it was used as the standard reference for piezoelectric materials. The word *piezo* is derived from ancient greek word "*piezein*" and it means to "*press*" or "*squeeze*" [35, 17]. Piezoelectric materials were not extensively used until the First World War. During this era thin quartz crystals were used as resonators for ultrasound sources in SOUNd Navigation And Ranging (SONAR) to detect submarines. During the Second World War, certain ceramic materials were discovered to have dielectric constants up to 100 times higher than common cut crystals. This led to the development of man-made materials with their piezoelectric properties 100 times higher than those of natural materials. during this period, the Americans advanced to the following developments:

- Development of the barium titanate( $\text{BaTiO}_3$ ) piezo-ceramics[36];
- Development of an understanding of the crystal structures and the electro-mechanical principle[36];

- and the development of extrinsic materials to achieve desired properties, e.g. piezoelectricity[17][36].

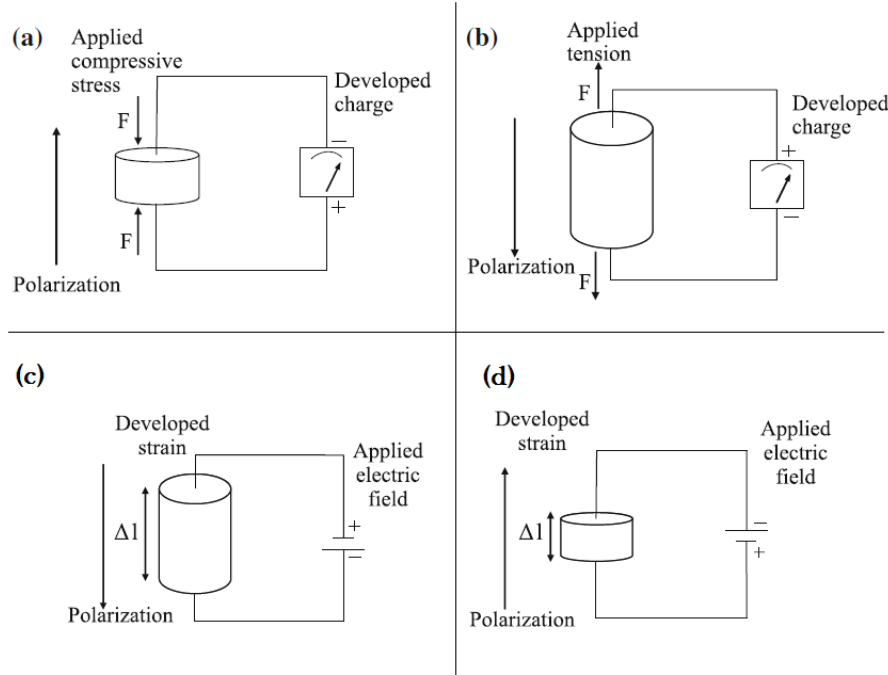


Figure 2.6: A schematic diagram showing both direct and inverse piezoelectric effects respectively. Direct piezoelectric effect:(a) at applied compressive force, (b) at applied tensile force. Inverse piezoelectric effect:(c) at applied positive voltage and (d) at applied negative voltage Both (c) and (d) are the same in terms of length change due to internal polarization as well as the reversed external voltage[36].

### 2.1.2.1 Piezoelectric effect in ZnO

ZnO nanostructures have attracted tremendous attention in recent years. Intense research by many different groups has focused on novel nanostructures with different shapes ranging from nanowires to nanobelts[37]. ZnO is a group II-VI metal oxide semiconductor material and it is known for its versatility. This nanostructures possesses anisotropic piezoelectric properties due to the fact that its structure lacks central symmetry[35]. Other ZnO nanostructure properties include:

- A higher (about 14 times) piezoelectric effect on ZnO nanostructures than that of the bulk material[17];
- Being biocompatible and environmental friendly[17];



- The power density of ZnO is estimated at  $2.7 \text{ mW/cm}^3$  which is ten times higher than for other piezoelectric materials[17].

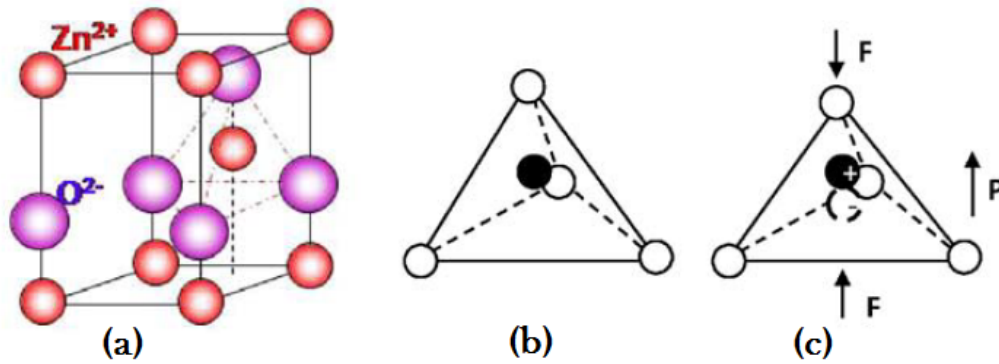


Figure 2.7: A schematic diagram of (a) a ZnO wurtzite structure, (b) tetrahedral organization between Zn and O atoms, (c) an applied force which displaces the positive charge with respect to the negative charge, resulting a potential difference in the structure[38].

Crystal Structure	Hexagonal Wurtzite
Piezoelectric Coefficient	12 pC/N
Molecular Weight	81.38
Lattice Constants (300K)	$a = 0.32469 \text{ \AA}$ , $c = 0.52069 \text{ \AA}$
Melting Point	2248 K
Density	$5.606 \text{ g/cm}^3$
Thermal Conductivity	$25 \text{ W/mK}$ at $20^\circ\text{C}$
Fusion Heat	$4.470 \text{ cal/mole}$
Band Gap	$3.37 \text{ eV}$ at room temperature
Thermal Expansion Coefficient	$4.3 \times 10^{-6}/^\circ\text{K}$ at $20^\circ\text{C}$ and $7.7 \times 10^{-6}/^\circ\text{K}$ at $600^\circ\text{C}$
Refractive Index	2.008
Lattice Energy	$964 \text{ kcal/mole}$
Exciton Binding Energy	$60 \text{ meV}$
Electron and Hole Effective Mass	$m_e^* = 0.24$ , $m_h^* = 0.59$
Dielectric Constant	$\epsilon_0 = 8.75$ , $\epsilon_\infty = 3.75$
Intrinsic Carrier Concentration	$< 10^6 \text{ cm}^{-3}$
Electron and Hole Mobility (300K)	$\mu_e = 200 \text{ cm}^2/(\text{V.s})$ , $\mu_h = 50 \text{ cm}^2/(\text{V.s})$

Table 2.2: Zinc oxide properties[35].

ZnO has a wide bandgap of approximately 3.3 eV with a large exciton binding energy of 60 meV. ZnO can be viewed to have a wurtzite crystal structure with the  $\text{Zn}^{+2}$  and  $\text{O}^{-2}$  atoms arranged in a specific order as shown in Figure 2.7. A summary of the important properties of ZnO are also given in Table 2.2. Figure 2.7(a) shows the wurtzite crystal structure of the ZnO with its anions and cations arrangement. The wurtzite structure is a hexagonal lattice and is characterised by two interconnecting sublattices of  $\text{Zn}^{2+}$  and  $\text{O}^{2-}$  atoms.

The lattice parameters of the nanomaterial crystal structure are given as follows:  $a = 0.32495 \text{ nm}$  and  $c = 0.52069 \text{ nm}$ . The tetrahedral arrangement of the ZnO atoms shows that there exist a covalent bond between the Zn and the O cations and anions respectively. This tetrahedral arrangement of the  $\text{O}^{2-}$  atoms give rise to the polar symmetry along the hexagonal axis. The

polar symmetry plays a significant role for most of the ZnO properties, such as the piezoelectric effect and the growth of different nanostructures. The ZnO wurtzite structure consist of four face terminations[17]: the polar Zn termination face  $[0001]$ , the polar O-terminated  $[000\bar{1}]$  and the two non-polar faces;  $[11\bar{2}0]$  and  $[10\bar{1}0]$  termination faces.

In Figure 2.7(b-c) shows the piezoelectric effect, in ZnO crystal structure, on the tetrahedral arrangement of the  $\text{Zn}^{2+}$  cations and  $\text{O}^{2-}$  anions. As shown, a cation is surrounded by four anions in a tetrahedral manner. The negatively charged atom are centred at the tetrahedron centre overlapping with the location of the positively charged atom. When a mechanical force is applied, the centre of gravity of the negatively charged atoms is distorted, shifting position and thus generating a pair of equal and oppositely charged poles[35].

Since ZnO is piezoelectric, the nanostructures fabricated from ZnO materials are also piezoelectric. As mentioned before that the NWs are said to possess high elasticity, and hence can be bent to a large degree. The principle of piezoelectricity in NWs is discussed next.

### 2.1.3 Piezoelectricity in a single ZnO NW

The principle of piezoelectric effect on a single nanowire comes from the coupled piezoelectric and semiconducting properties of ZnO. If a vertical ZnO NW(Figure 2.8A) is deflected by an AFM tip, a strain( $\epsilon_Z$ ) field is observed. The compressed side of the NW experience negative strain while the stretched side of the NW experience a positive strain as shown in Figure 2.8B. An Electric field along the NW is then generated as results of the bending or deflection. The Electric field is given by:  $E_z = \epsilon_Z/d$ , where  $d$  is the coefficient of the piezoelectric effect along  $c$  axis and  $\epsilon_Z$  is strain in the NW[38][17]. Due to piezoelectric effect an electri voltage is observed in both the compressed( $V_s^-$ ) and stretched( $V_s^+$ ) sides of the NW(Figure 2.8D).

When the platinum(Pt) electrode is in contact and bends the nanowire, the stretched side of the NW has positive voltage( $V_s^+$ ). If there in no applied external voltage, the electrode is at potential ground( $V_m=0$ ). So this means that the metal tip-ZnO interface is negatively biased, meaning  $\Delta V = V_m - V_s^+ = -V_s^+ < 0$ . The negative  $\Delta V$  results in n-type NWs, and a Schottky contact between the NW and Pt metal tip forms. The Schottky contact is said to be reverse-biased Schottky diode(Figure 2.8E)[38][17].

The Pt electrode moves across the NW until it reaches the negatively charged side of the NW. When the electrode reaches the negatively charged NW side, it has accumulated enough voltage( $V_m \neq 0$ ). In this instant,  $V_m > V_s^-$ , so this means that  $\Delta V = V_m - V_s^+ > 0$ . With  $\Delta V > 0$  means that the Pt metal-semiconductor interface is biased in a positive direction and a positive biased Schottky diode forms as shown in Figure 2.8F. A positive biased Schottky contact causes a gradual increase in current (I-V characteristic insert). The magnitudes of the voltages,  $V_s^+$  and  $V_s^-$ , will drop due to the

ionic charges being neutralised. The load voltage across the resistor,  $V_L$ , will drop according with  $V_s^+$  and  $V_s^-$  to zero after the neutralization the ionic charges[38][17].

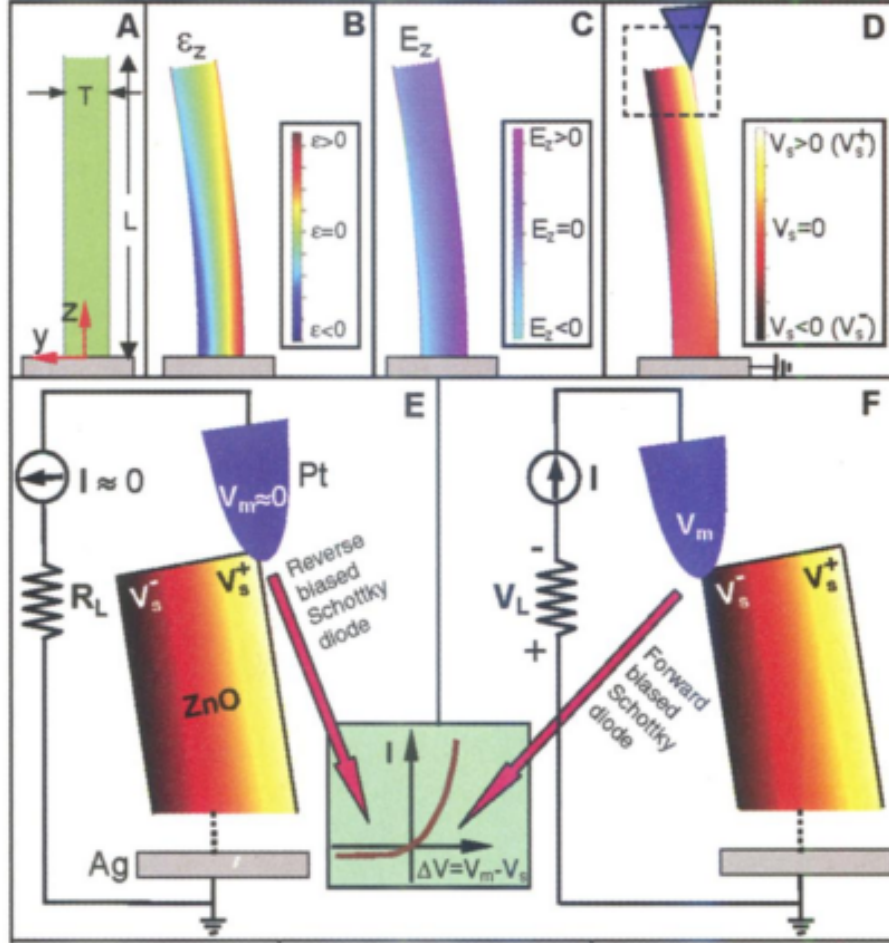


Figure 2.8: (A) schematic diagram of a NW governed by a set of axis, (B) longitudinal strain( $\epsilon_z$ ) distribution in the NW after deflected by an AFM tip, (C) induced electric field( $E_z$ ) in the NW due to deflection, (D) voltage distribution due to the piezoelectric effect, (E and F) the contact between the AFM tip and the NW with the I-V insert showing the forward and reverse Schottky diode[38][17].

### 2.1.4 Governing Equations

The relationship between the nanoforce and the generated voltage in piezoelectric NWs can be derived. Authors [17, 39] and [36] fully describe the steps taken to derive this relationship. Both authors start with the following two constitutive equations for piezoelectricity:

$$\sigma_p = C_{pq}\epsilon_q - e_{kp}E_k \quad (2.1.1)$$

$$D_i = e_{iq}\epsilon_q + \kappa_{ik}E_k \quad (2.1.2)$$

where each term is defined as follows:

- $\sigma_P$  is the stress tensor, which is related to strain  $\epsilon_q$ [39, 36].
- $E_k$  is the electric field[39, 36].
- $D_i$  the electric displacement[39, 36].
- $e_{kp}$  is the linear piezoelectric coefficient[39, 36].
- $\kappa_{ik}$  is the dielectric constant[39, 36].

These two equations can be solved by employing the perturbation theory. In this case the perturbation theory is used to simplify the equations in order to approximate a model that describes the output voltage of a single ZnO nanowire due to an external mechanical force or strain. The aim of deriving these equations is to roughly understand how is the piezoelectric potential generated due to an external stress. A state of zero external force is described by equation(2.1.3), while equation (2.1.4) describe a state of zero net electric charge or free charge[39].

$$\nabla \cdot \sigma = 0 \quad (2.1.3)$$

$$\nabla \cdot \vec{D} = \rho_e^{(b)} = 0 \quad (2.1.4)$$

Equation 2.1.5 is a geometrical constraint that must be satisfied by all means [39] and 2.1.4 assumes that there is no free charge in the NW which applies to insulator piezoelectric materials[40];

$$e_{ilm}e_{jpq}\frac{\partial^2 \epsilon_{mp}}{\partial x_l \partial x_q} = 0 \quad (2.1.5)$$

by considering the  $c_{6v}$  symmetry of ZnO crystal, the matrices in equations (2.1.1) and (2.1.2) can be written as follows[40]:

$$c_{pq} = \begin{bmatrix} c_{11} & c_{12} & c_{13} & 0 & 0 & 0 \\ c_{12} & c_{11} & c_{13} & 0 & 0 & 0 \\ c_{13} & c_{13} & c_{33} & 0 & 0 & 0 \\ 0 & 0 & 0 & c_{44} & 0 & 0 \\ 0 & 0 & 0 & 0 & c_{44} & 0 \\ 0 & 0 & 0 & 0 & 0 & c_{66} \end{bmatrix}$$

where  $c_{66} = \frac{c_{11}-c_{12}}{2}$ ,

$$e_{kp} = \begin{bmatrix} c_{11} & c_{12} & c_{13} & 0 & e_{15} & 0 \\ 0 & 0 & 0 & e_{15} & 0 & 0 \\ e_{31} & e_{31} & e_{33} & 0 & 0 & 0 \end{bmatrix}$$

and

$$\kappa_{ik} = \begin{bmatrix} \kappa_{11} & 0 & 0 \\ 0 & \kappa_{22} & 0 \\ 0 & 0 & \kappa_{33} \end{bmatrix} \quad (2.1.6)$$

A Book written by Wang et al.[40] titled "*Nanogenerators for Self-powered Devices and Systems*" thoroughly derives the equations that governs the piezo-electric potential generation in response to an applied force or external stress to a single NW. The aim of this section is to obtain the force-piezo-potential relationship equation without fully understanding the underlying substitution and steps to solve the equations.

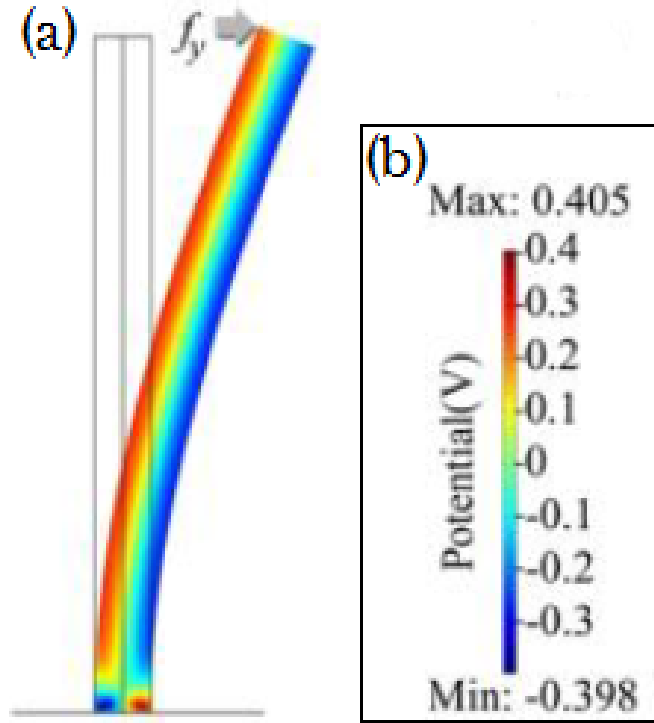


Figure 2.9: A schematic diagram of a cross section of a NW deflected by a force  $f_y$  producing a typical voltage demonstrated by the insert (b)[38].

Equations 2.1.1 and 2.1.2 can be solved by using complicated mathematical tricks. Such tricks include the perturbation theory, as mentioned before, combined with certain simplified parameters. Applying the perturbation theory, final solutions as presented in equations (2.1.7) and (2.1.8) are obtained[40][17][36]:

$$\varphi^C = \frac{1}{8\kappa_{\perp}} \frac{f_y}{I_x x E} [2(1+v)e_1 5 + 2ve_3 1 - e_3 3] \left[ \frac{\kappa_o + 3\kappa_{\perp}}{\kappa_o + \kappa_{\perp}} \frac{r}{a} - \frac{r^3}{a^3} \right] a^3 \sin \theta, r < a \quad (2.1.7)$$

$$\varphi^T = \frac{1}{8\kappa_{\perp}} \frac{f_y}{I_x x E} [2(1+v)e_1 5 + 2ve_3 1 - e_3 3] \left[ \frac{2\kappa_{\perp}}{\kappa_o + \kappa_{\perp}} \frac{a}{r} - \frac{r^3}{a^3} \right] a^3 \sin \theta, r > a \quad (2.1.8)$$

From Equations (2.1.7) and (2.1.8), the maximum potential occur at the NW surface, where  $r = a$ . The compressive (denoted by C) side fo the NW corresponds to  $\theta = -90^\circ$  and the tensile (denoted by T) side corresponds to  $\theta = 90^\circ$ . These equations can be simplified to give:

$$\varphi_{max}^{C,T} = \pm \frac{1}{\pi \kappa_o + \kappa_{\perp}} \frac{f_y}{E} [e_3 3 - 2(1+v)e_1 5 - 2ve_3 1] \frac{1}{a} \quad (2.1.9)$$

By the definition of elementary elastic theory (for small lateral displacement), the lateral force  $f_y$  can be related to the maximum deflection of the NW tip as  $v_{max} = v|_{(z=l)}$  as shown in Figure 2.9[40, 17]:

$$v_{max} = \frac{f_y l^3}{3EI_{xx}} \quad (2.1.10)$$

and thus equation (2.1.9) solve to equation (2.1.10) given by:

$$\varphi_{max}^{C,T} = \pm \frac{3}{4(\kappa_o + \kappa_{\perp})} [e_3 3 - 2(1+v)e_1 5 - 2ve_3 1] \frac{a^3}{l^3} \quad (2.1.11)$$

This final equations means that the piezo-potential in a NW can be related via the aspect ration rather than its dimensionality [40].

### 2.1.5 ZnO Nanowires Synthesis Methods

ZnO nanostructures can be synthesized using two approaches, which is the bottom-up and top-down approach. Bottom-up approach refers to nanofabrication with chemical or physical forces operating at the nanoscale to assemble basic atomic units into larger structures. In simple words, it is an arrangement of small scale (nanoscale) components to a more complex visible body. Chemical vapour deposition method is a typical example. In contrast, top-down approach refers to nanofabrication from bulk material to nannoscale. Optical lithography and Etching have been serving as examples of such approach [17]. There numerous types of synthesis methods used to fabricate NWs. Many techniques such as the use of the metal-catalyst-assisted Vapor Liquid Solid (VLS), Vapor Phase Epitaxy, Solution Liquid Solid (SLS) and the Vapor Solid (VS) methods have been studied. Among these, this project will only discuss the VLS and hydrothermal technique because of the availability of equipment at Stellenbosch University Electrical and Electronic Nanolaboratory. This section reviews the growth of ZnO NWs by the vapour liquid solid and hydrothermal techniques.

#### 2.1.5.1 Vapour Liquid Solid Technique

The VLS mechanism is a 1D-crystal growth mechanism that is assisted by a metal catalyst (e.g. Gold (Au)). 1D crystal growth was originally developed



approximately 50 years ago in the Silicon industry and the mechanism was suggested for wider use by Wagner in 1964. This method is called the VLS because vapor (which carries solid components), liquid (the catalyst alloy), and solid (the precipitated one-dimensional structures) phases are involved [41].

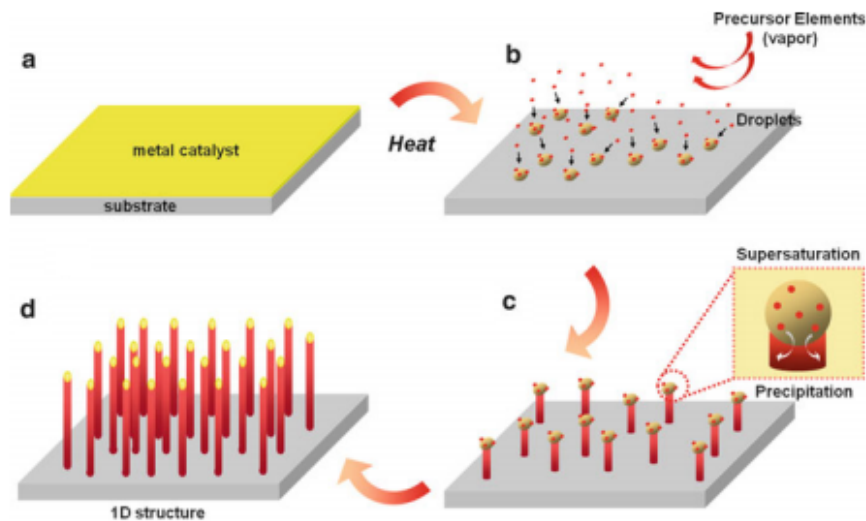


Figure 2.10: Schematic representation of the growth of ZnO nanowires by VLS mechanism[41].

In this method, a metal catalyst is sputtered onto a substrate, shown in Figure 2.10(a) then annealed at high temperatures to form liquid alloy droplets by adsorbing vapor components, shown in Figure 2.10(b). Due to temperature fluctuation, the alloy becomes a solution in which the actual concentration of the components is higher than the equilibrium concentration. It then drives the precipitation of the component at the liquid-solid interface to achieve minimum free energy of the alloy system, shown in Figure 2.10(c). Consequently, the 1D crystal growth begins, and it continues as long as the vapor components are supplied, see Figure 2.10(d). The growth takes place inside an open-ended quartz tube inside a furnace which operates at very high temperatures (e.g. 1200 °C).

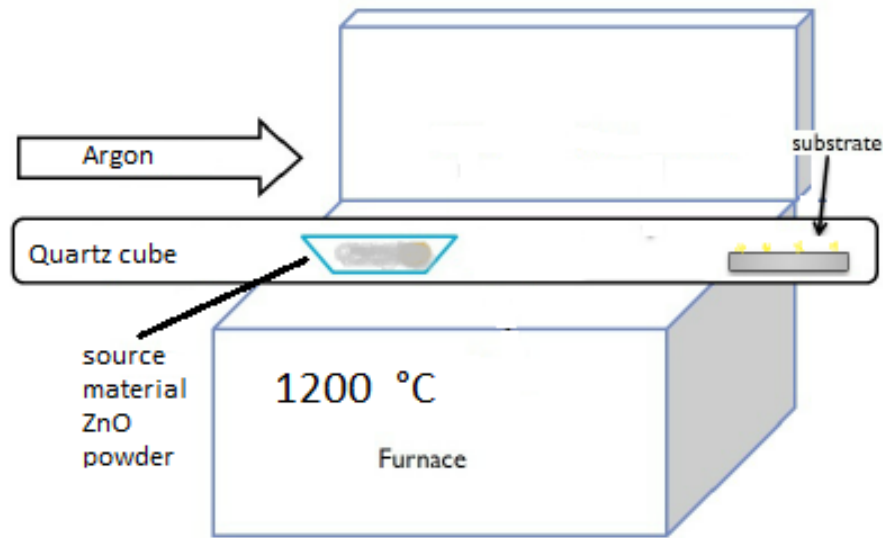
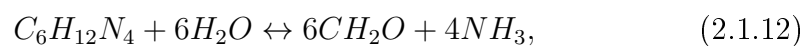


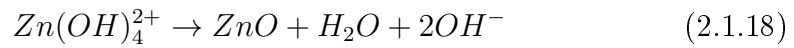
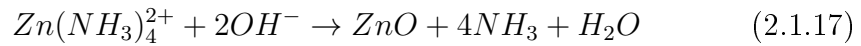
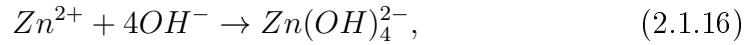
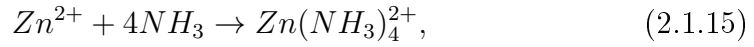
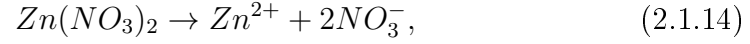
Figure 2.11: Schematic representation of the VLS setup mechanism. Showing the Argon gas flow direction, the position of the source material and the substrate[42].

For ZnO nanowire growth, the gold is annealed to form Au alloy droplets, then the source material is introduced in a ceramic boat, which is either Zn or ZnO powder, and heated up to 1200 °C causing the source material to evaporate. A carrier gas, Argon(Ar), is used to carry the evaporated source material to the sample or substrate, which are fixed far from the source material at a lower temperature as shown in Figure 2.11. The vapour then reacts with the Au droplets and initiates the growth[17].

#### 2.1.5.2 Hydrothermal Technique

Hydrothermal method is one of the widely used synthesis method for fabricating 1D metal oxide nanostructures. 1D metal oxide nanostructures can be easily prepared by solution based fabrication as compared to other methods. The hydrothermal method opens up a rich variety of precursors and solvents. The growth takes place in an aqueous solution containing metal ions and an oxidizing agent at a specific low temperature [43]. The aqueous solution is prepared by mixing  $C_6H_{12}N_4$  (Hexamethylenetetramine) and  $Zn(NO_3)_2 \cdot 6H_2O$  (zinc nitrate hexahydrate) in deionized (DI) water. The solution is clear with some white particles,  $Zn(OH)_2$  distributed throughout the volume. The reactions in the solution are described as follows[17]:





The solution contains oxides that facilitates the growth of 1D nanostructures along a certain axis, for instance ZnO NWs have been successfully grown from basic strong solutions[43]. The resulting ZnO (in Eq. 2.1.18) originates from zinc salts that dissolve in DI-water. The nanowire growth takes place in two stages. The first stage is the creation of nucleation sites, as shown in Figure 2.12(a), caused when the zinc salts initially dissolve in water. The NWs start to grow where the nucleation sites formed and these sites determine the diameter of the NWs.

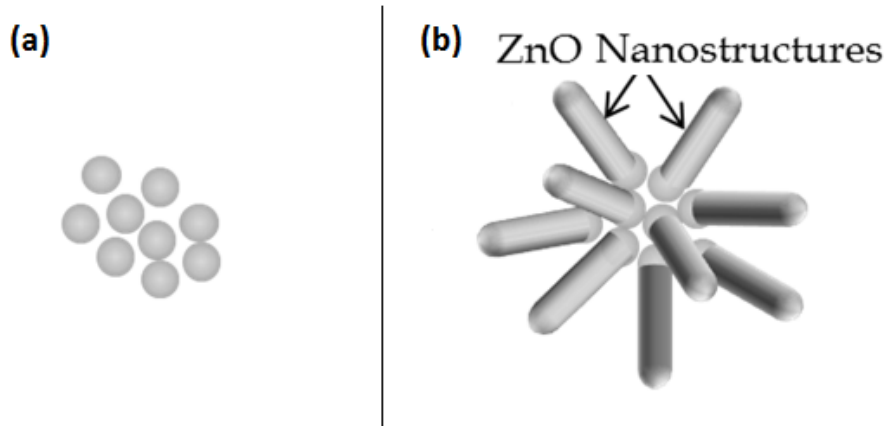


Figure 2.12: Schematic representation of the (a) formation of nucleation sites and (b) the growth of ZnO nanostructures (top view) from the nucleation sites in aqueous solutions.[44].

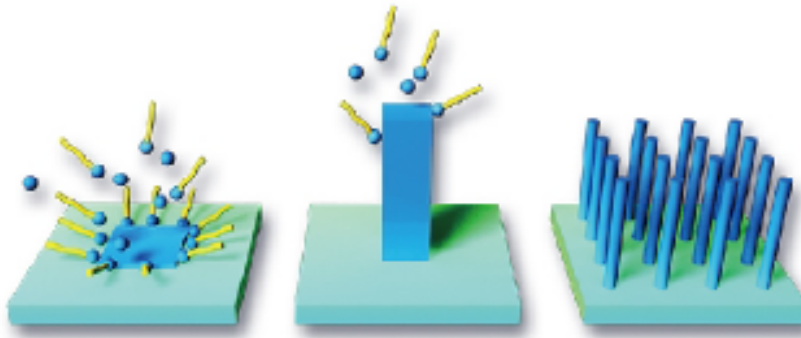


Figure 2.13: Schematic representation showing the zinc metals in the solution and oxygen from the water being attracted to the nucleation sites and form layers, which stack up to form the ZnO nanowires in an aqueous solution[43].

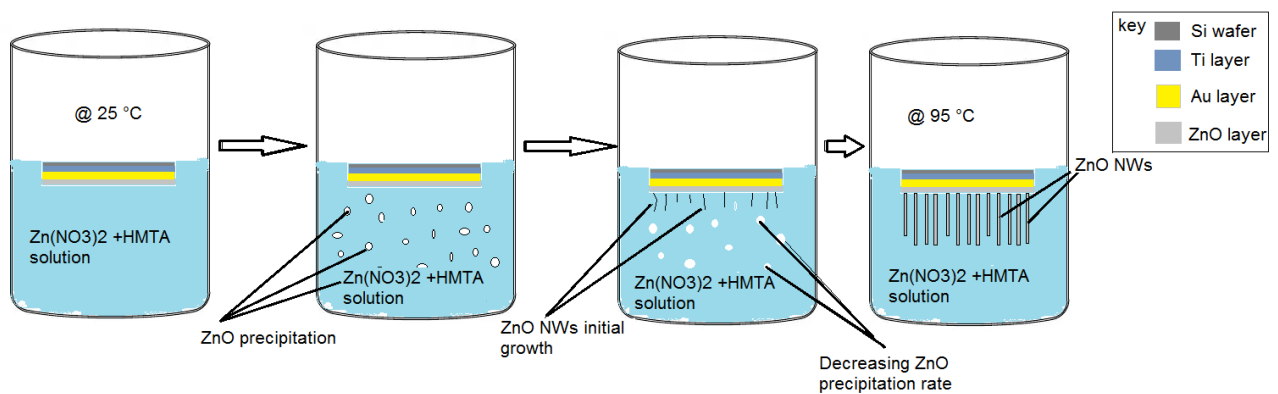


Figure 2.14: Schematic drawing to explain the hydrothermal method used to grow ZnO NWs. Schematic representation showing the zinc metals in the solution and oxygen from the water being attracted to the nucleation sites and form layers, which stack up to form the ZnO nanowires in an aqueous solution.

In simple words, the zinc solution molecular mass determines the size of the nucleation sites; the higher the molecular mass, the bigger the diameter of the NWs. The second stage is the growth of the NWs from the successfully formed nucleation sites as shown in Figure 2.12(b). The zinc metals in the solution and oxygen from the water are attracted to the nucleation sites and form layers, which stack up to form the ZnO nanowires as shown in figure Figure 2.13. The pH of the aqueous solution plays an important role in the NWs growth. HMTA is an additive that is added to modify the pH of the solution[17][44]. In general,

the hydrothermal method is one of the most highly flexible and adaptable for NW synthesis. The growth takes place in very low temperatures, it is simple, less hazardous and the costs are very low.

## 2.1.6 Piezoelectric Devices

### 2.1.6.1 Nanopiezotronics

Nanopiezotronics studies is very new in the field of nanotechnology. Nanopiezotronics was first introduced by Prof. Z.L Wang in 2006 at Georgia Institute of Technology [39]. Nanopiezotronics make use of the coupled semiconducting and piezoelectric properties of nanowires for fabricating novel electronic devices such as the Piezoelectric Field Effect Transistor shown in Figure 2.15 [45][39]. Nanopiezotronics applications stretches from Piezoelectric Diodes to nanogenerators.

#### Piezoelectric-FET

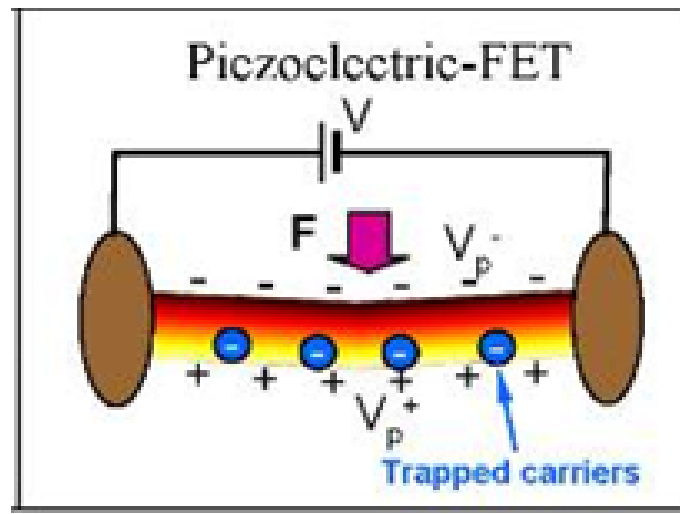


Figure 2.15: Schematic diagram of a typical PE-FET nanodevice based on a single nanowire. When an external nanoforce( $F$ ) is applied on the single nanowire connected between two electrodes, a proportional voltage( $V_p$ ) can be measured[39].

FETs based on nanowires are one of the most studied nanodevices. A typical NW FET is composed of a semiconducting NW that is connected by two electrodes at each end and normally placed on a silicon substrate. The Piezo Electric-FET can be switched on by applying mechanical force to bend the NW. The force is in the nano-newton range and even smaller[46].

### Piezoelectric-Gated Diode

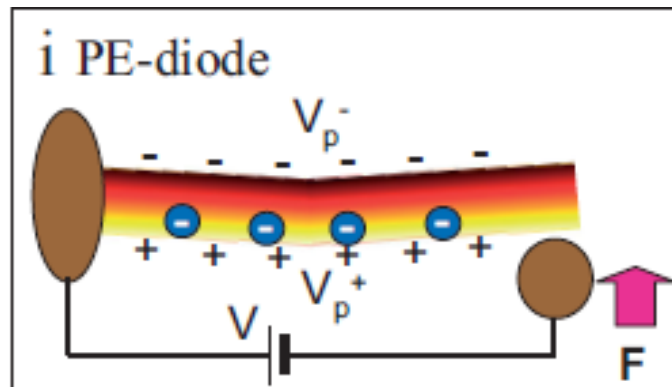


Figure 2.16: Schematic diagram of a typical PE-diode nanodevice based on a single nanowire. The single nanowire is held stationary by one probe and while the other is exerting force ( $F$ ) to end the NW to produce a voltage ( $V_p$ ) which can be measured[46].

The piezoelectric-gated diode, shown in Figure 2.16, works in the same principle as the piezoelectric-FET and uses the two probe technique. However, there is only one difference in the set up, the PE-diode has only one probe that is in contact with the bent nanowire. One of the probes holds the nanowire stationary while the other bends the nanowire from the stretched side. The piezoelectric FETs and diodes are outstanding examples of piezoelectric devices fabricated using NWs. Based on the electromechanical coupled properties of the nanostructures, novel and unique applications will be explored in areas of sensors, actuators, switches, and nanoelectrochemical systems (NEMS) [46].

## 2.2 Nucleic Acid Probe Immobilisation Techniques

Immobilization procedure is very crucial particularly for the sensitivity and selectivity of the biochemical reactions. The support (i.e. transducer) on which the biological material will be immobilized plays a huge role as a reaction medium for biochemical reaction. There are three types of immobilisation techniques for nucleic acids: (i) physical adsorption immobilisation, (ii) streptavidin-biotin immobilisation and (iii) covalent immobilisation [47]. The choice of the immobilisation technique is determined by the biocomponent to be immobilized, the nature of the transducer and the transduction mechanism. The following aspects need to be considered in order to select the type of immobilisation to employ [48]:

- the activity and stability of the biomolecule must be conserved;
- the selectivity of the biomolecule must remain unchanged;
- the method of immobilisation must be consistent and reliable.

The three types of immobilisation techniques for nucleic acids are discussed next.

### 2.2.1 Physical Adsorption

Physical immobilisation is preferred as compared to chemical immobilisation due to the fact that there are no structural modifications required for the single-side nucleic acids(ssNA) and the transducer [48]. This type of immobilisation technique has been reported to be based on ionic interface occurring between the negatively charged phosphate backbone of the ssNA probe and positive charges covering the surface as shown in Figure 2.17. The resulting layer is likely to be heterogeneous and randomly oriented, since each molecule can form many contacts in different orientations to minimize repulsive interactions with the substrate[16].

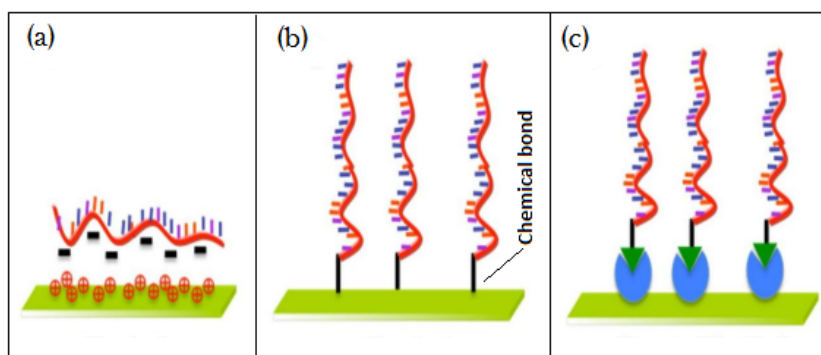


Figure 2.17: Schematic diagram showing the immobilisation techniques: (a) Physical adsorption (b) Covalent binding and (c) Streptavidin-Biotin Immobilization [47].

Physical Adsorption is very simple, fast and suitable for ssDNA, ssRNA and ssPNA immobilisation. However, there are limitations of random orientation, crowding effect and weak attachment of nucleic acid probes to the transducer or substrate. Due to the weak probe binding, some buffers when performing the assays can wash-away the nucleic acid probes [47].

## 2.2.2 Covalent Immobilization

A covalent bond occurs by a sharing of electrons between two atoms. Covalent bonding exploits the phenomenon of chemical bond formation between the sensing molecule and the transducer as shown in Figure (b) [49]. Covalent attachment belongs to the chemical immobilisation class. The covalent immobilisation method involves chemical alteration of the surface (i.e. transducer) when fabricating microarrays. The surface is usually modified to either nucleophilic or electrophilic functionalities which then react with the amine or carboxylated nucleic acid probes. Table 2.3 summarizes the functional groups which are used to modify surfaces for different covalent chemistries with their advantages and disadvantages [47].

Surface Function	Interaction or Reaction	Advantages	Drawbacks
Carboxyl (EDC coupling)	Chemical bonding with amine-DNA	- Simple method of immobilization	- Efficiency of immobilization depends on pH, concentration, ionic strength, and reaction time.
		- High surface coverage of DNA's	
		- Easy coupling reaction	
Aldehyde	Chemical bonding with amine-DNA	- Good stability	- Long hybridization time
		- High binding strength	- Limits the absolute signal intensity
		- Stable enough for long term use	- High hybridization temperature
		- Less random immobilization	
Epoxy	Chemical bonding with hydroxyl, amine and sulfhydryl groups	- Easy protocol for immobilization	- Reactions between DNA and epoxy supports are extremely slow.
		- Good stability	- Low Immobilization density
		- High binding strength	
		- Stable enough for long term use	
Isothiocyanate	Chemical bonding amine-DNA	- Well-ordered surface	- High non-specific hybridizations
		- Re-usability	- Long hybridization time
		- High density DNA/area	
		- Stable enough for long term use	
Maleimide	Chemical bonding with sulfhydryl group of DNA	- Faster immobilization reaction	- Degradation in aqueous solutions
		- Good stability.	- High non-specific interaction
		- Re-usability	
		- High binding strength	
Mercaptosilane	Chemical bonding DNA-SH	- Good stability	- High non-specific interaction
		- Re-usability	- High hybridization temperature
		- High binding strength	
		- Stable enough for long term use	

Table 2.3: The functional groups which are used to modify surfaces for different covalent chemistries with their advantages and disadvantages[47].

The thiol-metal interactions are commonly used for immobilisation of nucleic acids by covalent attachment on Au surfaces. The thiol groups prove to possess a strong affinity towards the metal surfaces allowing the formation of covalent bonds between the sulfur and gold molecules . In this case, the single-strand nucleic acids have to be modified using thiol [50]. Covalent bonding immobilisation technique has longer life span as compared to physical adsorption due to very strong bonds forming between the molecule and the substrate. Factors



like pH and ionic strength affect the covalent bonds. However, the process is very complex and time consuming, and may involve dangerous chemicals [49].

### 2.2.3 Bio-affinity Immobilization

Streptavidin-Biotin attachment is a type of bio-affinity immobilisation. Avidin is a 66-kDa glycoprotein comprising of four polypeptides that are interlinked with carbohydrates by glycosidic bonds. Avidin known as a protein with a quaternary structure of four subunits that forms a highly specific site for biotin, a 244-kilo Dalton (kDa) water-soluble vitamin H. Streptavidin is a 60-kDa, extracted from *Streptomyces avidinii*, which contains no glycosidic bonds. The Avidin-Biotin bond is one of the known strongest non-covalent bonds in the field of biology [51]. The absorption of Streptavidin on substrates is based on the formation of electrostatic interactions and hydrogen bonds, Van der Waals and hydrophobic interactions. The Streptavidin-biotin layer serves as an immobilizer for the nucleic acid probe to the transducer. The interaction between streptavidin and biotin causes the single stranded nucleic acid to assume position at the affine layer as shown in Figure 2.18 and Figure 2.17(c). The streptavidin-biotin interaction is frequently used to fabricate DNA microarrays.

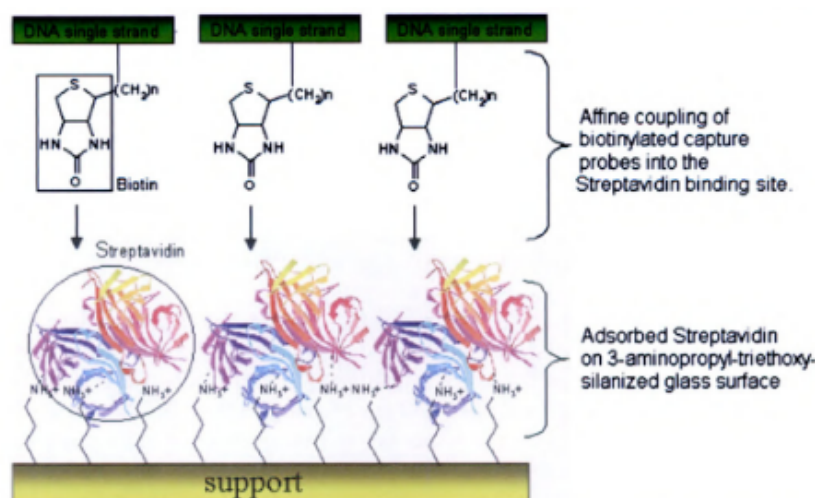


Figure 2.18: Schematic diagram showing the Streptavidin-Biotin immobilisation technique with a nucleic acid probe at the affine layer[51].

This type of immobilisation strategy is reasonably popular because it can be used for any biotinylated probe. But then again, it is very expensive due to the amount of Avidin needed to cover the transducer surface. Moreover, the synthesis of streptavidin-immobilized surfaces involves numerous steps, these include artificial surface modification, streptavidin immobilisation, and

use of blocking agents. Each step increases the production time and cost. Furthermore, streptavidin immobilisation on the surface have disadvantages like the immobilized proteins instability and non-specific interactions, hence the low sensitivity and specificity [47].

## 2.3 Self-Assembled Monolayers of Thiols on Metals as a part of Nanotechnology

Self-assembly is a process that implicates the spontaneous formation and arrangement of pre-existing atoms or a group of atoms bonded together in an ordered functional assembly. SAMs are themselves categorized as nanostructures because of their thickness ranging in the nanometer-scale. SAMs come with numerous useful properties and applications. Table.2.4 shows some of the functional headgroups and substrates used in forming SAMs on metals, oxides, and semiconductors. A typical example of how SAMs are formed is illustrated in Fig.2.19. The formation of SAMs is the most ingenious, flexible and simple way of creating thick organic films on which the biomolecules could be immobilized without. SAMs provide a protective thick layer between a metal and the immobilized biomolecule (i.e oligopeptides, nucleic acids, and proteins), the layer protects the biomolecules from degradation due to metal-biomolecule contact. The degradation processes may alter the molecular integrity and reduce its functionality [52]. SAMs can fabricated from both gaseous and solution phase methods.

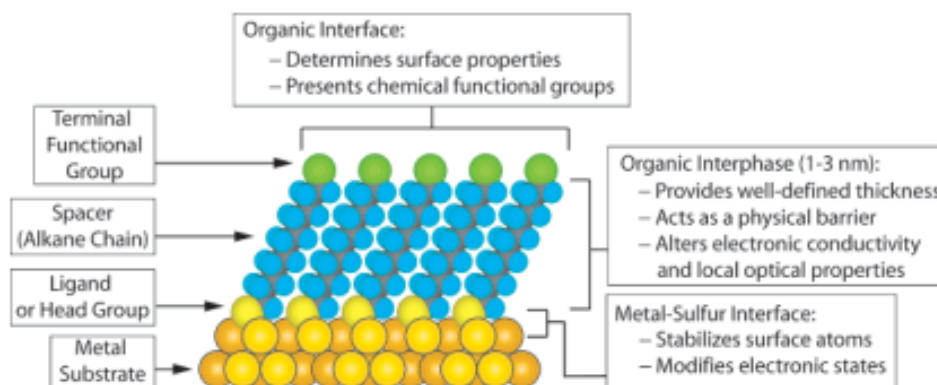


Figure 2.19: A typical building blocks of SAMs. Showing the terminal functional group, alkane chain, functional headgroup and the gold substrate. The formation of SAMs starts from the functional headgroup on the substrate to the terminal functional group[52]

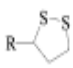


Ligand	Substrates	Morphology of Substrate		Ligand	Substrates	Morphology of Substrate	
		Thin Films or Bulk Material	Nanoparticles or Other Nanostructures			Thin Films or Bulk Material	Nanoparticles or Other Nanostructures
ROH	Fe <sub>2</sub> O <sub>3</sub>		35	RSSR'	Ag	89	90
	Si-H	36			Au	20	90-92
RCOO-/RCOOH	Si	37			CdS		61
	α-Al <sub>2</sub> O <sub>3</sub>	38,39			Pd	30	
	Fe <sub>2</sub> O <sub>3</sub>		40		Au	93	
	Ni		41,42				
RCOO-OOCR	Ti/TiO <sub>2</sub>	43		RCSSH	Au	94	
	Si(111):H	44			CdSe		95
Ene-diol	Si(100):H			RS <sub>2</sub> O <sub>3</sub> /Na <sup>+</sup>	Au	96	98
	Fe <sub>2</sub> O <sub>3</sub>		45		Cu	97	
RNH <sub>2</sub>	FeS <sub>2</sub>	46		RSeH	Ag	99	
	Mica	47			Au	100,101	
	Stainless Steel 316L	48			CdS		60
	YBa <sub>2</sub> Cu <sub>3</sub> O <sub>7-δ</sub>	49		RSeSeR'	CdSe		102
RC≡N	CdSe		50		Au	101	
	Ag	51		R <sub>3</sub> P	Au		103
R-N≡N <sup>+</sup> (BF <sub>4</sub> <sup>-</sup> )	Au				FeS <sub>2</sub>	46	
	GaAs(100)	52			CdS		104
	Pd	52			CdSe		104
RSH	Si(111):H	52		R <sub>3</sub> P=O	CdTe		104
	Ag	26	53,54		Co		105,106
R 	Ag <sub>90</sub> Ni <sub>10</sub>	55			CdS		104
	AgS		56		CdSe		104
	Au	26	57		CdTe		104
	AuAg		58	RPO <sub>3</sub> <sup>2-</sup> /RP(O)(OH) <sub>2</sub>	Al	107	
	AuCu		58		Al-OH	108	
	Au <sub>3</sub> Pd <sub>1-x</sub>		58		Ca <sub>10</sub> (PO <sub>4</sub> CO <sub>3</sub> ) <sub>6</sub> (OH) <sub>2</sub>	109	
	CdTe		59		GaAs	110	
	CdSe		60	RPO <sub>4</sub> <sup>2-</sup>	GaN	110	
	CdS		61,62		Indium tin oxide	111	
	Cu	26	58		(ITO)		
	FePt		63-66		Mica	112	
	GaAs	67			TiO <sub>2</sub>	113,114	
	Ge	68			ZrO <sub>2</sub>	114,115	
	Hg	69-71			CdSe		116-118
	HgTe		72		CdTe		118,119
	InP	73			Al <sub>2</sub> O <sub>3</sub>	120	
	Ir		74		Nb <sub>2</sub> O <sub>5</sub>	120	
	Ni	75			Ta <sub>2</sub> O <sub>5</sub>	121	
	PbS		76-78		TiO <sub>2</sub>	120,122	
	Pd	30	74,79	RN≡C	Pt	123	124
	PdAg		58		Si	37	
	Pt	32	80	RHC=CH <sub>2</sub>	Si(111):H	125	
	Ru		81				
	Stainless Steel 316L	48		RC≡CH			
	YBa <sub>2</sub> Cu <sub>3</sub> O <sub>7-δ</sub>	82					
	Zn	83		RSEX <sub>3</sub> X = H, Cl, OCH <sub>2</sub> CH <sub>3</sub>	HfO <sub>2</sub>	126	
	ZnSe	84			ITO	127	
	ZnS		85		PtO	128	
					TiO <sub>2</sub>	113,126,129	
RSAc	Au	86			ZrO <sub>2</sub>	126,129	
R 	Au		87				
RSSR'	Au	88					

Table 2.4: Combinations of Headgroups and Substrates Used in Forming SAMs on Metals, Oxides, and Semiconductors[52].

The formation of SAMs takes place in two processes; (i) a fast process of absorption, followed by (ii) a slower process of monolayer organization. Thiolates, the headgroup, adsorb spontaneously onto the metal surfaces (i.e. Au, silver, Pt etc). Au forms the standard frequently used substrate, because (1) Au forms good SAMs and (2) it is historically the most studied. After the adsorption of the headgroup, the alkyl group forms resulting in the formation of densely packed and highly ordered monolayers. As more molecules absorb to the surface, the molecules form a 3D crystalline structure on the metal surface. The forces known as the Van der Waals forces between the alkyl chains enhance the stability and the order of the SAMs. The formation of SAMs has to take place on a very smooth surface because the roughness of the surface influences the orientation of the SAMs. Long alkanethiols produce more uniform and ordered SAMs hence the requirement for smooth surface.

## 2.4 Factors affecting SAMs

There are several factors that need to be controlled during the fabrication of SAMs employing the solution phase technique, which is the most common technique for preparing SAMs on gold, silver, palladium, mercury, and other materials. These factors include how clean is the substrate, type of solvent used during the process of assembly, the incubation temperature, the immersion time, chain length and surface roughness.

**Cleanliness.** Cleanliness and crystallinity of the substrate plays an important role in determining the compactness of the monolayers, as bare metal tends to absorb organic substances which results in monolayer defects. For smoother and clean substrates, the density of defects are lower due to fewer grain impurities on the surface, step edges and other surface features that are known to cause defects in SAMs.

**Solvents.** Various solvents can be used for SAM formation. However, ethanol is the most widely used solvent for preparing SAMs. There are at least four other factors that contributed to the widespread use of ethanol: it dissolves a variety of alkanethiols with varying degrees of polar character and chain length; it is very inexpensive; available in high purity, it is a high polar solvent and with low toxicity.

**Incubation Temperature.** For the SAMs to form, a stable temperature of at least 25 °C is needed. However, forming SAMs at temperatures above 25 °C can result in improved kinetics of SAM formation and also results in less monolayer defects. The increase in temperature increases the rate at which

desorption of adventitious materials and physisorption of solvent molecules on the substrate surface. Increased temperatures allow for chain reorganization and lateral rearrangements.

**Concentration and Immersion Time.** concentration and immersion time are actually inversely proportional, this means that a solution with less concentration of thiols requires a longer immersion time (i.e weeks). However, solutions with low thiol concentrations results in more regular SAMs, compared to high thiol concentrations.

SAMs are well-suited for researches in the field of nanotechnology because they are easy to prepare, they don't require specialized equipment, they form on objects of all sizes and are critical components for stabilizing and adding function to be preformed, nanometer-scale objects for thin metal films, nanowires, and other nanostructures, they can couple the external environment to the electronic (current-voltage responses).

## 2.5 Biosensors

A biosensor is defined as an analytical device that converts the biorecognition event into an electrical signal. The event only occurs between a bioreceptor and a target analyte[14][15]. Ever since the pioneers biosensors, Clark and Lyons, proposed the initial concept of glucose enzyme electrodes in the early 1960s, there have been many progressive implementations in the biosensor field. Even though there are several types of biosensors, depending upon what they are intended to detect and the type of technology employed, all biosensors have some common features[53]. Firstly, they consist of a bioreceptor; which is normally immobilized onto a transducer surface. In molecular biology, a bioreceptor is a group of molecules used to study the properties of other molecules or structures such as a target analyte. A bioreceptor is an element that is capable of recognizing a molecule or pathogen it is designed to identify.

Secondly, they consist of a transducer. A transducer is a physical device that performs signal transduction by converting one form of energy into another form of energy. Thirdly, they consist of a signal processing system. The processing system usually consist of signal amplification, filtering and display of the output in an appropriate format. These components are the essential building blocks of a biosensor as shown in Figure 2.20. The main ideal purpose of a biosensor is to provide an accurate, real-time, rapid and reliable information about the analyte under investigation. Ideally, these analytical devices should respond in a continuous and reversible manner. Biosensors have numerous applications; such applications include, to name a few, bio-diagnosis, medical and food and safety fields. This section highlights the different types

of biosensors based on their biorecognition element and the type transducer they employ.

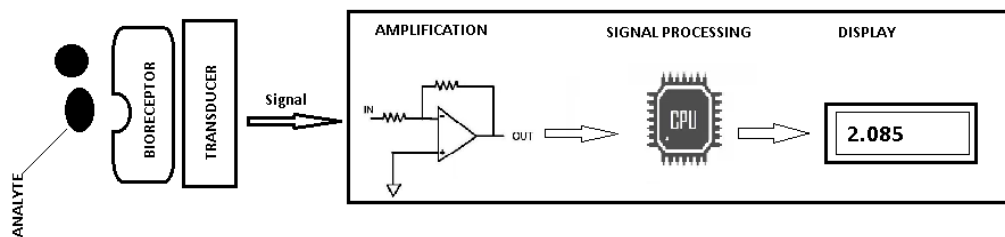


Figure 2.20: The building blocks of a typical biosensor. Showing the bioreceptor, transducer and the signal processing electronics. The signal processing electronics consist of the amplifying, the signal processing and the display stages.

### 2.5.1 Types Of Biosensors

There are several types of biosensors and they are classified by either the type of bioreceptors or the type of transducers they employ. The types of bioreceptors discussed in this section are whole cells, nucleic acids, enzymes, antibodies and the biomimetic materials. Similarly, the types of transduction material discussed in this section include optical, electrochemical, colourmetric and piezoelectric. Figure 2.21 can be used to categorize a biosensor accordingly. The categorization can be used to properly select a biosensor.

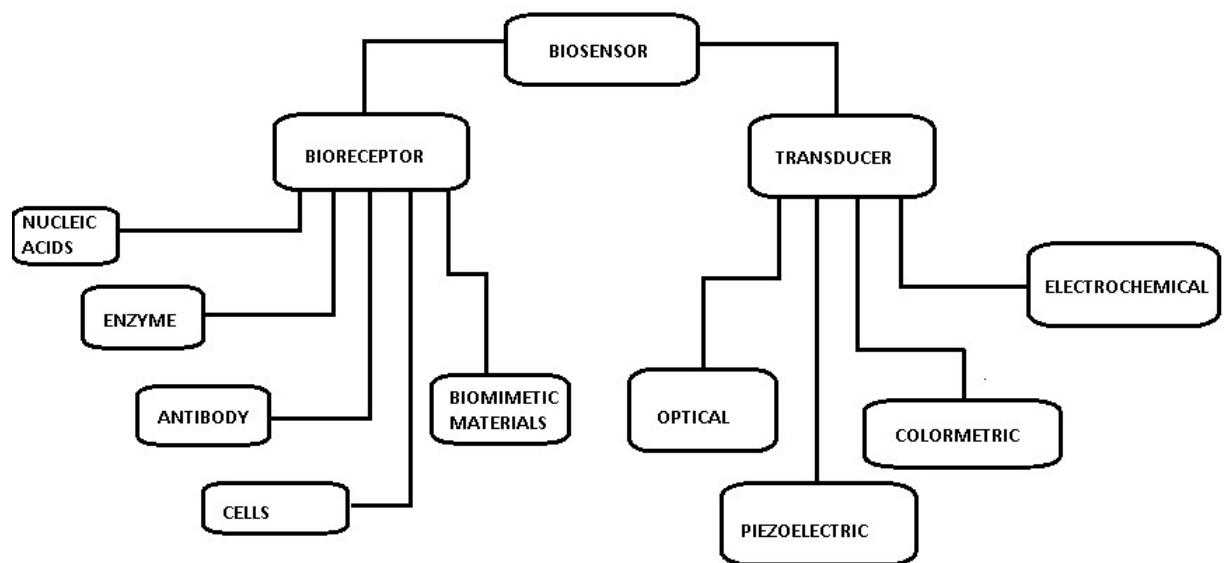


Figure 2.21: Categories of biosensors based on bioreceptors and transducers.

## 2.5.2 Bio-receptor Categorization

As stated before, a bioreceptor is one of the significant and distinguishing element of a biosensor. Designing the bioreceptor to be highly specific and sensitive to the target analyte is very important. Selectivity refers to the bioreceptor being able to identify specific substances in an analyte unambiguously. And sensitivity refers to the bioreceptor to being able to identify a substance even at very low concentrations. The bioreceptors utilized by biosensors can be divided into five mechanisms, as shown in Figure 2.21. So in simple word the role of the bio-receptor element is to control the selectivity and specificity that allows the biosensor to respond to a particular target analyte and to produce accurate, real-time, rapid and reliable information about the analyte. In this section the types of biosensors based on the biorecognition elements they employ are discussed.

### 2.5.2.1 Cell-Based Biosensors

Cell-based biosensors are sensor devices that utilize living cells as the bioreceptor[54], as shown in Figure 2.22. They rely on the ability of the living cell to detect the intracellular and extracellular microenvironment conditions, physiological parameters and produces response through the interaction between stimulus and cells[53]. These types of biosensors are capable of measuring useful information to help us understand the cellular mechanisms behind specific diseases to advance the development of targeted treatment[54].

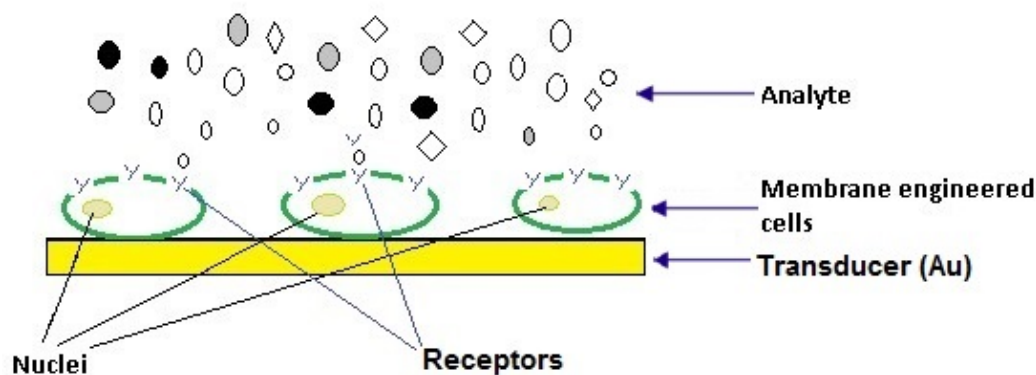


Figure 2.22: A schematic of a cell-based biosensor. Showing the living cells as the bioreceptors immobilized on a gold electrode interacting with an analyte.

Bioreceptor layers on such biosensors can be designed in various ways. They can be fabricated to either detect a response of a single cell or network of cells. In essence, cell based biosensors are unique biosensors as compared to other types of biosensors, they contain materials extracted from biotic factors. They are very versatile and therefore applicable in various fields such as food safety, medical diagnostics and environmental monitoring. However, even though they emerge as the promising technology, cell based biosensors have several issues that might limit their application scope. Major limitations issues such as specificity, reliability and robustness, Long-term stability and shelf life and also scalability with low price [55]. These types of biosensors lack specificity for a proper identification of the analyte due to cellular events such as cell death or cell path signaling. Moreover, the mammalian cellular cultures are fragile prone to damage and they are also quite expensive. Regardless of these drawbacks, cell based biosensor are still advantageous over the enzymes based biosensor. They are less sensitive to solutes inhibition. They are also more tolerant of suboptimal pH and temperatures and a longer lifetime can be expected than the enzyme based biosensor[53].

### 2.5.2.2 Enzyme-Based Biosensors

Biosensors that makes use of enzymes as their bio-recognition elements and still represents the most thoroughly studied area [56]. Enzyme-based biosensors are still the mostly used biosensors for biomedical or clinical analysis. The most broadly utilized enzyme biosensors in the medical field are those manufactured for glucose glutamate, lactate, cholesterol, and urea. Glucose is the most widely studied analyte [57]. Enzymes have properties such as being very effective biocatalysts, which have the ability to specifically identify their substrates and to catalyze their transformation. These properties makes enzymes to be perceived as the powerful tools to develop analytical devices. However, an



enzyme catalytic reaction can be influenced by numerous factors such as; substrate concentration, temperature, pH and inhibitors (both competitive and none-competitive)[53].

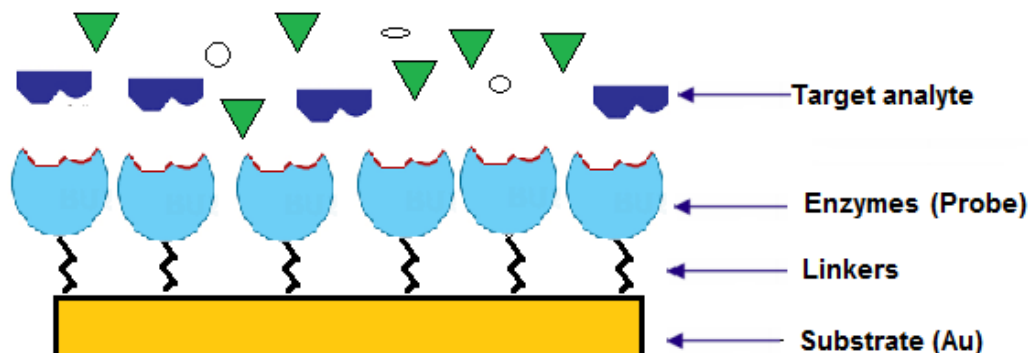


Figure 2.23: A schematic diagram of an Enzyme-based biosensor. Showing the enzyme as the bioreceptors immobilized onto a transducer and interacting with a target analyte.

Figure 2.22 above shows the basic schematic diagram of an enzyme based biosensor. The enzyme selectively reacts with its designated substrate and provides the correct analytic results. A basic principle of an enzyme-based biosensor incorporates, after the addition of an analyte, an enzymatic reaction that occurs when the analyte or product transfers an electron with the electrode surface to be oxidised or reduced[58].

This enzymatic response is controlled by the frequency of two processes that occur during the same time, and these processes are; the enzymatic conversion of the substrate and the diffusion of the product from the enzyme layer. This results in an altered constant flow of electrons (current) that can be measured. The magnitude of the current is directly proportional to the substrate concentration[59].

### 2.5.2.3 Antibody-Based Biosensors

Antibody-based biosensors, also known as immunosensors, make use of antibodies as their bio-recognition element. An antibody molecule is a large, Y-shaped immunoglobulin (Ig) that is made up of two light and two heavy chains with each containing constant and variable part as shown in Figure 2.24. The variable part is specific to the antigen that attaches with the corresponding antigen, which is highly specific and selective[53].

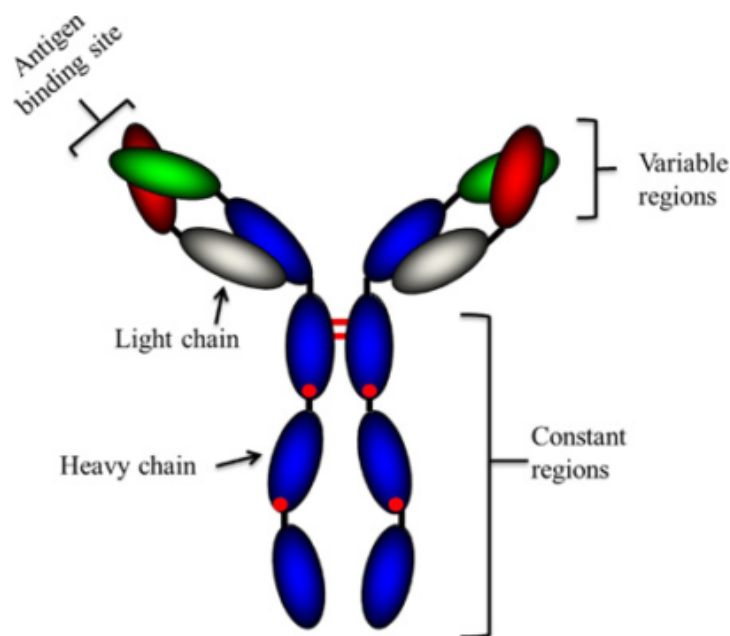


Figure 2.24: A diagram of an antibody. The antibody is 'Y' shaped immunoglobulin with two heavy chains and two light chains. The diagram also shows the antigen binding sites[60].

Immunosensors, show in Figure 2.25, are basically more useful than enzyme-based biosensors due to the fact that antibodies have been generated to specifically bind to individual compounds or groups of structurally similar compounds with a wide range of affinities[61]. This type of sensor was first developed and applied for the first time in the early 1950s, thus introducing the opportunity of immuno-diagnosis. The development of immunosensors for bacteria and pathogen detection has gained a plenty of attention due to its application in the point of care diagnostics. However, immunosensors have been significantly explored and developed only for the early detection of tumor[53].

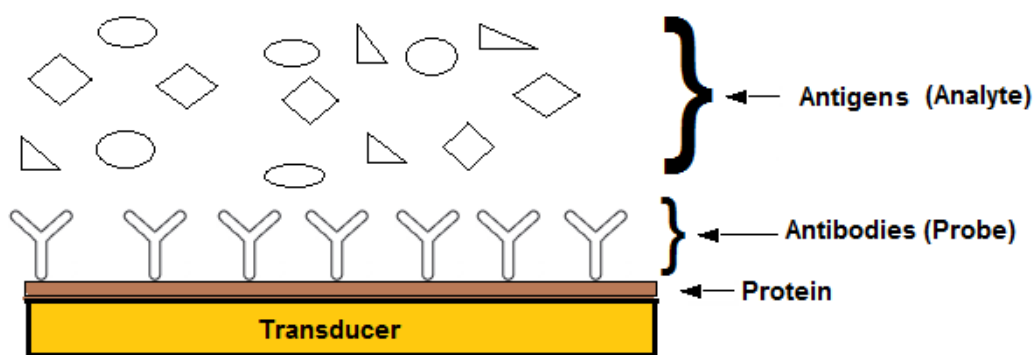


Figure 2.25: A schematic diagram of an Antibody-based biosensor. Showing the antibody used as the bioreceptors immobilized onto a transducer and interacting with a target analyte (specific antigens with markers).

#### 2.5.2.4 Nucleic Acid Based Biosensors

Nucleic acid biosensors (NABs), also known as genosensors, make use of the nucleic acids oligonucleotide as their biorecognition element[62]. The nucleic acid group consists of deoxyribonucleic acid (DNA), ribonucleic acid (RNA), peptide nucleic acid (PNA), and aptamers (both DNA and RNA). The use of nucleic acid as a biorecognition element in biosensing is rather a new and exciting area in analytics[63]. A biosensor fabricated with nucleic acid (NA) is commonly made up of single-strand (ss) DNA probe which is immobilized onto a transducer surface as shown in Figure 2.26. The probe is normally synthesized to hybridize with a specific complementary strand. Owing to its highly efficient and good specificity, the detection of the complementary nucleic acid strand can be easily recognized[64]. Figure 2.26(c-d) shows the hybridization process.

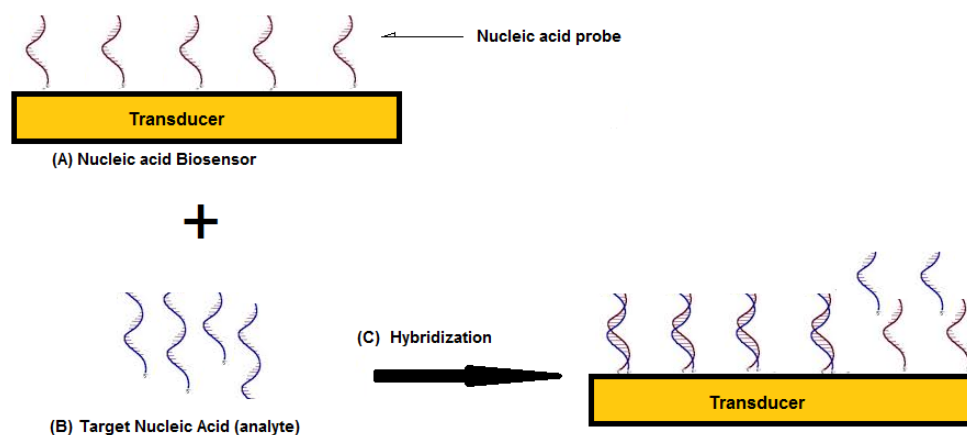


Figure 2.26: A schematic diagram of an ideal Nucleic acid-based biosensor. Showing (A) the biosensor and the probe used as the bioreceptors immobilized onto a transducer, (B) the target analyte, which is nucleic acids as well and (C-D) The hybridization process, which is the binding of target to the complementary probe.

There are two types of hybridization that can occur, a weak and strong hybridization. Weak hybridization occurs when the probe is too short such that hybridization takes place in few minutes (high rates) and that could result to a less specific biosensor, which may provide poor results. Having a less specific biosensor is a disadvantage. Strong hybridization occurs when the probe is quite long such that the hybridization process takes place for hours (low rate). Biosensors having a longer probe are advantageous as the biosensor is more specific and can provide reliable results. The fundamental principle behind NABs is the degree of complementarity of base pairs.

NABs have several clinical applications such as diagnostics of pathogenic diseases and infections at the point of care. They have proved to be promising analytical devices for the detection and diagnosis of various diseases like metabolic disorder such as cancer and infectious diseases like tuberculosis[63].

### 2.5.2.5 Biomimetic Based Biosensors

Biomimetic based biosensors make use of the biomimetic materials as their biorecognition element. Biomimetic materials are synthetic materials that mimic the processes of real and natural biomaterials. Therefore, that means that a biomimetic biosensor is an artificial sensor that mimics the function of a natural biosensor. Aptamers are short oligonucleotides (usually around 40-60 nucleotides) which can be chemically manufactured, modified and easily integrated with a variety of nanomaterials, such as gold nanoparticles, quantum dots, carbon nanotubes, and iron oxide nanoparticles [63]. Aptamers were first reported in the late 1980s where they were described as artificial nucleic acid

ligands[53]. Aptasensors can be designed to recognize peptides, amino acids and proteins. The most common biomimetic material is the peptide nucleic acid (PNA). PNAs are artificial DNA mimics with a neutral polyamide backbone structure instead of the negatively-charged sugar phosphate backbone structure (Figure 2.27).

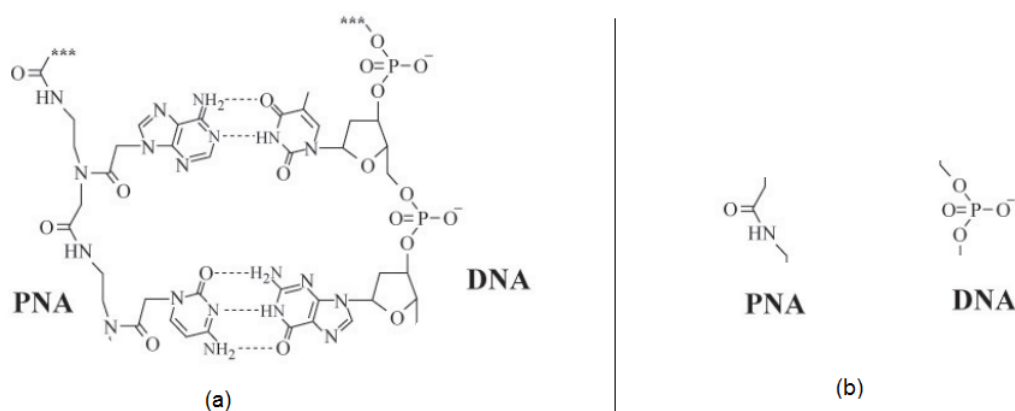


Figure 2.27: [A schematic diagram of a chemical model of peptide nucleic acid and deoxyribonucleic acid. Showing (a) the hybridized PNA-DNA duplex in terms of the Watson-Crick base pairing rule and (b) the difference in the backbone chemical structures of PNA and DNA[14].

Owing to its significance superior hybridization characteristics and improved chemical and enzymatic stability compared to nucleic acids, PNAs are ideal for biosensing. PNA can form both double and triple stranded complexes with other nucleotides[14]. Recently, a significant progress has been made in biomimetic biosensor for clinical application. This, therefore, means that biomimetic biosensor can be applied for medical diagnostics to detect pathogen and infectious diseases at an early stage.

### 2.5.3 Transducer Categorization

Biosensor can also be categorized using the type of transducer they employ for transduction. There are numerous types of transducers that can be used during the manufacturing stage of the biosensor. The types of transducers are shown in Figure 2.21. As stated before, a transducer is a physical device that performs signal transduction by converting one form of energy into another form of energy (see Table 2.5). In this section types of biosensors based on the transducers they employ are discussed and include piezoelectric, color metric, electrochemical and optical transducers.

Form of energy	Examples
Thermal	temperature, heat, heat flow
Mechanical	force, pressure, position
Chemical	concentration, composition, reaction rate
Optical	intensity, wavelength
Magnetic	field intensity, flux
Electrical	voltage, current

Table 2.5: The forms of energies that can be transduced and their typical input or output energy examples.

### 2.5.3.1 Electrochemical Based Biosensors

Electrochemical biosensors combine the sensitivity of electroanalytical methods with the inherent bioselectivity of the biological component. A typical transducer for this type of biosensor is an chemically modified electrode (CME)[65]. These biosensors use electrochemical detection for the transducer owing to its low cost, ease of use, portability, and simplicity of construction. The reaction is monitored electrochemically and it can generate a measurable current (amperometry), a measurable charge accumulation or potential (potentiometry), and it can alter the conductivity properties of the medium between electrodes (conductometry). A basic electrochemical biosensor setup consist of an electrochemical cell which is composed of a solution, working electrode(WE), reference electrode(RE), counter electrode(CE) and an electrochemical analyser as shown in Figure 2.28[66]. Amperometry is based on the measurement of the current resulting from the electrochemical oxidation or reduction of electroactive species. It is usually performed by maintaining a constant potential at a Carbon-or Gold- or Platinum-based working electrode. On the other hand, potentiometry is based on measurements of the potential difference between either an indicator and a reference electrode or two reference electrodes separated by a permeable selective membrane, when there is no significant current flowing between them. The transducer may be an ion-selective electrode (ISE), which is an electrochemical sensor based on selective membranes as recognition elements[65][67]. In conductometric detection the changes in the electrical conductivity of the sample solution are monitored. Conductometric biosensors often include enzymes whose charged products result in ionic strength changes, and thus increased conductivity. Conductometry has been used as the detection mode in biosensors for environmental monitoring and clinical analysis [67].

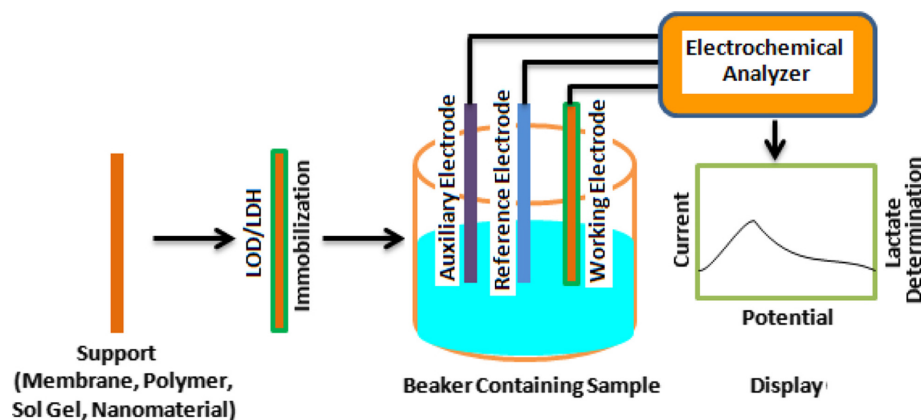


Figure 2.28: A basic electrochemical biosensor setup consisting of an electrochemical cell which is composed of working electrode(WE), reference electrode(RE), counter electrode(CE) in a solution and an electrochemical analyser[66].

For portability purposes, these biosensors are manufactured using miniaturized electrodes, this means that the biosensor is designed to small as possible through the use of micro-electrodes. Micro-electrodes are defined as electrodes with a radius in the range of micrometre scale, and thier shapes are usually in the form of disks or cylinders made from carbon fibers or metal microwires [67]. Some of these biosensors have reached the commercial stage and are normally used in clinical, environmental, industrial, and agricultural applications.

### 2.5.3.2 Colorimetric Based Biosensors

Colorimetric biosensors are based on the principle of temperature or heat detection. In more simple words, these biosensors measure the changes in temperature of the reaction between probe and an analyte under analysis. This type of biosensor, shown in Figure 2.30, takes advantage of the fact that all chemical and biochemical reaction involve the exchange of heat[68]. This principle of heat in biochemical reactions has inspired and attracted researchers' interest in developing calorimetric based transduction[53]. A typical type of biosensor mostly used is the thermistor(Figure 2.29), which is a temperature transducer whose resistance is dependent on temperature. Unlike other transducers, they are sensitive to optical and electrochemical properties of the sample and they do not need frequent recalibration. Typical applications for this type of biosensor include pesticide and pathogenic detection.

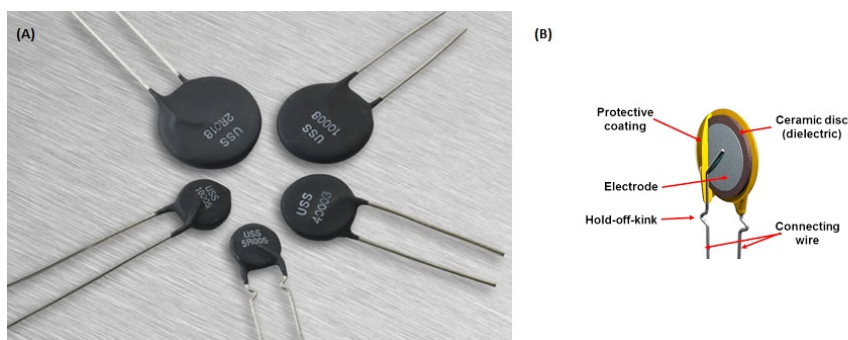


Figure 2.29: A basic (A)thermistor and its (B)schematic diagram showing vital components of the thermistor[69].

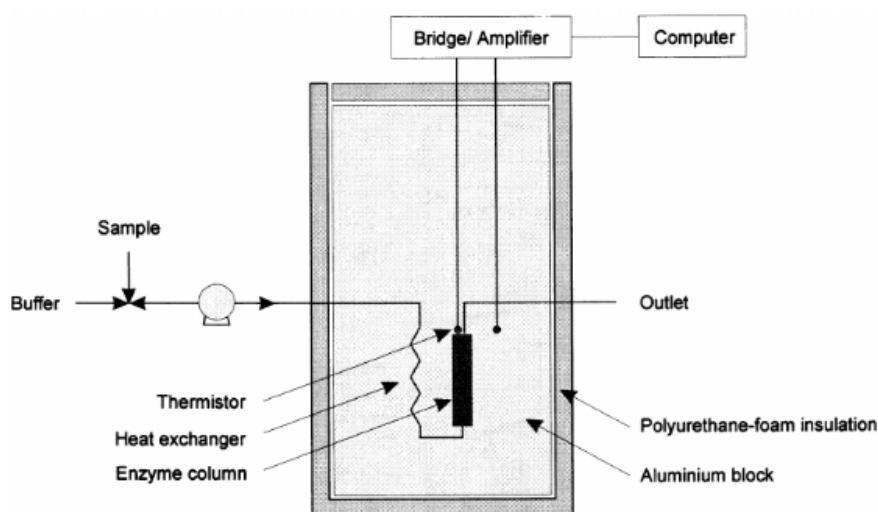


Figure 2.30: A basic calorimetric biosensor(also know as Enzyme thermistor) setup consisting of a thermistor as the transducer, heat exchanger, enzyme column[68].

### 2.5.3.3 Optical Based Biosensor

An optical biosensor is an analytic device, which contains a bio-recognition sensing element (e.g. enzymes, antibodies, antigens etc), combined with an optical transducer system(Figure 2.31)[70]. The main aim behind an optical biosensor is to produce a signal that is directly proportional to the concentration of the analyte under investigation. Optical transduction uses the changes in optical properties(e.g. phase, frequency, amplitude etc)A typical transducer that is used for optical transduction is a working electrode. The electrode maintained at a specific potential, at which the products, catalytically converted by an enzyme from the analyte, are oxidized or reduced. One



of the major advantages of this optical transducer is the low cost and the use of biodegradable electrodes[71]. There are many other optical biosensors and these include: Surface Plasmon Resonance (SPR), localized surface plasmon resonance (LSPR), Evanescent wave Fluorescence, Bioluminescent optical fibre, Reflectometric interference spectroscopy biosensors. The surface plasmon resonance which can be combined with optical fiber is most popular method available optical based biosensing.

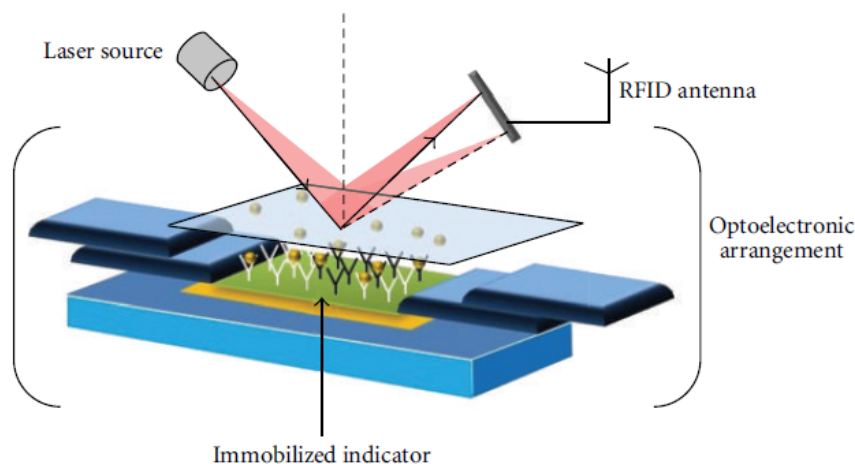


Figure 2.31: An optical biosensor architecture showing the scattering of light from the laser source to the detection device(antenna), optoelectronic setup and the immobilised probe[70].

Over the past few years, optical biosensors have been applied in a numerous number of fields and these include food safety, environmental monitoring and health care. In the health care field, optical biosensor has been applied in both medical diagnostics and medical research [53].

#### 2.5.3.4 Piezoelectric Based Biosensor

Piezoelectric based biosensors work on the basic principle of direct piezoelectric effect or inverse of piezoelectric effect. Direct piezoelectric effect refers to the ability of certain materials to produce electric current in response to an applied force. Inverse piezoelectric effect refers to deformation of these materials that results from the application of an electric field. All piezoelectric transducers can be fabricated to employ both the inverse and direct piezoelectric effect. Recently it has been shown that this method can be extremely interesting when integrated with Microelectromechanical systems (MEMS) for biosensing application [53]. The transducers employed by these types of biosensors are made up of piezoelectric materials, as shown in Table 2.1.

The most widely used transducers in the biosensing field are the quartz crystal microbalance (QCM), cantilever beam, surface acoustic wave (SAW) and Bulk wave (BW). QCM transducers are recognized as the highly accurate and stable oscillators. They are also used to measure the change in resonant frequency due to mass changes [72]. Figure 2.32 shows the basic schematic setup of a QCM biosensor. These transducers are also highly capable of detecting mass changes from the range of  $10^{-12}$  (pg) [73]. QCM based biosensors mostly make use of the inverse piezoelectric effect as they require current to produce vibrations.

However, the cantilever beam-based biosensors make use of either the direct or indirect effects of piezoelectricity depending on the output measured. The deflection of a cantilever beam transducer can be monitored by different methods; these methods include optical beam deflection, embedded transistor semiconductivity, and piezoelectricity and piezoresistivity.

In the piezoresistive method (Figure 2.33), the resistance of an unequally doped cantilever varies as a function of the applied force. The piezoresistive method has been widely studied as a signal transduction technique for cantilever beam deflection for biosensor applications [74]. In the piezoelectric, energy from the deflected cantilever beam also varies as a function of deflection or applied force [75].

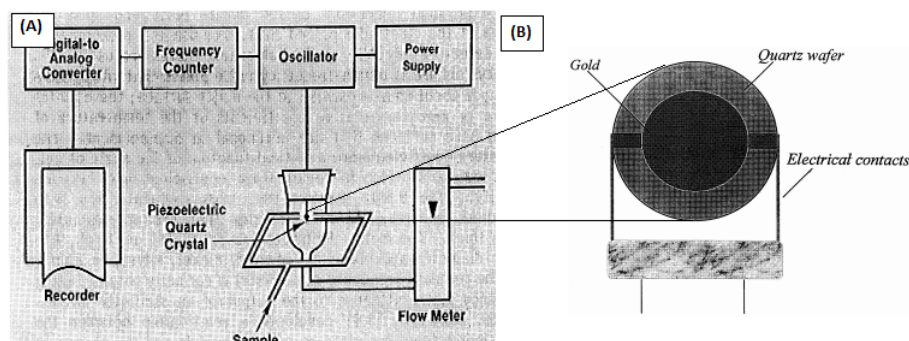


Figure 2.32: (A) Schematic setup of a typical QCM biosensing technique. Showing an oscillator and a frequency counter which will record the changes in frequency from the QCM. (B) Schematic of a typical piezoelectric crystal [72].

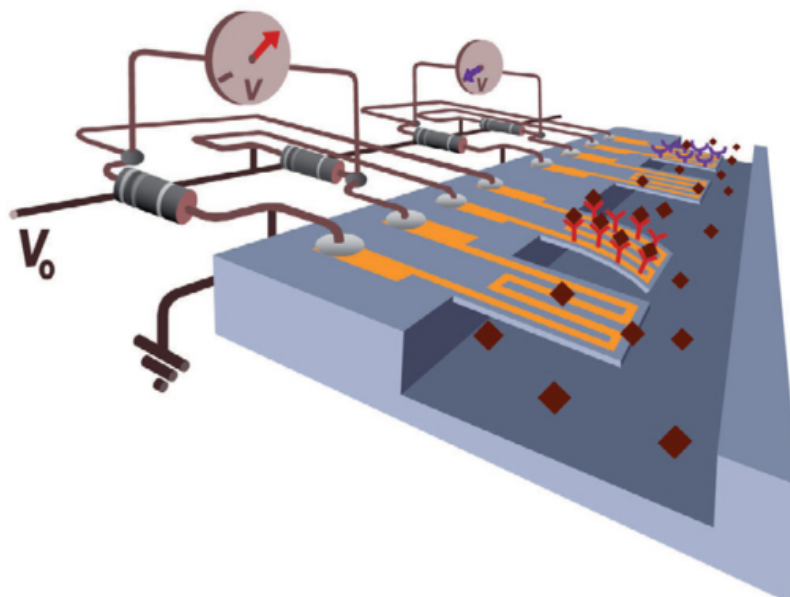


Figure 2.33: Schematic diagram of a typical piezoresistive cantilever beam sensing technique. When the biomolecules attach to the cantilever beam, the cantilever bends and causes a change in the resistance of the resistor placed inside the cantilever[74].

Of all piezoelectric nanodevices, the field effect transistor (FET) is one of the most studied systems because, in its simplest form, it is an electronic device and it exhibits a wide spectrum of applications especially in sensing and energy harvesting technologies. This PE-FET, as shown in Figure 2.15, is composed of a single semiconducting nanowire that is connected by two electrodes (source and drain electrodes) at the ends on a silicon substrate[76]. The working principle of PE-FET is dependent on the piezoelectric voltage produced when the nanowire, under strain, serves as the gate voltage for controlling the current flow from the drain to source electrodes[13].

Piezoelectric sensors have numerous advantages such as fast response, portability, simplicity, stable output signals, possibility for array sensors and self-powering, low cost of readout devices or electronics.

## 2.6 Conclusions

Nanotechnology implicates the study, manipulation, creation and use of materials, devices and systems normally with dimensions smaller than 100 nm. Nanotechnology is playing a progressively significant role in the development of biosensors. Sensitivity, selectivity and other attributes of biosensors can be optimized with nanomaterials during their fabrication. Nanomaterials display unique physical, electrical and chemical features because of effects such as the quantum size effect. Use of nanomaterials and nanoparticles in biosensors allows the use of many new signal transduction technologies in their manufacture. Because of their submicron size, nanosensors, nanoprobess and other nanosystems are transforming the fields of chemical and biological analysis, to enable rapid and early point of care diagnosis of infectious diseases (in this case; Tuberculosis).

## Chapter 3

# Design and Simulation Of 3D ZnO Nanowire Based Mass Sensor

### 3.1 Introduction

Modeling and simulation plays a critical role in any experiment as it gives a better understanding of the expected outcomes and shed light the underlying mechanisms of the system. There are different reasons why modeling and simulation is very important and these are as follows:

- The cost of experimentation might be too high;
- The experiments might be in a scale or dimensions which cannot not be perceived with a naked eye;
- and the results obtained from a simulated model can also be used for optimization purposes.

In summary, modeling and simulation provides an easy way to observe how the object or system of objects will behave under certain conditions. In this project, a Comsol Multiphysics software is used to simulate a 3D ZnO NW based mass sensor. COMSOL Multiphysics software is developed by the COMSOL company to simulate and model scientific and engineering problems[77]. The model will be studied and observed under certain conditions such as when under mechanical strain(force). The modeling and simulation takes place in a 3D space dimension in an x,y and z coordinate system.Fpor this project, COMSOL is used to simulate Zinc Oxide nanowires to study the effect applied force, nanowire radii and the length of the nanowire on the generated electric potential.

## 3.2 Comsol Modeling

Comsol modeling and simulation involves 8 different steps:

- Selecting the appropriate space dimension (0D, 1D, 2D, 3D);
- Selecting the appropriate study;
- Defining the geometry of your model;
- Defining materials for model;
- Setting up the physics (e.g Piezoelectric module);
- Meshing of the model;
- Simulation;
- And analysis of the results.

The aim in this chapter is to simulate the ZnO pressure sensor. The mass sensor is modeled and simulated in such a way that it should resemble and respond the same way the real life model would. The mass sensor is composed of a Silicon wafer(Si<100>) substrate on which the ZnO nanowires are grown. First the silicon wafer is modeled as shown in figure 3.1 and the dimensions are listed in table. 3.1 below. Figure. 3.2, shows a complete mesh of the silicon wafer consisting of 9242 elements.

Geometry	Value
Thickness	0.1 $\mu$
Depth	10 mm
Width	10 mm

Table 3.1: The silicon wafer X, Y and Z dimensions used during modeling.

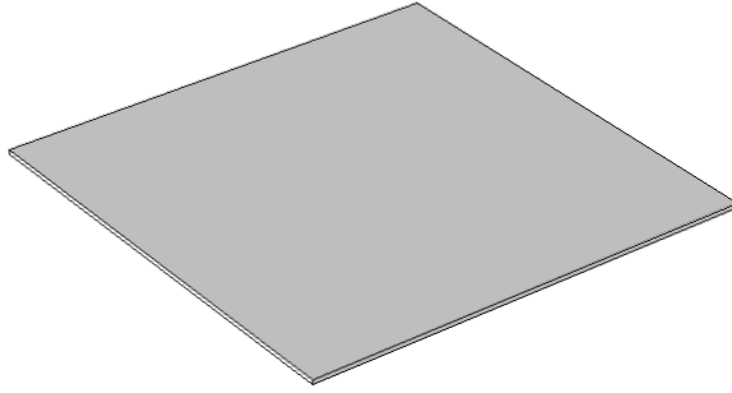


Figure 3.1: A Comsol model of a 3D ZnO Silicon wafer(p-type Si<100>). The Silicon wafer is modeled such that it has a thickness of  $0.1\mu\text{m}$  and an area of  $10\times 10\text{ mm}^2$ .

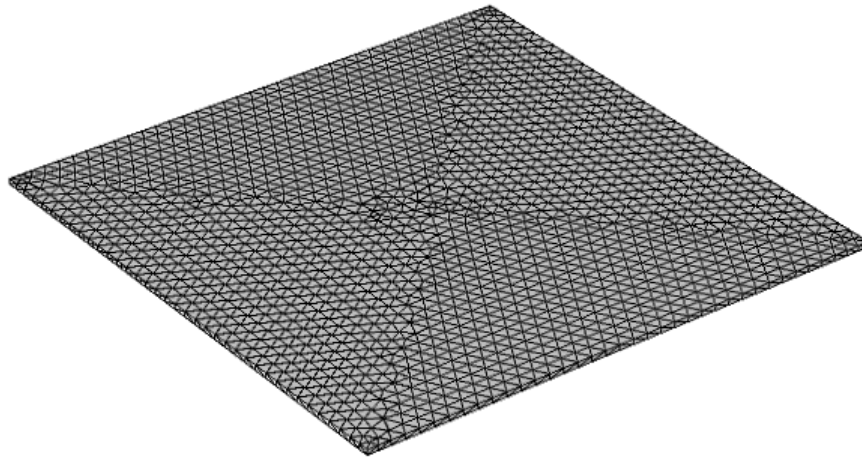


Figure 3.2: A meshed model of a 3D Silicon wafer with 9242 elements.

After the silicon wafer is modeled, the next part is to model an array of nanowires on top of the Silicon wafer. The nanowires are modeled as cylindrical objects to simplify their geometry. However, in real life nanowires have a polygon geometry. Figure. 3.3 shows the modeled ZnO nanosensor. The nanosensor consist of ZnO nanowires and a Silicon wafer as a substrate. Figure. 3.4 shows the meshed ZnO nanosensor. The whole system serves as a piezoelectric transducer for the biosensor. The model depicts a silicon wafer on which upright ZnO NWs are grown. The upright ZnO Nws have lengths of 600 nm and radii of 30 nm. As mentioned, the NWs are defined as uniform cylindrical objects with fixed lengths and radii for easy computational simulations as shown in Figure. 3.3 and Figure. 3.4.

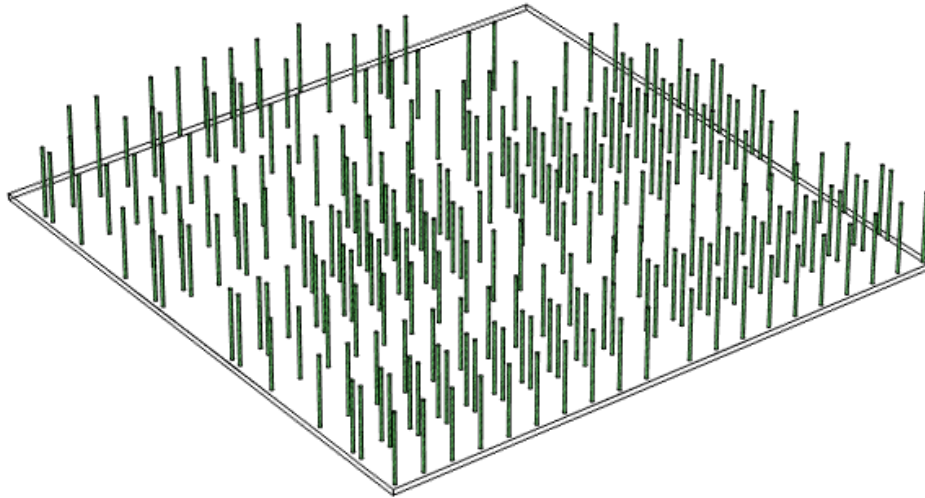


Figure 3.3: A Comsol model of a 3D ZnO nanowire sensor. Showing the Zinc oxide nanowires(green colour) which are supported by a silicon wafer (Si(100)) substrate.

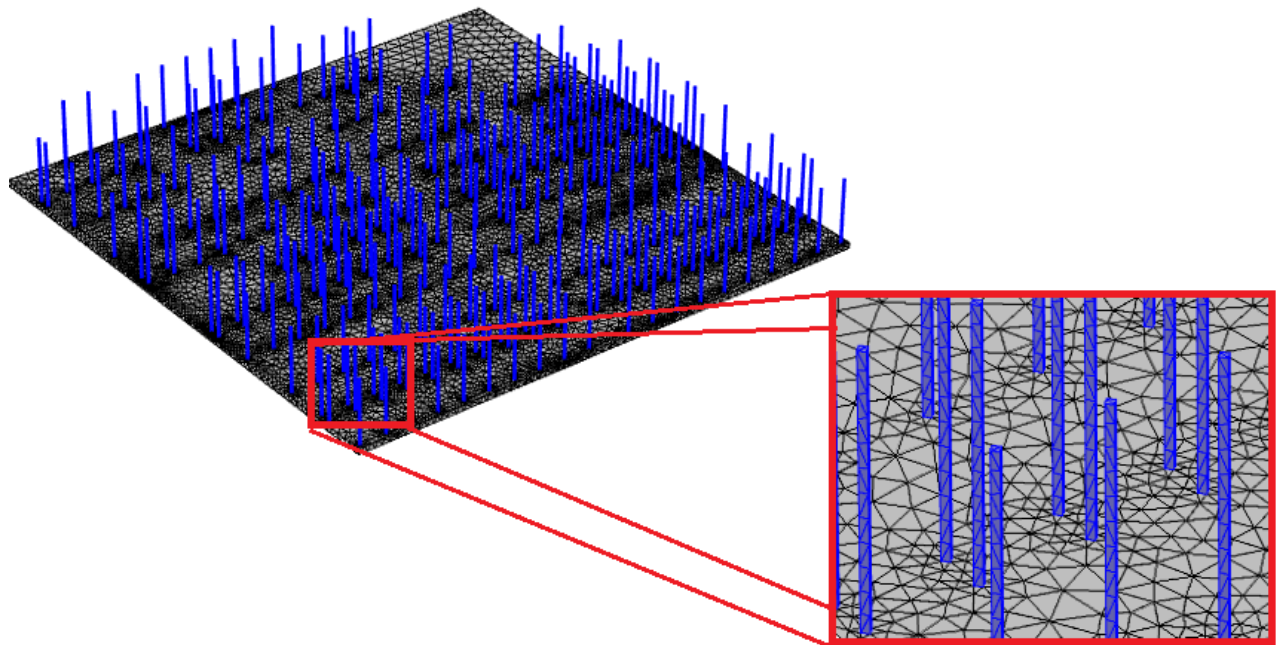


Figure 3.4: A meshed model of a 3D ZnO nanowire sensor. Showing the Zinc oxide nanowires(blue colour) which are supported by a silicon wafer (Si(100)) substrate(grey colour). The meshed sensor consist of complete meshed of 61070 elements.



### 3.3 Comsol Simulation

The COMSOL MULTIPHYSICS software contains the MEMS module in which it was used when simulating the ZnO NWs using the FEM (Finite Element Method). The MEMS module adds unique characteristics to the model at a nanoscale level; such traits include the piezoelectric effect of the ZnO NWs. The software solves equations (2.1.1) and (2.1.2) shown in Section 2.1.4. The NWs had not initial charge applied to them. Each NW has a number of entities or boundaries such as domains, faces, edges and points of which could be used for computational purposes.

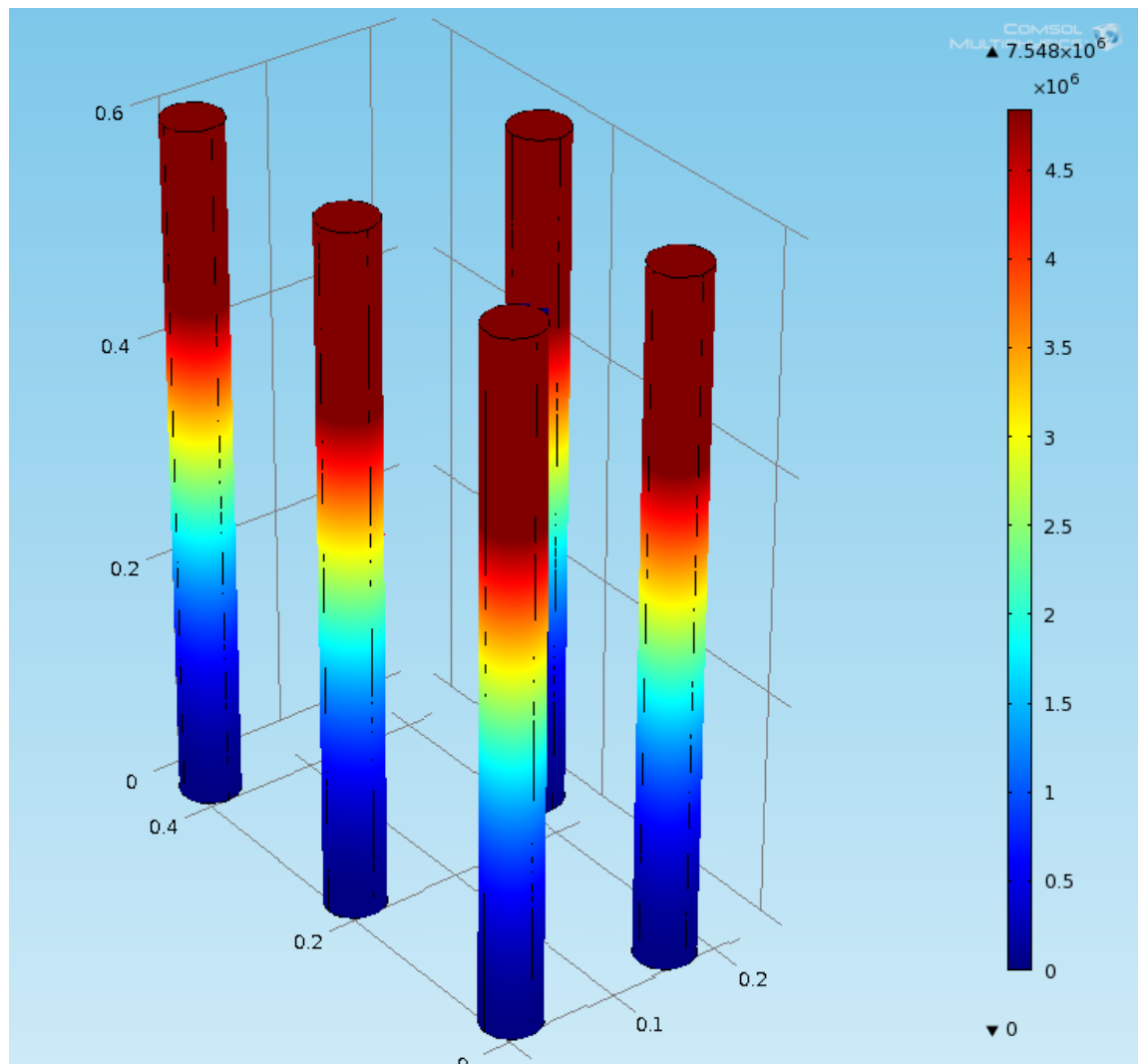


Figure 3.5: A 3D simulated nanosensor. The nanosensor consist of 5 activated ZnO nanowires. Only 5 nanowires were chose to represent the nanosensor due to computational time and memory space.

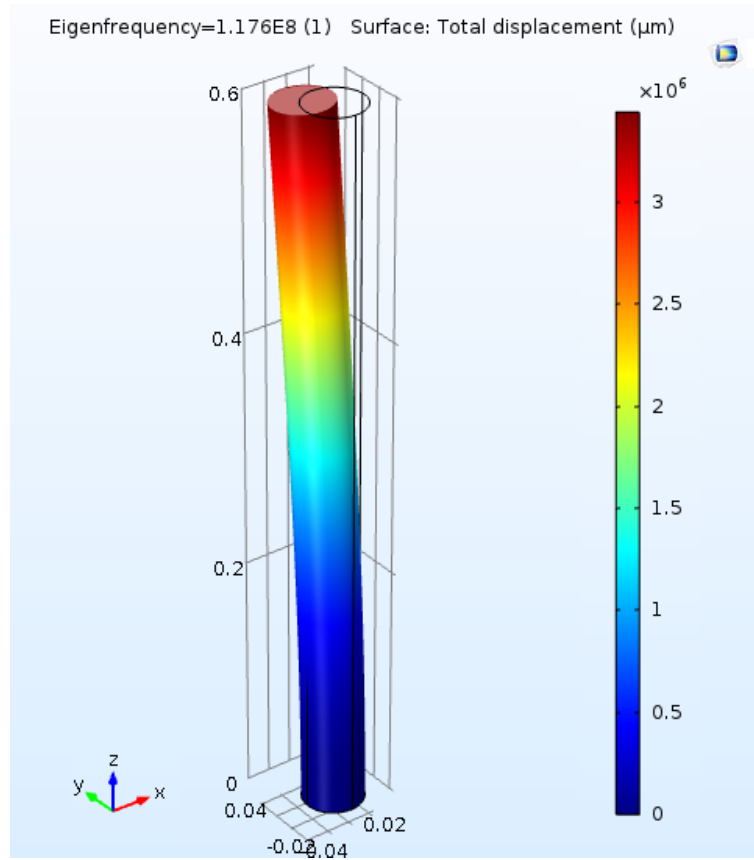


Figure 3.6: A displaced 3D simulated ZnO nanowire with an applied force of 10 nN in the y-direction.

For better simulation, a single nanowire was simulated and point load was applied to the NW as shown in Figure. 3.6. Using the single NW a number of conditions were defined and a set of outcomes were observed. The Electric Potential was observed for different variable parameters (see Table. 3.2) and these were used to optimize the sensor.

Variable Parameter	Observed Output
Mechanical Stress / Force	Electric Potential(E)
Length of the Nanowire	Electric Potential(E)
Radius of the Nanowire	Electric Potential(E)

Table 3.2: The parameters used to optimize NW growth.

### 3.4 Comsol Simulation Results And Discussions

For this project, COMSOL simulation was successfully used to verify theoretical claims about the piezoelectric phenomenon. Moreover, it was used to optimize the nanosensor in terms of the output electric potential energy. Figures. 3.7(a) and 3.7(b) show the generated and calculated electric potential, respectively, as a function of an applied force. The graphs, also show that the electric potential is directly proportional to the applied force. In turn, this proves the piezoelectricity due to mechanical stress. Moreover, Figure 3.7(c) shows the relationship between the length of the nanowire and the generated voltage under a constant pressure. The graph proves that longer nanowires have more bending degree as compared to shorter nanowire and thus results in more electric potential to be generated by the nanowires. Hence, nanowires with more thinner diameter produce higher electric potential as shown in Figure. 3.7(d).

The zinc oxide nanowires were successfully modelled and simulated using COMSOL Multiphysics software. The simulation served two purposes :

- To prove the literature and theoretical claims about piezoelectric material such as 1D nanowires;
- and for obtaining the optimal dimensions of the nanowires for a highly sensitive nanosensor.

As stated above, Figures. 3.7(a) and (b) proved that the piezoelectric effect holds as the literature study claims. Also, Figures. 3.7(c) and (d) proved that nanowires that are thinner in diameter and longer in length will produce higher electric potential across the nanowires as they have a higher degree of bending than thick and short nanowires.

The optimal nanowire radii and lengths which will produce higher output voltage for the nanosensor to be more sensitive were obtained and the experiments will be set up to meet the optimal parameters.

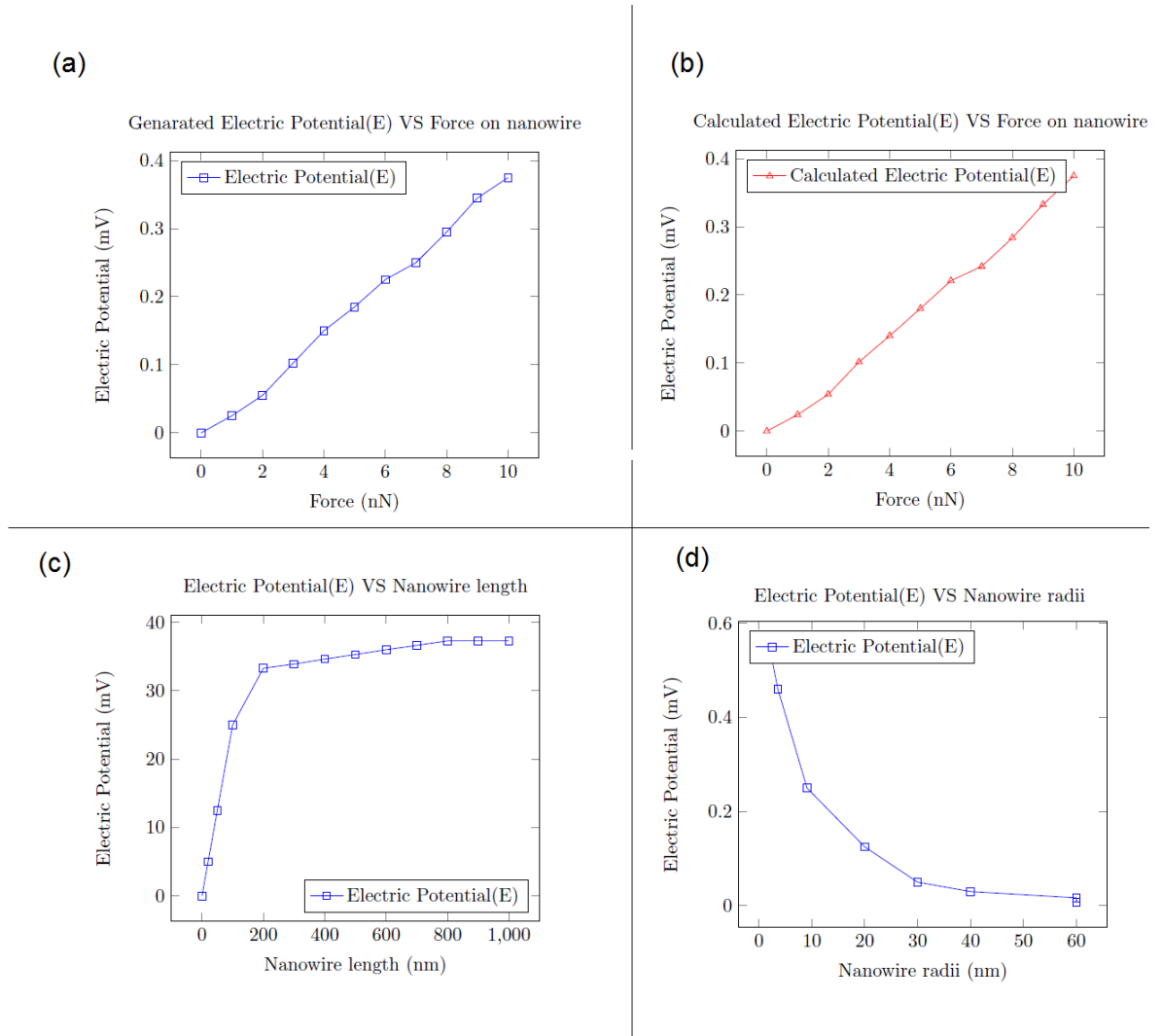


Figure 3.7: Simulated graphs showing the (a) generated Electric Potential Energy as function of an applied force on the simulated nanowire. Note that the Electric Potential Energy is directly proportional to the applied force. (b) Calculated Electric Potential Energy as function of an applied force using equation 2.1.11. Note the graph has the same trend as the simulated graph from (a) and also that the Electric Potential Energy is directly proportional to the applied force. (c) Generated Electric Potential Energy as function of the length of the simulated nanowire. Note that the graph saturates at length more 1000 nm. (d) Generated Electric Potential Energy as function of the radii of the simulated nanowire. Note that the Electric Potential Energy is indirectly proportional to the nanowire radii.

## Chapter 4

# ZnO Transducer Design And Fabrication

### 4.1 Introduction

One of the main aims of this project was to identify, design and manufacture an optimal transducer for the biosensor. ZnO nanowires makes it possible to successfully manufacture an optimal transducer as required. The main aim in this chapter is grow the ZnO nanowires and use them to design and manufacture the transducer element. A piezoelectric (ZnO nanosensor) transducer is chosen because it is quite easy to optimize as compared to others and the output signal can be measured directly from the transducer itself with no external power input. The types of transducers considered for this project are discussed in Chapter 2. The transducer will convert the hybridization process into a measurable electrical signal through the piezoelectric effect.

### 4.2 Materials and Methods

#### 4.2.1 Preparation of silicon wafers

The p-type <100> silicon wafers, with thickness in the range of 250-300  $\mu\text{m}$ , were cut into smaller sizes of 10 x 10  $\text{mm}^2$  and used as the substrate for the ZnO nanowire growth to manufacture the nanosensor. The p-type Silicon (100) wafers were cut by cleaving. The silicon samples were then cleaned via sonication for 10 min in acetone, absolute ethanol and DI-water respectively to remove surface impurities such as dust particles. Then silicon samples were air dried and placed on a hot plate at 110  $^{\circ}\text{C}$  for 10 mins to remove any liquid.

### 4.2.2 Deposition of the Aluminum layer

The wafers were then placed inside a thermal evaporator and a thin layer of aluminum, about 9-15 nm, was successfully deposited on the silicon samples. The main purpose of aluminum deposition is to improve and serve as the adhesion layer between the SiO<sub>2</sub> and Au layers. Then they were rinsed in DI-water, air dried and heated on a hot plate at 110 °C for 10 mins.

### 4.2.3 Deposition of the Gold layer

Now that an adhesion layer has been achieved, the next step was to sputter a thin layer of Au film. The etched samples were placed in an Edwards sputter coater S150B (Edwards, West Sussex, UK). A 40 nm Au film layer was successfully sputtered onto the rough surface silicon samples at 1.5 kV and 20 mA, under a pressure of  $2 \times 10^{-1}$  mbar in a chamber of non-reactive argon gas.

### 4.2.4 Deposition of the ZnO seed layer

The Au-Si samples were also cleaned by rapid soaking in absolute ethanol to remove surface impurities, air dried and then placed on a hot plate at 110°C for 5 min. For this project, the seed layer was sputtered using two methods. The first method is the ICM sputtering and the second method is sol-gel coat spinning. The two methods were compared.

#### 4.2.4.1 Sol-gel coat spinning method

The sol-gel spin coating method was implemented as follows: zinc acetate dihydrate ( $\text{Zn}(\text{CH}_3\text{COO})_2 \cdot 2\text{H}_2\text{O}$ ) was dissolved in a mixture of 2-methoxyethanol, also known as methyl cellosolve, and monoethanolamine (MEA) at a temperature of 25 °C. The concentration of zinc acetate was 0.1 M and the molar ratio of monoethanolamine to zinc acetate was 1:1. The solution was stirred for 2 h at 60 °C using a magnetic stirrer until a clear and homogeneous solution was achieved. After that, a 25  $\mu\text{l}$  of the solution was placed onto the gold-plated Si wafers and spun using the spin coater (Laurell Technologies, Pennsylvania, USA) at 3000 rpm for 30 sec. After spin coating, the samples were baked at 200 °C for 5 min on a hot plate to evaporate the solvent and remove the residual organic components. The process was repeated until a uniform ZnO layer was achieved. The ZnO uniform seed layer was annealed in air at 700 °C for 10 min.

### 4.2.5 Synthesis of ZnO nanowires And Insulation

Two methods were used to grow ZnO nanowires along the c-axis. Firstly they were grown via the hydrothermal method then the electrodeposition method.

**Hydrothermal Method.** ZnO Nws were synthesized using the hydrothermal growth method. An equimolar aqueous solution of zinc nitrate hexahydrate (1 mM) and hexamethylenetetramine (HMTA) (1 mM) dissolved in DI-water was prepared. The samples were placed upside down in the solution. The solution was then closed and placed inside an oven at 95°C for 12 hrs. After 12 hrs has elapsed, the substrates were rinsed with DI water and then dried with nitrogen gas to remove any contaminants and salts. After that, a mixture of SWCNTs and PMMA (ratio = 1:3) was dissolved in DI-water with a ratio of 2:3 [39]. The mixture was then dripped into the sample and spun using a spin coater at 1000 rpm for 15 s. Then the samples were placed on a hot plate at 100°C for 30 s. The SWCNTs-PMMA solution was spun until it had filled inbetween but not covering the nanowire tips. The main purpose of the SWCNTs was to increase the sensitivity of the nanosensor or transducer. The last step was to sputter a thin gold layer (20 nm) for a Schottky contact, as shown in Figure 4.3.

**Electrodeposition Method** A homebuilt electrochemical cell with two electrodes was used for the growth of ZnO nanowires. The substrate was cleaned as before and a thin layer of gold was sputtered on top of the substrate. The gold plated substrate was then spun coated with the sol-gel mentioned above the heated and rinsed as before. The clean sol-gel-Au-Si substrate was then connected on the negative(-) terminal of the electrode while the Zinc electrode was connected to the positive(+) terminal of the electrode inside the electrochemical cell containing a solution of Zinc nitrate hexahydrate (1 mM concentration). The solution was heated to 70 °C and a voltage of -1V was applied. After 1 hour the growth was terminated. The insulating polymer was spun as mentioned before and then a thin layer of gold was also sputtered for a Schottky contact. This then concludes the piezoelectric transducer. The next step is to immobilise the probe onto the transducer gold surface.

#### 4.2.6 Results And Discussions

For this project, two methods were employed to grow the perpendicular ZnO nanowires or ZnO nanowires along the c-axis. The two methods were the hydrothermal method and the electrodeposition method as mentioned. Figure. 4.1 shows poorly grown nanowires and according to the author's knowledge that is due to the poor formation of the ZnO seed layer and also no control of direction. Different concentrations, pH levels, substrates and temperatures were tried for the hydrothermal method but to no avail.



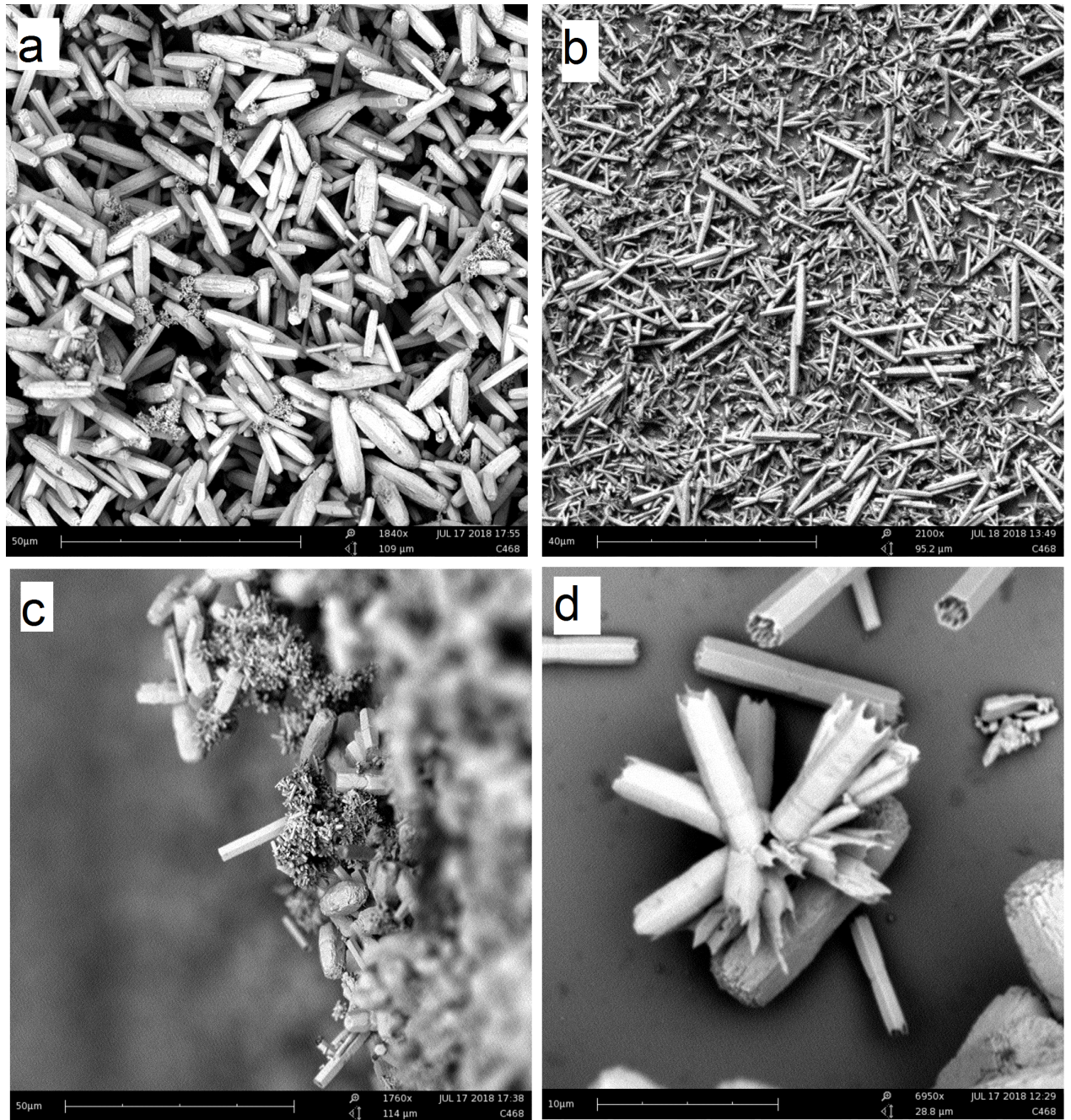


Figure 4.1: SEM images obtained via the FIE-SEM of non-optimised nanowires grown via the Hydrothermal method. Images (a) and (b) show the top view of the randomly grown nanowires. Image (c) shows the side view of the nanowires. Image (d) shows the nanowire growth branched at different directions other than the c-axis which is a huge problem.



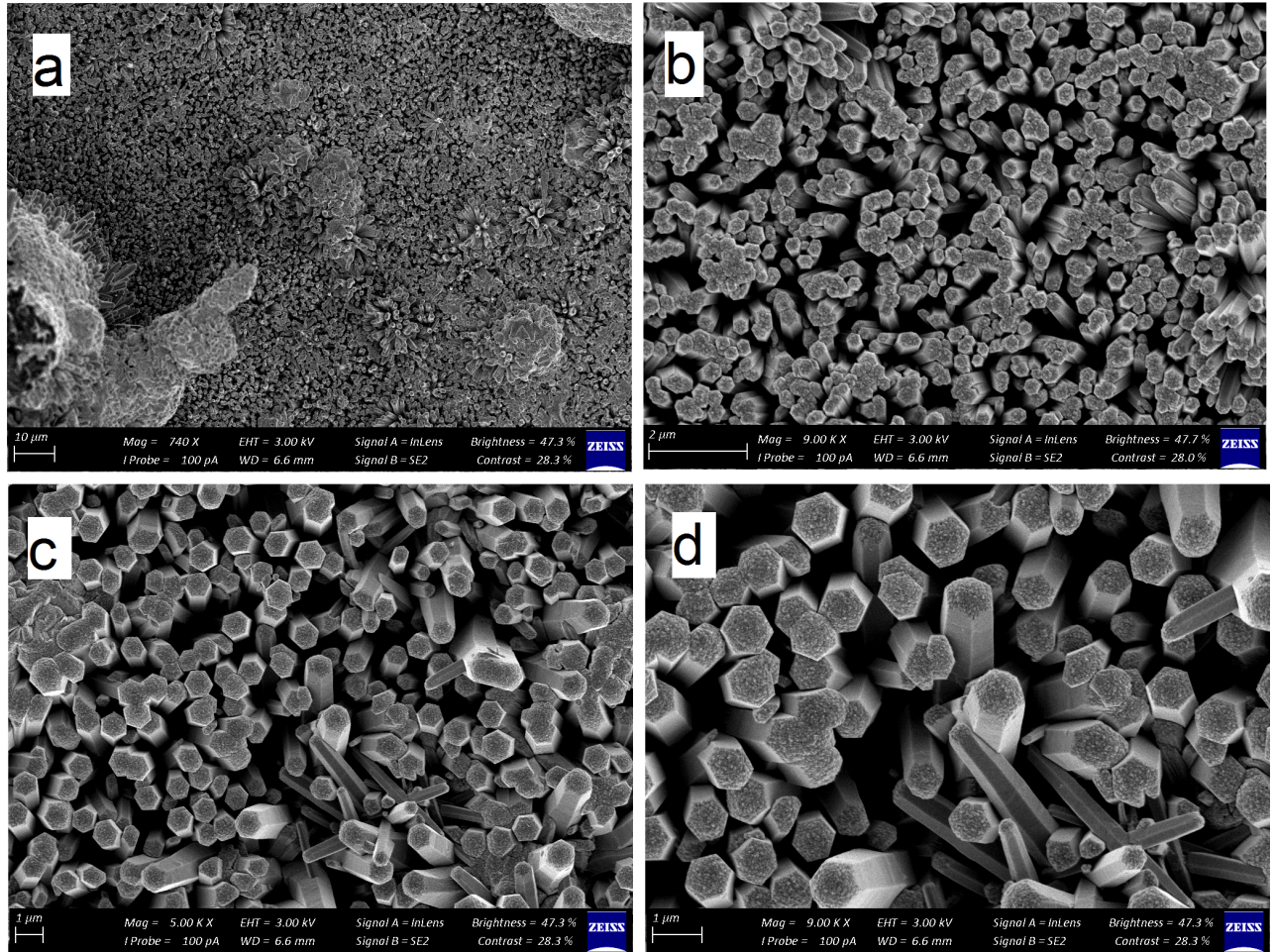


Figure 4.2: SEM images obtained via the ZIESS SEM of optimised nanowires grown via the Electrodeposition method. Figures. 4.2(a)-(d) show the top view of the nanowires. Figure. 4.2(b) shows the zoomed version (at  $2\mu\text{m}$ ) of Figure. 4.2(a). Figures. 4.2(c) and (d) show the nanowires at scale of  $1\mu\text{m}$ . The nanowires successfully grew perpendicular to the substrate via the electrodeposition method just under an hour.

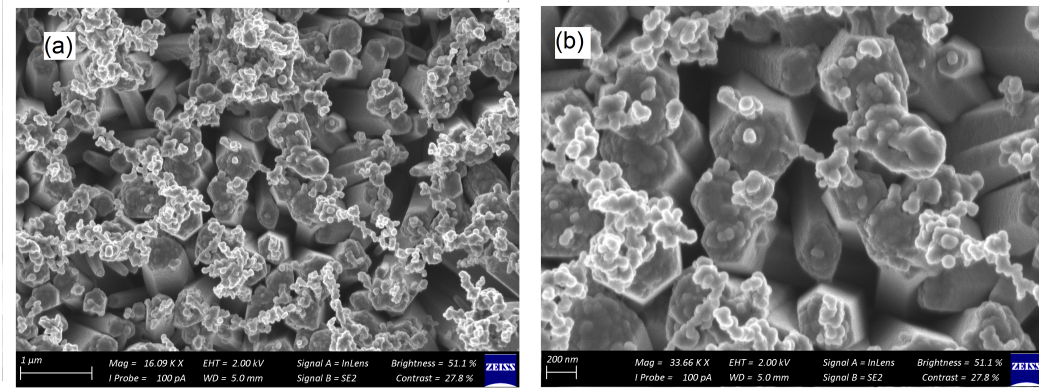


Figure 4.3: ZnO nanowires grown via the Electrodeposition method characterised using an ZEISS-SEM at Stellenbosch University, shown in Figure. 4.3 (a) and (b), zoomed at  $1\mu\text{m}$  and  $200\text{ nm}$ , is an array of ZnO nanowires with a thin layer of gold on top of the nanowires to form a Schottky contact.

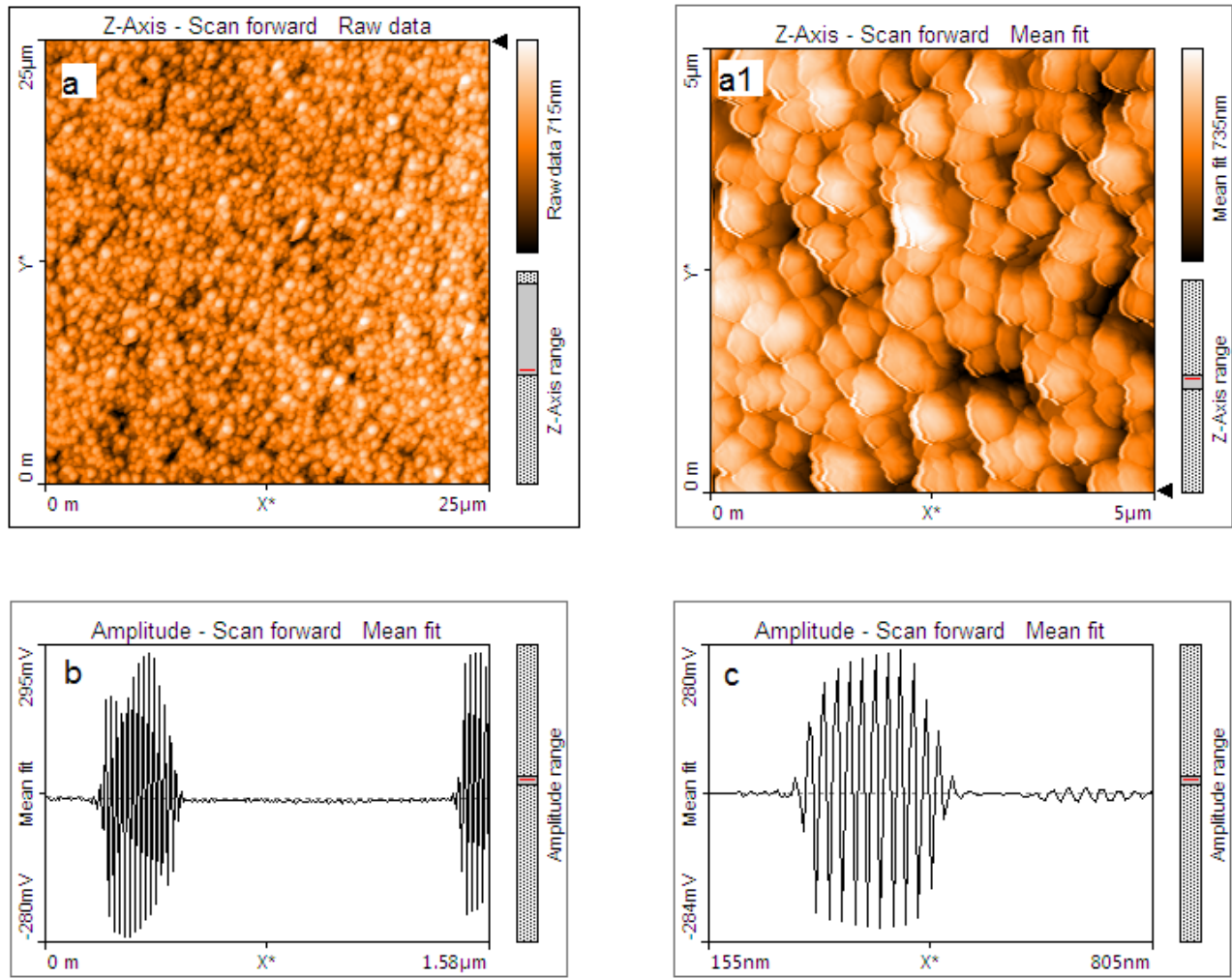


Figure 4.4: ZnO nanowires grown via the Electrodeposition method characterised using an AFM in our nanolaboratory at Stellenbosch University, shown in Figure 4.3 (a) and (a1). Figures 4.3 (b) and (c) show the output voltage of a nanosensor under the tapping mode of the AFM. The tapping mode of an AFM is when the AFM tip is in contact with a defined number of nanowires causing them, through the applied force, to bend and generate potential energy of about 295 mV. Figure 4.3 (c) shows a zoomed-in version voltage response of Figure 4.3 (b).

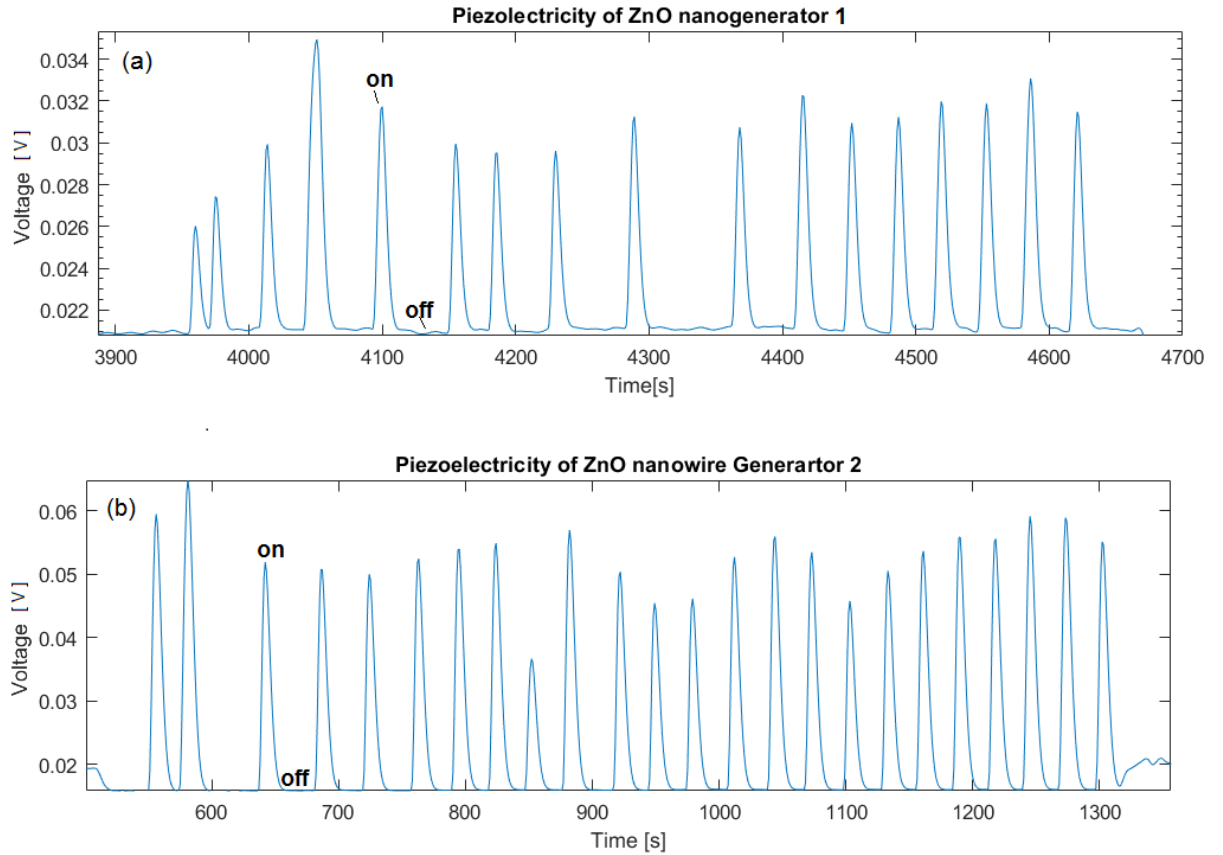


Figure 4.5: A generated voltage of a ZnO nanosensor obtained by a digital multimeter (Agilent, 34401A Digital Multimeter) which uses the BenchVue software. When the pressure is applied on the nanosensor the nanowires bend to generate a specific voltage which depicts the "on" state and when no pressure is applied there is no voltage which depicts the "off" state of the sensor. The first nanosensor, shown in Fig. 4.5(a), generated an average voltage of 0.032 mV. On the other hand, a different nanosensor, shown in Fig. 4.5(b), generated an average voltage of 0.05 mV.

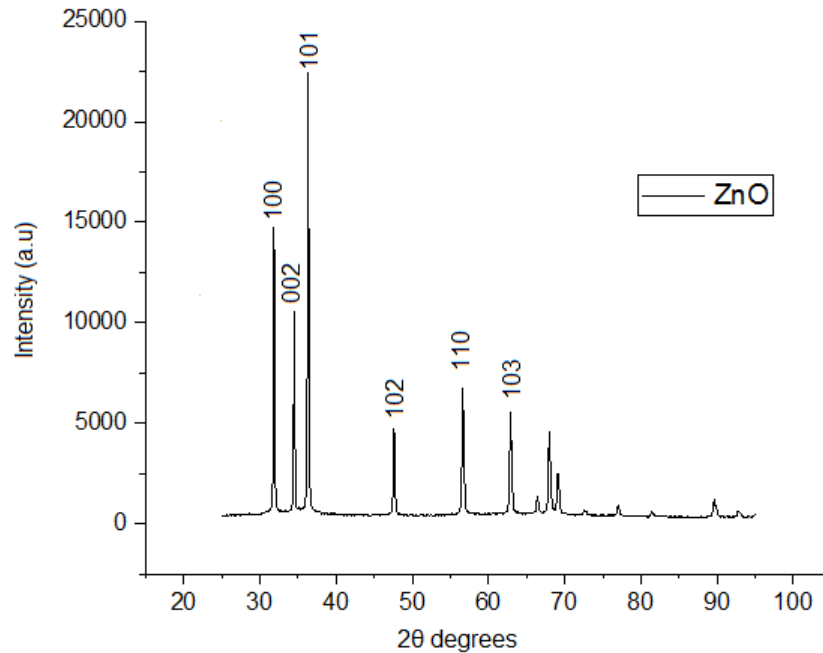


Figure 4.6: X-ray diffraction pattern of ZnO Nws synthesized on a glass substrate via the electrodeposition method. The major diffraction planes, such as (100), (101) and (102), could be easily indexed.

On the other hand, the electrodeposition method was very promising as the nanowires were successfully grown along the *c*-axis as shown in Figure. 4.2, which is perpendicular to the substrate. One advantage the method had over the hydrothermal method is that the substrate did not need a seed layer to initiate the ZnO nanowire growth along the *c*-axis. Different temperatures, applied voltages, concentrations had a huge effect on the quality and quantity of the ZnO nanowires. Temperatures above 70 °C accelerated the growth such that the layer of ZnO forms instead of nanowires. Voltages between -0.6V to -1V were ideal for the growth of nanowires while anything less than -0.6V produces ZnO nanotubes or nanowalls and voltages above -1V produces thin layers of ZnO.

Furthermore, the nanowires grown using the electrodeposition technique were further characterized using an AFM and XRD. Figures 4.4 and 4.6 show an AFM image and an XRD pattern of the ZnO NWs respectively. The AFM image, figure. 4.4, shows a top-down view of dense ZnO nanowires. The AFM-tip was used in the tapping mode to apply a force and bend the nanowires in which a response voltage was observed due to piezoelectricity as shown in figure. 4.4 (b)-(c). The sinusoidal nature of the signal is caused by the fact that the AFM tip moves in both forward and backward direction when bending the nanowires. This is also explained in the literature, see Chapter 2. The average



voltage produced by the AFM tip is about 295 mV.

A proper voltage, as shown in Figure. 4.5, was successfully obtained using a digital multimeter (Agilent, 34401A Digital Multimeter) which can be easily connected to a PC. Both responses show the "on" and "off" states of the nanosensor when pressure is applied and when there is no applied pressure respectively. The first nanosensor produced an average voltage of 0.032 mV as shown in Figure. 4.5(a), while the second nanosensor, shown in 4.5(b), produced an average voltage of 0.05 mV. The sudden decrease in output voltage for the digital multimeter is due to the fact that the multimeter has a series resistance of 10 M $\Omega$ . The series resistance decreases the voltage when the current passes through it. Further supporting information about the generated piezoelectric voltage using the digital multimeter can be found in Appendix blah.. Figure. 4.6 shows the XRD pattern of the ZnO nanowires. The XRD peaks and planes are so well aligned when compared with the standard XRD pattern for ZnO nanowires. The major diffraction planes, such as 100, 101 and 102, could be easily indexed and compared.

### 4.3 Conclusion

The electrodeposition method holds a promising future for the growth of nanowires as it is easily repeatable and simple as compared to the hydrothermal method. It also gives one more control over the growth. Electrodeposition is by far the simplest method to use. It requires the lowest temperature and pressure, moreover it is very cost-effective and scalable than any other methods. Zinc oxide nanowires grown via electrodeposition technique are found to show better crystallization and piezoelectric properties than those grown via other methods. The applied voltage or electric potential across the electrolyte plays a huge role on the growth of the nanowires as it directs the growth in a specific direction (from the negative terminal to the positive terminal/electrode).

Nanowires successfully grown using the Electrodeposition method were used as the transducer for the biosensor as the nanowires grew along the c-axis as compared to nanowires grown using the hydrothermal method. Electrodeposition technique made it possible to fabricate the nanosensor successfully. The nanosensors were characterised using an AFM in tapping mode to confirm the piezoelectricity of the ZnO nanosensors and the voltage response was successfully obtained. Furthermore, a digital multimeter was also used to confirm and validate the piezoelectricity of the ZnO nanosensor, the results were successfully confirmed and support the theoretical claims in chapter 2, and the digital multimeter results are shown in the appendix.

## Chapter 5

# Probe Design And Manufacturing

### 5.1 Introduction

Designing a probe for pathogen detection means that one should be able to sequence and study the genomic material of a particular organism. The genomic materials under study should be specific and unique to that particular organism or group of organisms. In this section, the main focus is on designing a ss-DNA probe which will be immobilised onto the gold plated transducer using biotin-streptavidin interaction for the detection of Mycobacterium Tuberculosis Complex. This chapter also focuses on predicting the structure of the 16S rRNA folding and the location of chosen bases through automated DNA computer softwares such as NCBI BLAST.

### 5.2 Chemical And Biological Materials

### 5.3 Methodology

**Probe design.** A 16S rRNA strain from the Mycobacterium Tuberculosis Complex (MTBC) was obtained from an online gene bank through blasting[78]. Table 5.1 below shows the target sequence and its complementary probe used in this study. The probe was designed to be specific to the 154 to 210 loci on the 16S rRNA of MTBC as shown in Figure. 5.1. The complete 16s rRNA sequence of the MTBC, which consist of 1532 base pairs, can be seen in Figure. 5.1. The NCBI BLAST(basic local alignment search tool) software was used to properly choose the MTB-specific oligonucleotide probe sequences.

16S rRNA Target Sequence
5'—aac tgg gtc taa tac cgg ata gga caa cgg gat gca tgt ctt gtg gtg gaa agc gct—3'
Probe Sequence
3'— acc cag att atg gcc tat cct ggt gcc cta cgt aca gaa cac cac ctt tcg cga—biotin—5'

Table 5.1: The 16S rRNA target sequence and its complementary DNA probe used in this study. The probe was labeled at the 5' end of the probe with biotin.

The Standard Nucleotide BLAST software, which runs on an online database, allows users to successfully design probes and successfully locate the sequence loci[78]. For this study, the online software is used for the design and simulation of the DNA probe specific to the 16S rRNA. The probe was designed to consist of 57 base pairs nucleotide. After the design of the probe complementary a region on the 16s rRNA, the identified sequence was sent for manufacturing. The probe was successfully manufactured and modified with biotin. The 5' end biotinylated oligonucleotides were obtained from Inqaba Biotechnical Industries(PTY) LTD and were used as a probe for the biosensor. After the probes were successfully manufactured, the next step was to isolate the total RNA for the mycobacterium tuberculosis through the help of Dr. Melanie Grobbelaar at Stellenbosch University.



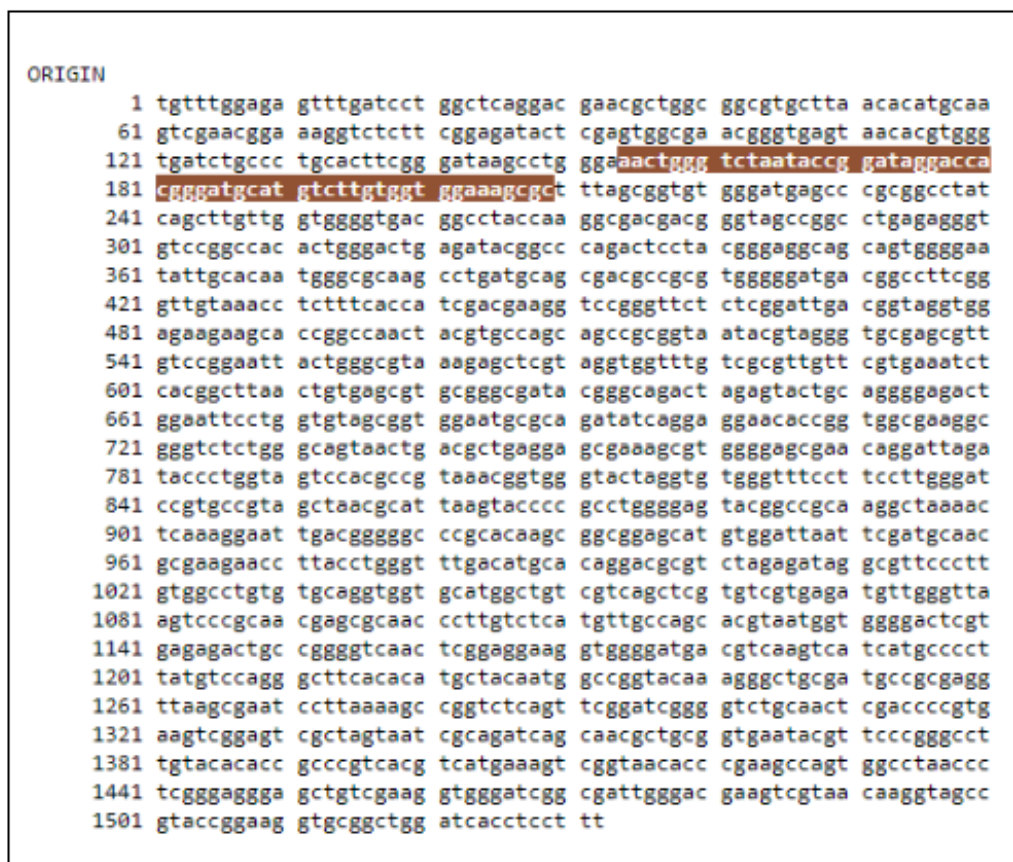


Figure 5.1: The blast results of 16 rRNA *Mycobacterium Tuberculosis* obtained from an online NCBI BLAST. The highlighted region shows the region of interest in complete genome of the bacterium.

### 5.3.1 *Mycobacterium* Cell Lysis And RNA Extraction.

During the lysing stage of the tuberculosis bacterium, a fastRNA ProTMBlue kit was used in conjunction with the ryzolizing step. This is where the cells were mixed with 0.2  $\mu\text{m}$  silica beads in a conical tube and beating everything together at a certain angular speed and time in a Ryzolizer machine. For this project, the total RNA extraction was performed at Stellenbosch University Tygerberg Campus (Division of Molecular Biology and Human Genetics) and is summarized below and a full version can be found in the appendix:

- A 1 ml of an overnight bacterial culture was diluted into 14 ml of fresh media in a sterile 50 ml tube. Then, the tube was incubated for 6 hours at 37 °C while shaking at 200 rpm to reach an  $\text{OD}_{600}$  that is between 0.9 and 1.0.

- 10 ml of bacteria cells were pelleted by centrifugation at 3000 rpm for 10 min, then the remaining liquid was discarded.
- Then 1ml of RNAPro solution was added to the pellet, which was resuspended by pipetting.  
**NOTE:** RNAPro solution contains Guanidine Thiocyanate and phenol which are very toxic and harmful-avoid exposure.
- The next step is to transfer 1mL of solution into lysing matrix B, 2 mL tubes. The tubes contain about 0.1 mm silica beads that are mainly used for lysing positive and negative gram bacteria.
- Then the tubes were homogenized or processed using the FastPrep-24 instrument for 25 sec with a setting of 4.5. The tubes were then placed on ice for 1 min.
- The solution was again transferred into a lysing matrix B, 2 mL tubes, this was repeated 3 times.
- The tubes were removed and centrifuged at 12 000 rpm for 5 min at 4°C.
- Then the liquid was transferred onto a new tube while avoiding transferring the cell organic waste and silica beads.
- 300  $\mu$ l of chloroform was added to the same tube and vortexed for 10 sec and incubated at room temperature for 5 min. Chloroform help to isolate the nucleic acids from proteins. Chloroform denatures protein and becomes soluble.
- The tubes were then centrifuged at 12 000 rpm for 10 min at 4 °C. The aqueous upper phase of the tubes contains only nucleic acids, which is transferred into a new tube.
- 500  $\mu$ l of cold ethanol was then added to the tubes an vortexed for 5 sec.
- Then the tubes were incubated for 1 hour at -20°C.
- After an hour, the tubes were centrifuged at 12 000 rpm at 4°C for 20 min then the supernatant was removed and washed with 500  $\mu$ l of 75% ethanol by centrifugation for 1 min at 12 000 rpm. The solvent, 75% ethanol, helps with isolation and purification of RNA.
- After a minute, ethanol was discarded and the pellets were air dried for 10 min.
- After drying, the pellets were resuspended in 30  $\mu$ l of RNase free water and incubated for 15 min.
- Lastly, the RNA is stored at -80°C.

### 5.3.2 Hybridisation Through Electrophoresis.

This step is used to confirm and characterize hybridization between the probe and target RNA (16S rRNA) before the immobilisation of the probe onto the transducer or nanosensor. Two methods were considered: Confocal microscopy and electrophoresis. The latter was chosen due to its availability, easy of use and the DNA probe does not necessary need to be labeled which entails less cost. The Bioanalyzer instrument was used to study the hybridization of the target 16S rRNA and the DNA probe. The bioanalyzer produces electropherograms which, in detail, shows the concentration, purity, type of RNA, ratio of 16S to 23S, RIN and the hybridization peaks. All the above-mentioned parameters play a huge role on the quality of RNA. A baseline electropherogram was achieved with a Mycobacterium Tuberculosis control RNA as shown in Figure. 5.2.

#### 5.3.2.1 Experimental procedures

The NanoDrop 8000 Spectrophotometer and the Agilent Bioanalyzer RNA Nano Assay kit were used to assess the quality and integrity of the bacterial RNA samples.

#### 5.3.2.2 NanoDrop

RNA concentration and quality were determined using the NanoDrop 8000. Concentration of each sample was measured after blanking with 1.2 $\mu$ L of water. Both pedestals were wiped with a lint free paper and 1.2 $\mu$ L of sample was placed and measured. This was repeated until all samples had been measured.

#### 5.3.2.3 Bioanalyzer

RNA samples, control RNA and the Agilent RNA Nano Ladder were heat denatured at 70°C for 2 mins in a thermal cycler. These were then placed immediately on ice after a brief spin. After priming the chip on the chip priming station with Agilent RNA Nano gel-dye mix, 5 $\mu$ L Agilent RNA Nano Marker was added to all wells including the ladder well. 1 $\mu$ L of sample was then added to respective wells and the ladder (1  $\mu$ L) to the ladder well. The chip was vortexed with the IKA vortexer for 1 min at 2400 rpm and run in the Agilent 2100 Bioanalyzer.

Two sets of samples were prepared for the bioanalyser: one batch of samples was hybridized at room temperature while the other batch of sample set was hybridized at 52 °C for two hours. The experiments were conducted using RNA different concentration ranging from 50 to 100 ng/ $\mu$ L with increaments of 5 ng/ $\mu$ L, this was adapted from the baseline concentration or the Mycobacterium Tuberculosis control RNA as shown in Figure. 5.2. One should keep in mind that the bioanalyzer was not used to determine the limit of detection (LOD),

it was used to confirm that the hybridization process did take place between the DNA probe and the RNA target. The bioanalyser was used to annotate different samples under different conditions to eliminate any ambiguity, the conditions are listed in Table. 5.2 below. These sample conditions were tested in two different temperature zones.

Room temperature -2 hrs	52°C -2 hrs
RNA + Probe	RNA + Probe
RNA + TE(Tris-EDTA) buffer	RNA + TE buffer
RNA + RNase-free Water	RNA + RNase-free Water

Table 5.2: The sample conditions in which the bioanalyzer was used to annotate. These sample conditions were tested in two different temperature zones: at room temperature and at 52, 57 and 62 °C.

Different sample conditions under different temperatures annotated using the bioanalyser will produce different electropherograms. This means that the electropherogram for RNA and Probe hybridised at 52, 57 and 62 °C will not exhibit the same characteristic curves for RNA in water and Tris-EDTA buffer at 52 °C and at room temperature.

## 5.4 Results And Discussions

Thirty-two (32) Bacterial (*Mycobacterium tuberculosis*) RNA samples were analysed using the Agilent Bioanalyzer Prokaryote Total RNA Nano Assay and Nanodrop 8000 Spectrophotometer, see Appendix E . A base line or a control mycobacterium tuberculosis RNA electropherogram was first determined as shown in Figure.5.2. This serves as a baseline for none-hybridised RNA. As mentioned before, some of the RNA samples were incubated in TE(Tris-EDTA) buffer and RNase free water buffer. For both incubations in TE(Tris-EDTA) and RNase free water, the results are shown in Figures. 5.3 and 5.4. It is easily observable that there are no distinctive curve shifts for both buffers. When both TE and water incubated RNA electropherogram curves are compared with the base line electropherogram, they show no curve shifts. The curves are still reaching a highest point approximately around 1750[nt] for 16S rRNA and around 3800[nt] for 23S rRNA, which is still the same as the curves for the baseline electropherogram.

Another 13 Bacterial (*Mycobacterium tuberculosis*) RNA incubated cDNA samples were prepared and analysed using the Agilent Bioanalyzer Prokaryote Total RNA Nano Assay and Nanodrop 8000 Spectrophotometer hybridized

with the complementary DNA. The tests were carried out in different temperatures: 52 ° Figure 5.5 , 57° 5.6 and 62°. The samples were diluted as 500:1 and 1000:1 for a ratio of RNA to DNA as shown in Figure 5.5 (a) and (b), 500:1 and 100:1 for a ratio of RNA to DNA as shown in Figure 5.6(a) and (b) and lastly a ratio of 600:1 for RNA to DNA as shown in Figure 5.7. The mentioned electropherograms show a different curve response as compared to the base line electropherogram. However this does not necessary entail hybridization, other factors such as RIN number, RNA area and rRNA ratio should be carefully analysed to make a proper conclusion.

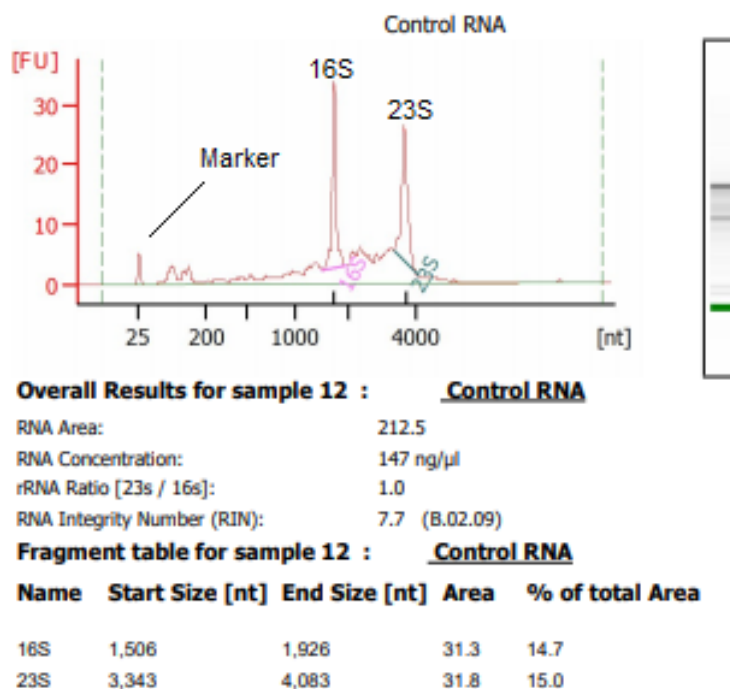


Figure 5.2: A base Electropherogram of the extracted total RNA showing the RNA area,contamination, concentration, RNA ratio and the RNA Intergrity Number(RIN). The electropherogram also shows 3 peaks which depict the maker, 16S rRNA and the 23S rRNA.

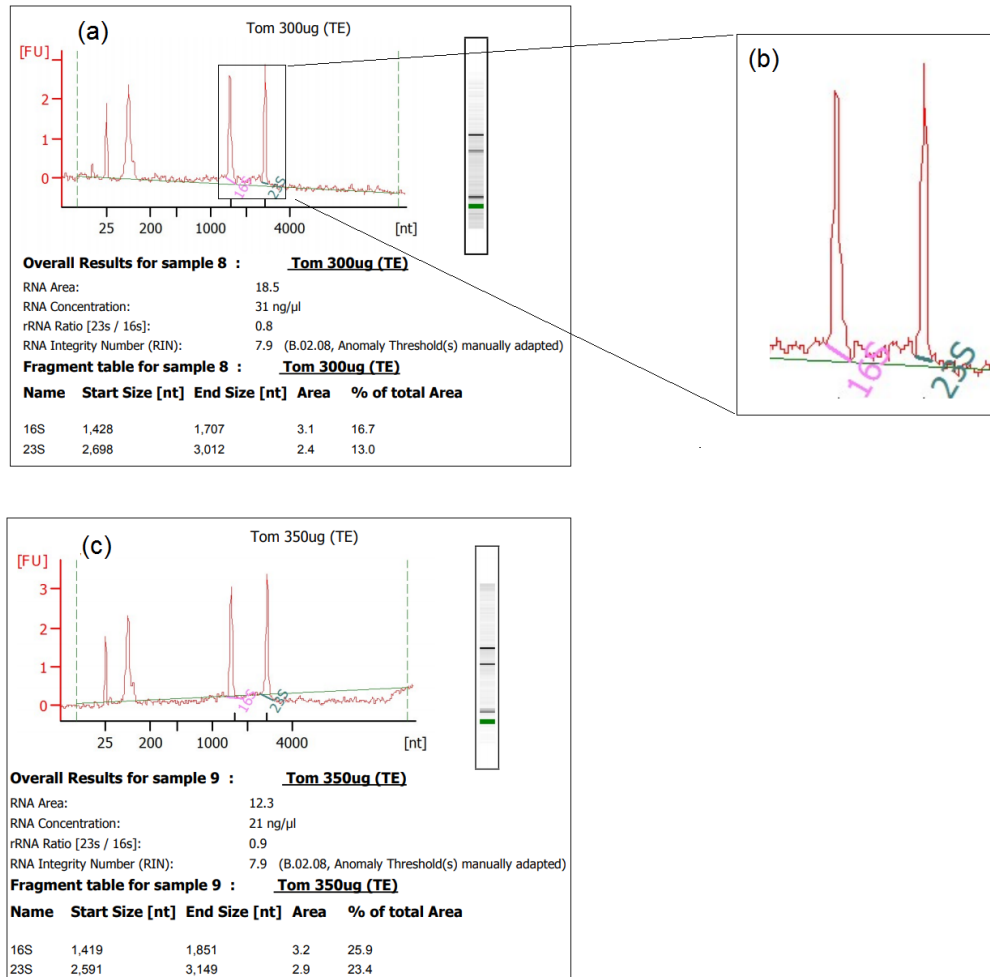


Figure 5.3: Bioanalyzer electropherogram results of the extracted *Mycobacterium tuberculosis* total RNA incubated in TE buffer at room temperature. The incubation was carried out in different RNA concentrations of 31 ng and 21 ng as shown in Figures.5.3(a) and (c) , respectively. The electropherograms show the RNA area,contamination, concentration, RNA ratio and the RNA Integrity Number(RIN) for each concentration. The inset in Figure5.3(b) electropherogram also shows 2 peaks which depict the 16S and the 23S rRNA concentrations.

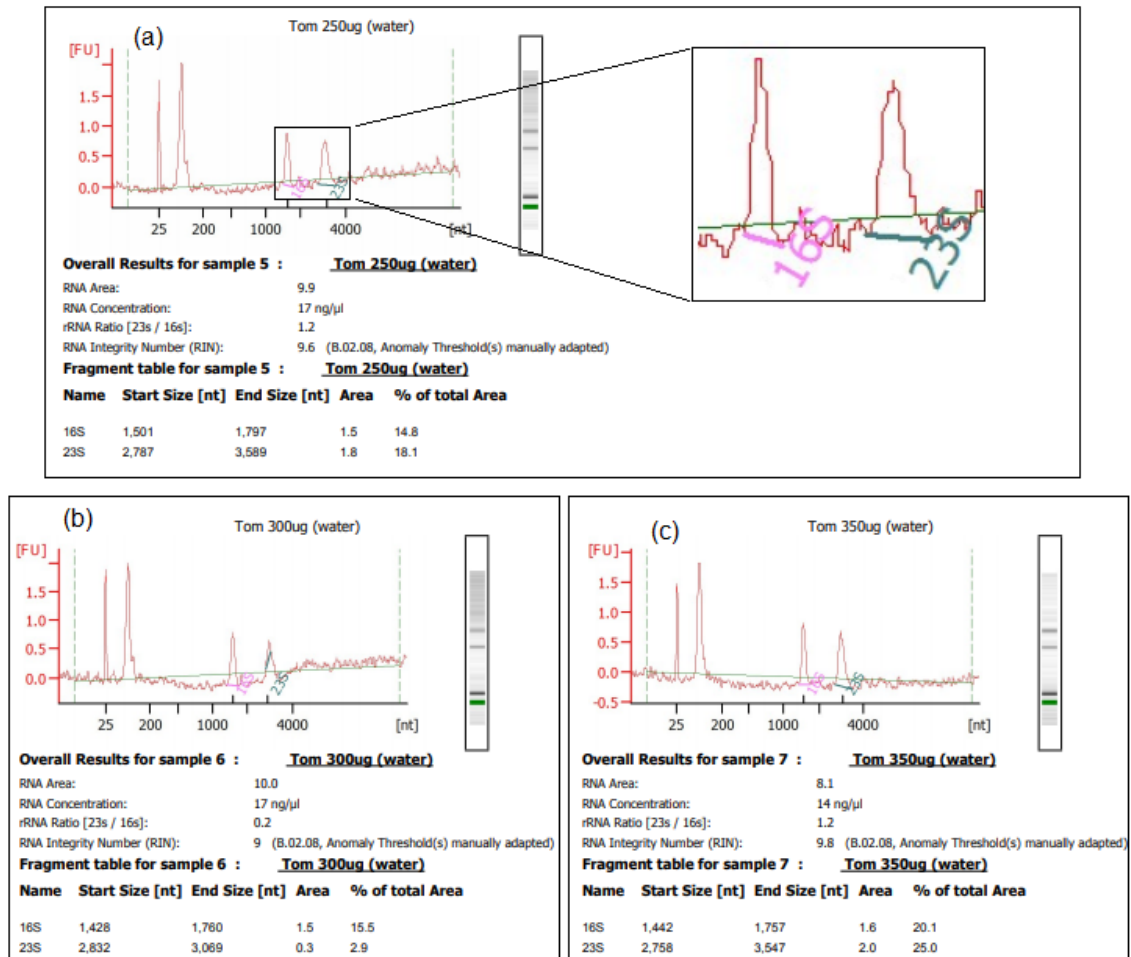


Figure 5.4: A base bioanalyzer electropherogram results of the extracted different concentrations of the *Mycobacterium tuberculosis* total RNA incubated in RNase free-water buffer at room temperature. The incubation was carried out in different RNA concentrations of 17 ng, 17 ng and 14 ng as shown in Figures.5.4(a)-(c) , respectively. The electropherograms show the RNA area,contamination, concentration, RNA ratio and the RNA Intergrity Number(RIN) for each concentration. The inset in Figure5.4 electropherogram also shows 2 peaks which depict the 16S and the 23S rRNA concentrations.

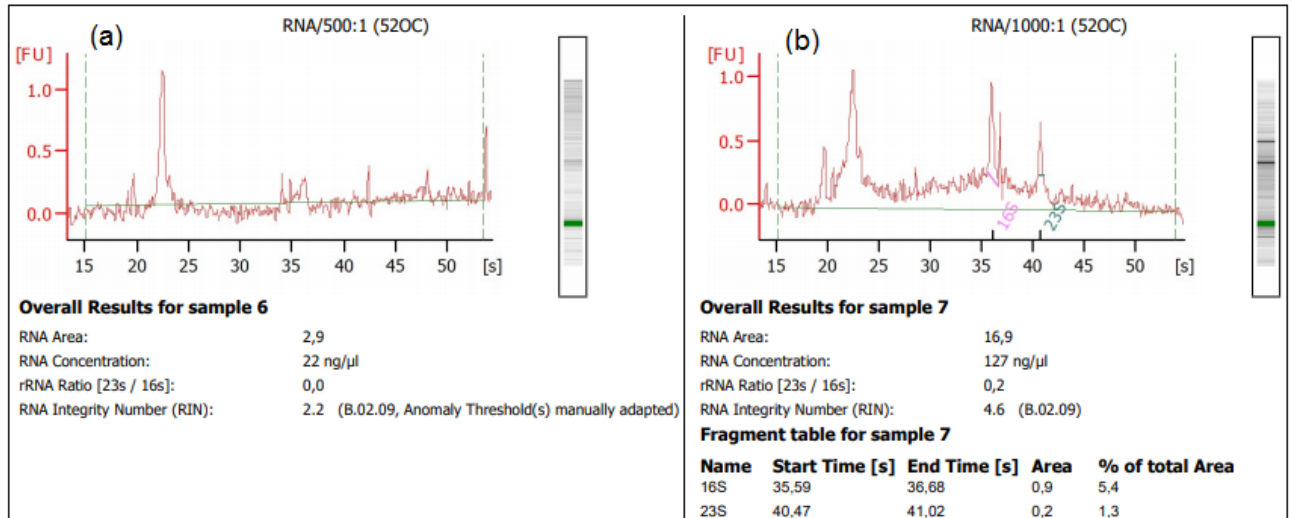


Figure 5.5: Bioanalyzer electropherogram results of the the cDNA probe incubated with the total RNA at different concentration ratios. the dilution ratio was 500:1 and 1000:1 as shown in Figures 5.5(a) and (b), respectively. The incubation was carried out in different RNA concentrations of 22 ng and 127 ng as shown in Figures.5.5(a) and (b) , respectively. The electropherograms show the RNA area,contamination, concentration, RNA ratio and the RNA Integrity Number(RIN) for each concentration.



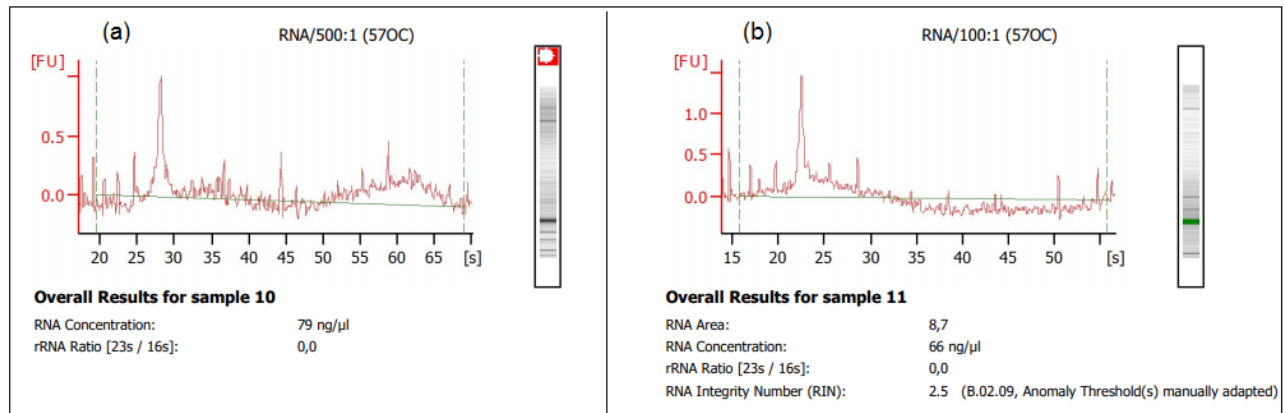


Figure 5.6: Bioanalyzer electropherogram results of the the cDNA probe incubated with the total RNA at different concentration ratios. the dilution ratio was 500:1 and 100:1 as shown in Figures 5.6(a) and (b), respectively. The incubation was carried out in different RNA concentrations of 79 ng/ul and 66 ng/ul as shown in Figures.5.6(a) and (b) , respectively. The electropherograms show the RNA area,contamination, concentration, RNA ratio and the RNA Intergrity Number(RIN) for each concentration.

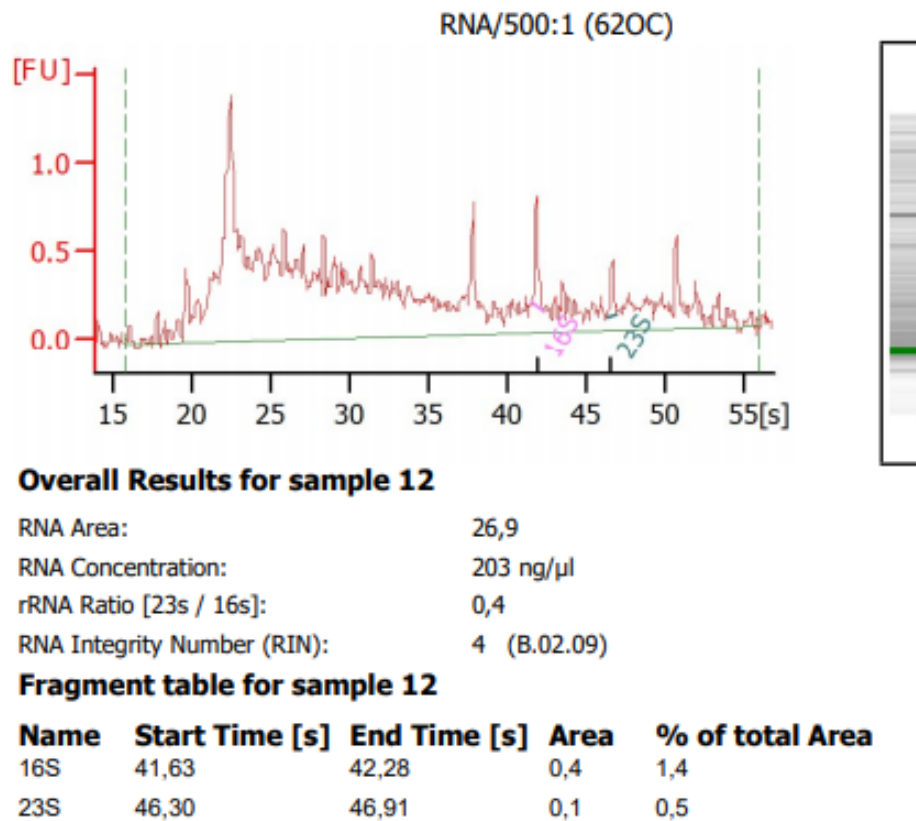


Figure 5.7: Bioanalyzer electropherogram results of the the cDNA probe incubated with the total RNA at a concentration of 203 ng/ul. The dilution ratio was 500:1 as shown in Figures 5.7. The incubation was carried out in different RNA concentrations of 203 ng/ul and . The electropherogram shows the RNA area,contamination, concentration, RNA ratio and the RNA Intergrity Number(RIN) for each concentration.

## 5.5 Conclusion

The bioanalyzer was successfully used for the analysis of the hybridization process between the DNA probe and an RNA target sequence. The bioanalyzer results confirmed that the DNA probe was successfully designed and manufactured to be specific and complementary to the 16S rRNA target sequence as it could hybridize with the complementary 16S rRNA target sequence. In other words, the 57 base pair probe demonstrated rather a fairly high specificity for the target. The electropherograms showed the same results for RNA incubated in TE and water buffers when compared to the baseline results. While, the electropherogram for the RNA probe incubated with the DNA probe in TE buffer was distinctively different. The distinctive shift in the electropherogram curves entails hybridization. During the process of characterisation some of the samples were degraded, such as the samples hybridized at 57° due to poor a RIN number. However, samples hybridized at 52 ° and 62 ° showed a promising level of success with partial degradation as well. The samples hybridized at 62 ° has an RIN number of 4 and 4.6 respectively, which is also poor. A good RIN should be between 7 and 10. comparing an RIN of 2.5 and an RIN of 4.6, that is almost a twice as much. And this evidence suggest that a temperature of 57° allowed high levels of successful hybridization with partial degradation as well.

## Chapter 6

# Data Capturing and Refining Electronics

### 6.1 Introduction

This chapter focuses on the design of the output circuitry for the biosensor. Without the output circuitry, the data from the biosensor would not make sense to the end-user. In general, the output voltage or current of the nanosensor is not easily understandable, hence a data refining circuitry has to be designed and built. As discussed in the previous chapters, the nature of the nanosensor voltage consist of several peaks, impulse like curves, of different amplitude and duration. These electronic circuits are designed to convert the impulse-like curve into a DC voltage. There are different circuits that can do this conversion with ease. However, in this project only a full bridge rectifier is investigated together with a driving microcontroller circuit. Each circuit is designed and simulated using LTSpice, which is a simulation tool for electronic and electrical circuits.

### 6.2 Simulation of Data Refining Circuitry

This section highlights the purpose of simulating circuits before building the actual practical circuits. In this project, LTSpice is used to simulate and execute the output circuitry in order to predict their behaviour under certain circumstances. Simulating circuits enables the designer to minimize the room of errors, improve the circuit efficiency and accuracy, demonstrate physical concepts and also optimize the circuit for excellent results before the system is actually built. The first circuit to be simulated is the equivalent circuit of the nanosensor, then the full bridge rectifier and lastly, the microcontroller driving circuit.

### 6.2.1 Ideal Piezoelectric Nanogenerator Equivalent Circuit

The first simulated circuit was of the nanosensor itself. An equivalent diagram of the nanosensor is designed and modelled as shown in Figure. 6.1. The purpose of designing, modelling and simulating the nanosensor is to imitate the piezoelectric response of the ZnO nanosensor in order to study and investigate how the other circuits would respond. the circuit is modeled with a voltage source in series with a resistance  $R_{in}$  and capacitance  $C_{in}$ . The input resistance,  $R_{in}$ , serves as the total resistance of all the ZnO nanowires inside the nanosensor. On the other side, the input capacitance,  $C_{in}$ , serves as the total capacitance in-between the the two conducting electrodes, meaning between the gold-plated silicon substrate and the top gold electrode.

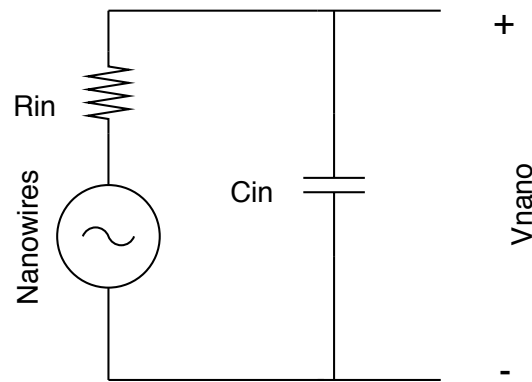


Figure 6.1: An equivalent circuit diagram of the nanosensor modeled with a voltage source in series with an input resistance and an input capacitor. The equivalent circuit is modeled to resemble a nanosensor on a rigid substrate.

The circuit was simulated to imitate a rigid nanosensor, meaning that the voltage response of the nanosensor has to have peaks that are positive. The simulated output voltage shows ideal peaks of about 270 mV as shown in Figure. 6.2. Compared to the actual piezoelectric response of the nanosensor shown in Figures. 4.5(a) and (b) there is no difference in the nature of the signal. Further supporting information can be found in Appendix blah blah.

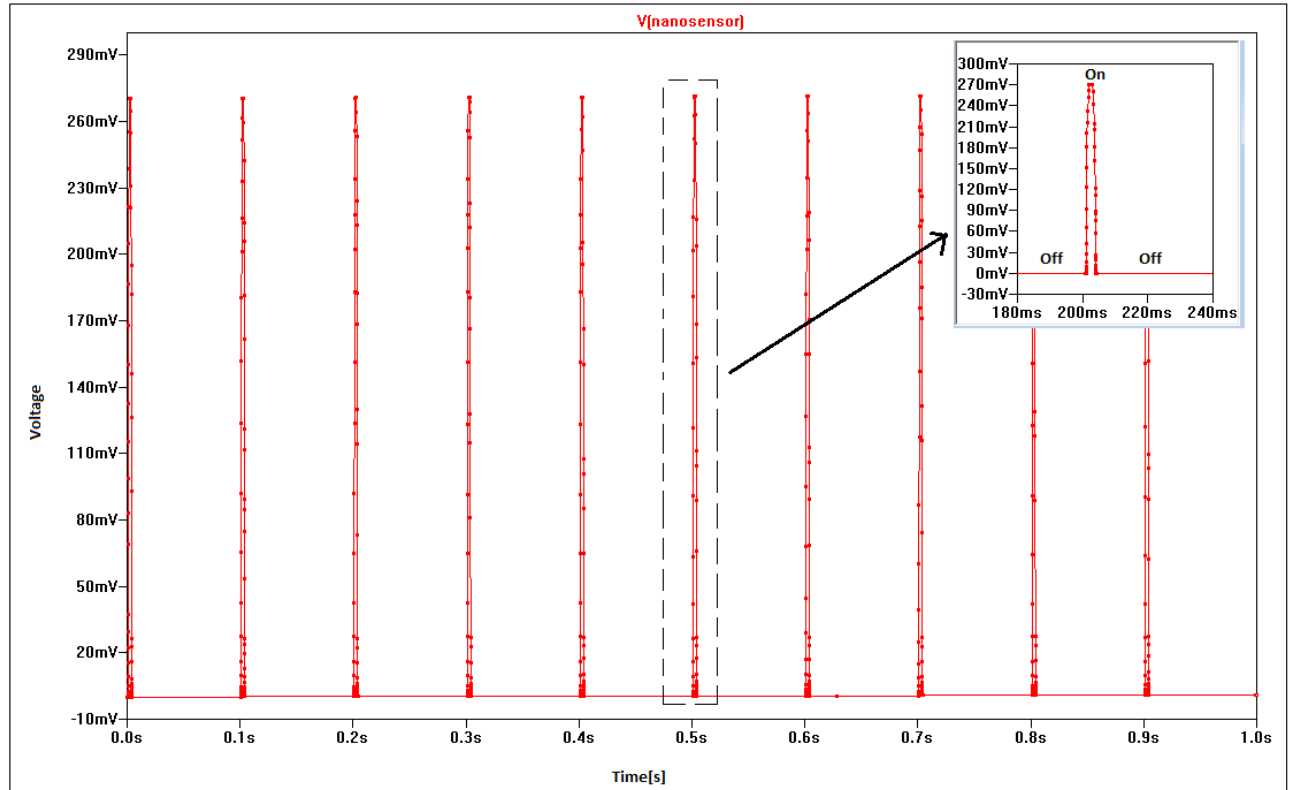


Figure 6.2: A simulated output voltage of the equivalent nanosensor circuit. The inset shows the magnified voltage of the nanosensor and also shows the "On" and "Off" states.

### 6.2.2 Simulation of a Rectifying Circuit

The second designed and simulated circuit was the full-bridge rectifier, as shown in Figure. 6.3. for the purpose of circuit behavioural investigation, the equivalent nanosensor circuit is used as the input source of voltage for the full bridge rectifying circuit. In this project, the full bridge is used to convert the impulse-like voltage signal from the nanosensor into a DC voltage. This means that the main goal is to get DC voltage signal irregardless of the magnitude of the nanosensor voltage. The DC voltage increases to a specific magnitude as long as the input voltage is supplied and the output capacitor charges. The full bridge conducts the input current along two paths through the switching of diode with respect to the input current. In other words, during a specific cycle (whether positive or negative cycle) only two diodes will switch "on" and the other two will be "off". The full bridge rectifier was chosen for only one reason : to fully rectify the signal, as the actual signal may sometimes contain negative values depending on the contact between the top electrode and the ZnO nanowires.

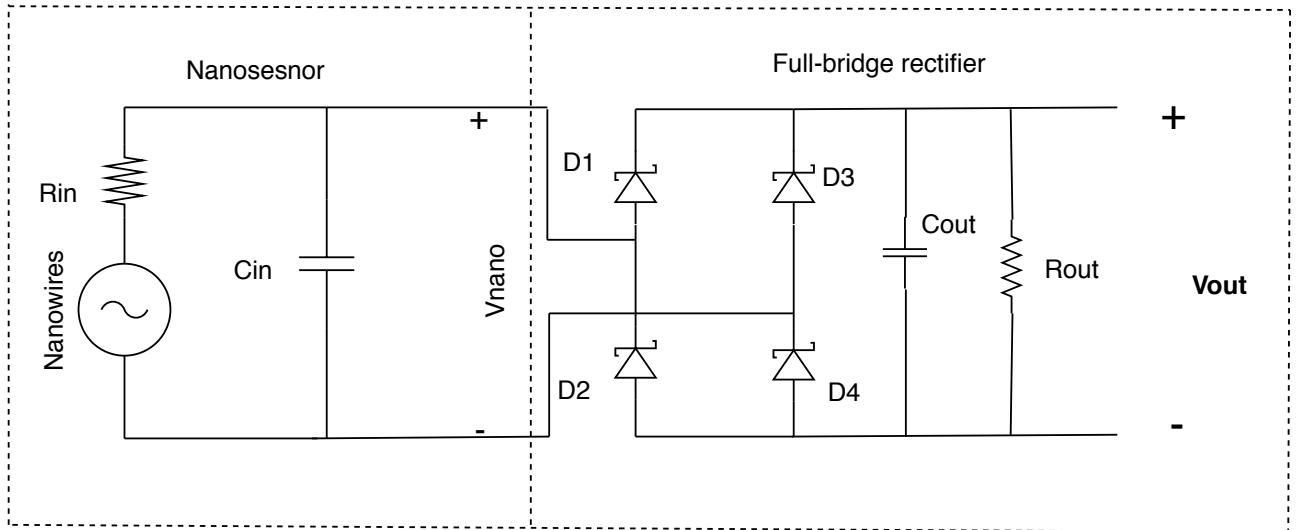


Figure 6.3: A circuit diagram of a full bridge rectifying circuit with the nanosensor circuit diagram connected as an input source of voltage. The Purpose of the rectifying circuit is to scavenge power from the nanosensor and convert it to a DC voltage.

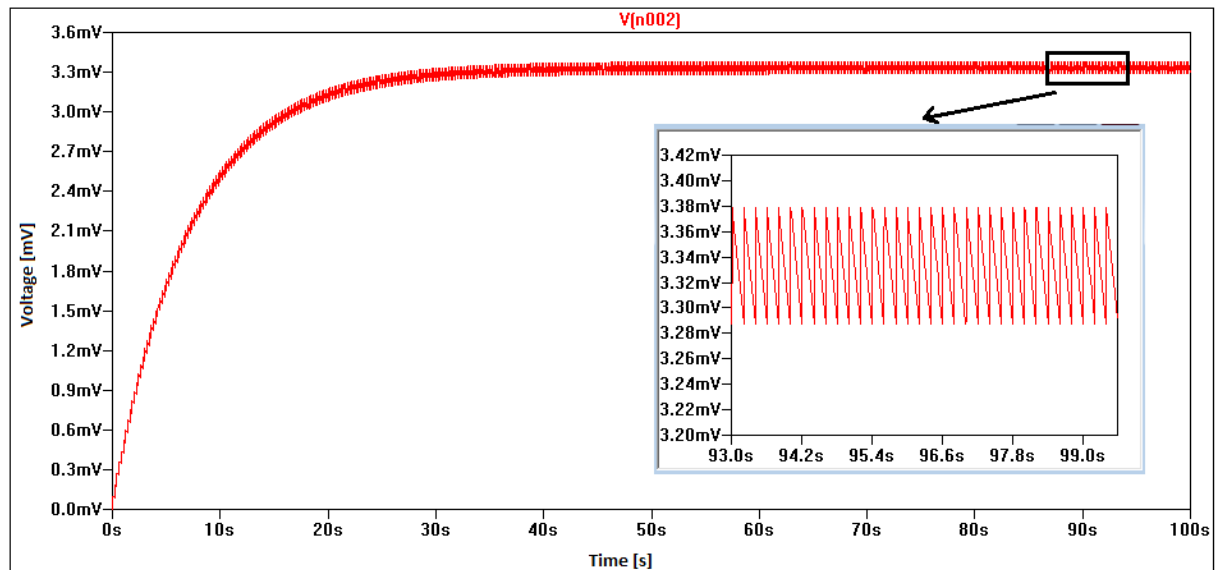


Figure 6.4: A simulated voltage output of the full bridge rectifying circuit with the nanosensor circuit diagram connected as an input source of voltage. The output capacitor charges and it reaches a steady state after 25 seconds of 3.33 mV DC and the ripple voltage is about  $81.6\mu\text{V}$  as shown by the inset.

A simulated voltage output of the full bridge rectifying circuit, shown in Figure. 6.4. The curve reaches a steady state voltage of 3.33 mV DC after 25 seconds and the ripple voltage is about  $81.6\mu\text{V}$  as shown by the inset. This curve shows that it is possible to convert the nanosensor impulse-like curves into a DC. Now that the voltage is in DC form, it can be used as an input to the driving microcontroller circuit to process and refine it further.

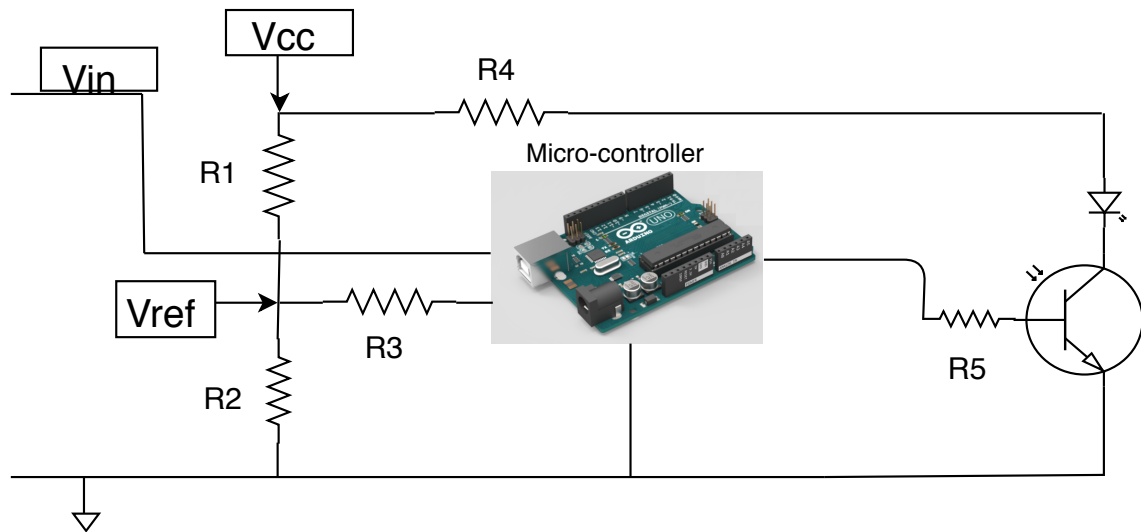


Figure 6.5: A circuit diagram of a driving circuit with a microcontroller. This circuit is used to interpret and make sense the processed data from the rectifying circuit and provides easy end-user interface.

A circuit diagram of a driving circuit with a microcontroller, shown in Figure. 6.5 above. This circuit is used to process and interpret data coming from the rectifying circuit and also it provides easy end-user interface. The circuit works in way that it compares the input and reference voltage and if the input voltage is greater than the reference voltage then the LED switches on and the results are displayed on the LCD.

After a limit of detection (LOD) for the biosensor have been found. The reference voltage is calculated as a result of the biosensor LOD. Furthermore, the input DC voltage from rectifying circuit will be compared to the reference voltage using the microcontroller. In simple word, this means that the circuit will check if the reference voltage is greater or less than the input voltage from the rectifier or vice-versa. Figure 6.6 below shows the full circuit connections, with the equivalent circuit replaced with a crystal oscillator.



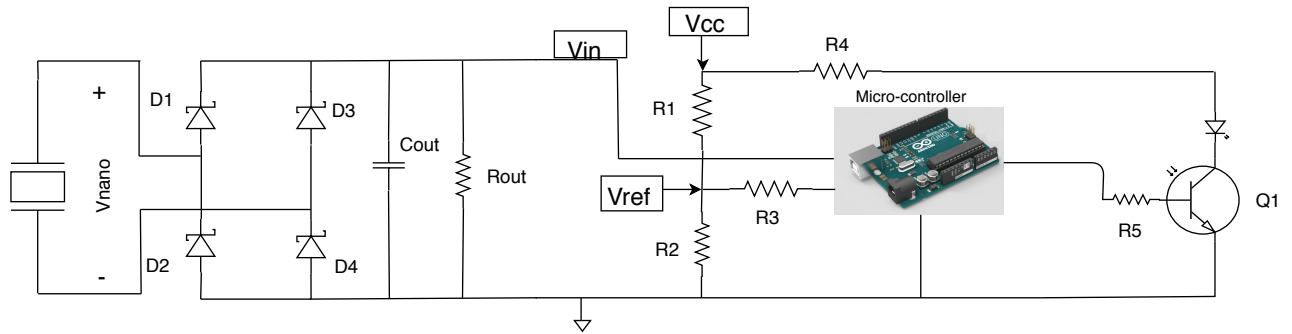


Figure 6.6: A full circuit diagram for data capturing and refining used for the biosensor.

### 6.3 Practical Circuitry

As stated before that the simulated circuits enabled the designer to minimize the room of errors, improve the circuit efficiency and accuracy, demonstrate physical concepts and also optimize the circuit for excellent results before the system is actually built. However, simulations have a number of parameters that are not taken into consideration such as heating, resistor and capacitor tolerances, and power loss. These factors will have a major impact on the practical circuits. All the simulated circuits, except the equivalent nanosensor circuit, were built, shown in Figure 6.7, with components purchased from RS components.

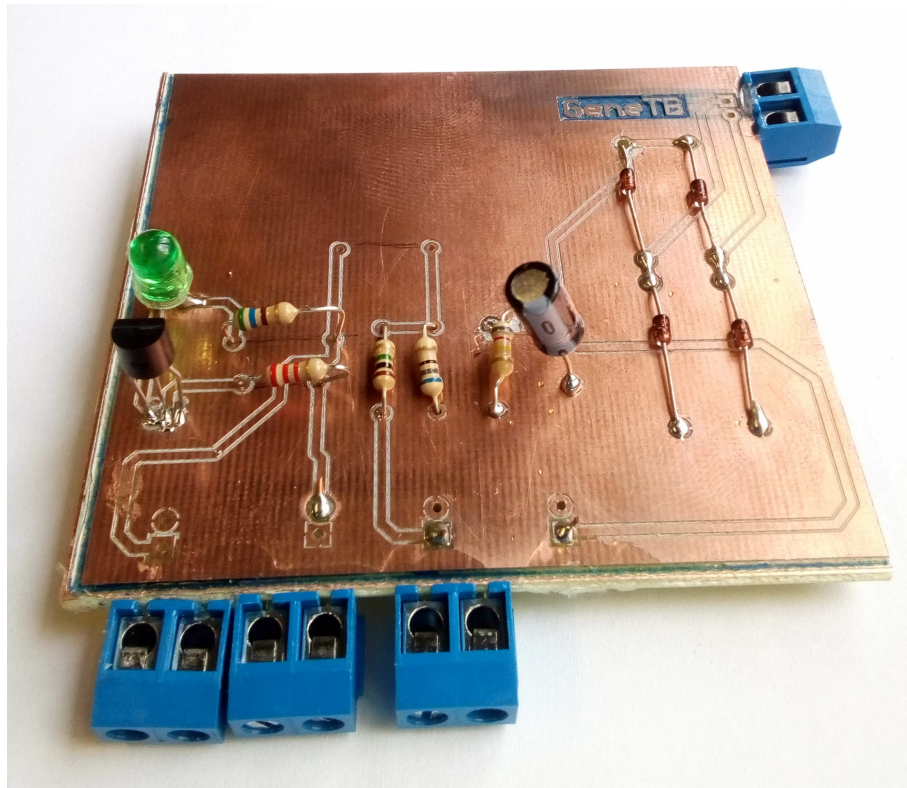


Figure 6.7: A built practical circuit for data capturing and refining used for the biosensor.

### 6.3.1 Rectifying Circuit

The full-bridge rectifier was built using the circuit designed and simulated in the previous section, see Figure. 6.4. The through-hole BZX55C-3V3 Zener diodes were used for the full bridge connection. A resistance and capacitance of  $850\text{ k}\Omega$  and  $10\text{ }\mu\text{F}$ , respectively were used as a load. Figure. 6.8 below, shows the measured output voltage of the rectifying circuit. The nanosensor was put under a constant pressure for 2 minutes and the output voltage was measured, across the load impedance. The measurements were recorded under a  $10\times$  probe, with a time scale of 5 seconds per division and a voltage scale of  $20\text{ mV}$  per division for the sinusoidal signal. For the nanosensor, the measurements recorded under the same probe and time scale, however, the only difference was the voltage division which was  $1\text{ mV/div}$ . The voltage is quite stable if there no other vibrations around the nanosensor. External vibrations may lead to incorrect data interpretation due to high level of noise that will contribute and generate a piezoelectric voltage from the nanosensor.

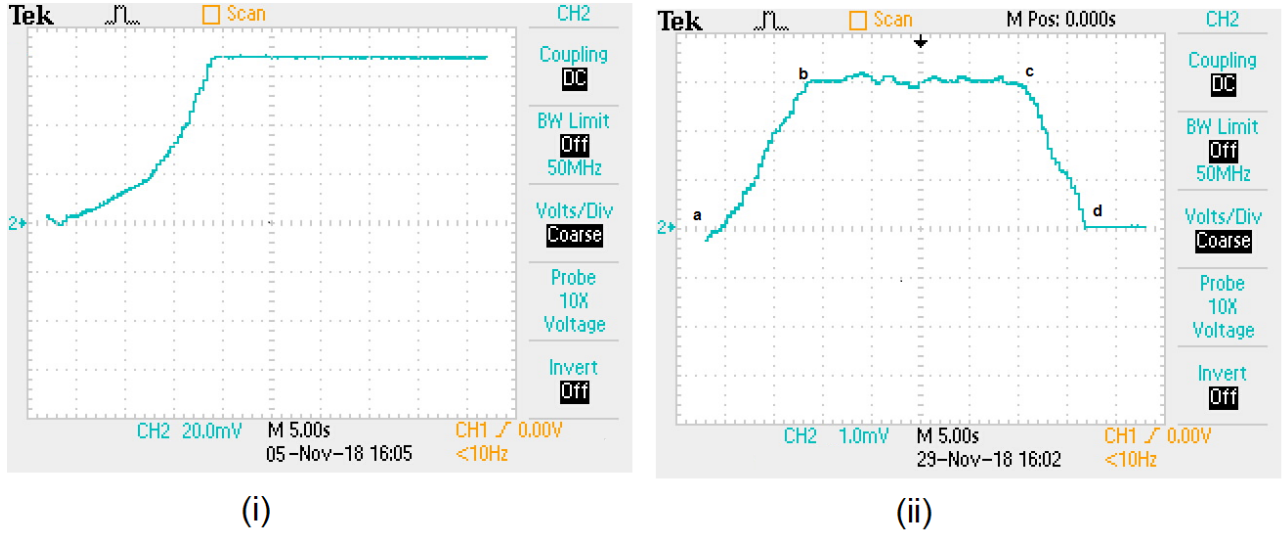


Figure 6.8: A measured output voltage of the full bridge rectifying circuit. Figure 6.8 (i) shows that the input signal can be rectified by the scavenging circuit using a sinusoidal input voltage. Figure 6.8(ii) shows the charging capacitor (curve: a-b), the fully charged capacitor (curve: b-c) and the discharging capacitor through the load resistance (curve: c-d) due to change in input piezoelectric voltage.

The rectified measured output voltage of the sinusoidal input exhibits a more constant DC value as compared to the output signal for the nanosensor. The reason for the latter, is that the nanosensor does not in reality have a constant amplitude as compare to the sinusoidal input. To avoid such inconsistency, a larger load capacitor has to be used[80].

### 6.3.2 Microcontroller-Driving Circuit

An LED driving circuit was also built from the designed and simulated circuit shown in Figure. 6.5. The Arduino microcontroller was used to process the data from the two inputs,  $V_{in}$  and  $V_{ref}$ .  $V_{ref}$  is a DC supplied voltage and  $V_{in}$  is a DC voltage form the rectifier. These voltage inputs are compared by the Arduino and then drives the transistor-LED circuit accordingly. The Arduino drives the KSP 2222A transistor, which works as a switch for the LED and the LED will turn on or off with respect to transistor acting as an "on" or "off" switch. Figure 6.9 shows the measured voltage across the led when its switching on and off.

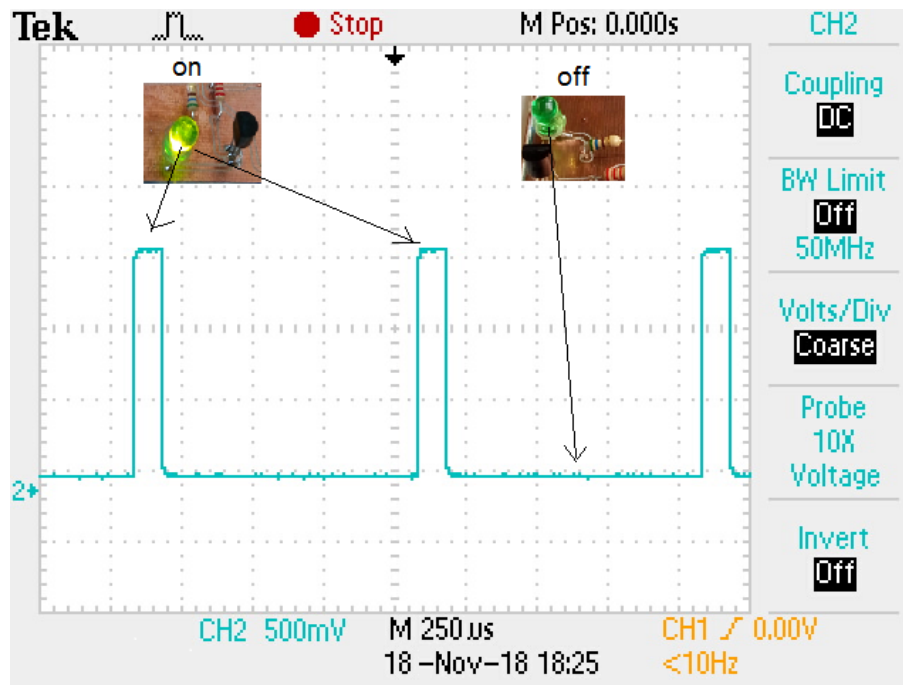


Figure 6.9: A measured output voltage across the LED when switching "on" and "off" as shown by the insets.

This circuit works on a simple concept: if the input voltage,  $V_{in}$ , is greater than the reference voltage,  $V_{ref}$ , then the arduino commands the transistor to switch "On", meaning driving it to the saturation region (act as a short circuit). Then the negative side of the LED will be connected to ground and switch "On". The opposite will happen if the transistor acts as an open circuit.

### 6.3.3 Conclusion

A data refining electronic circuit was successfully designed, simulated and built. The electronic circuit consisted of two parts: the full bridge rectifier and LED driving circuit. The full bridge circuit was successfully used to convert the impulse-like signal into a DC voltage signal for better and improved data interpretation. Secondly, the LED driving circuit was successfully used to process the data from the rectifying circuit and refine it further using the Arduino microcontroller.

The main purpose of designing and building the data refining electronics is to make data acquisition and interpretation way more easy for the end-user. Meaning that the end-user must be able to use the devices without intense training or deeper knowledge of the concepts behind the device. Visualisation displaying components, such as LCDs and LEDs, makes it easier for the end user to interpret processed data.

## Chapter 7

# ZnO nanowire-array biosensor construction for the detection and quantification of tuberculosis

### 7.1 Introduction

Immobilization of DNA probes is one of the most important and thought-provoking step when developing biosensors as the molecules are in close contact with surface which may alter or inhibit their biological activity. This chapter focusses on the immobilization of biotinylated probe through the streptavidin-biotin interaction as mentioned before. This chapter firstly focuses on the formation of biotin-self assembled monolayers on gold surfaces. Secondly, the coating of streptavidin after the formation of biotin-SAMs and lastly the immobilization of the biotinylated-Probe on streptavidin-biotin layer to conclude the manufacturing of the biosensor.

### 7.2 Materials And Methods

#### 7.2.1 immobilization of Biotin-SAMs on Nanosensor Surface

After the manufacturing of the nanosensor (details in Chapter 4), the next step was to immobilise a functional group on the surface of the sensor. The nanosensor was cleaned thoroughly with a Piranha solution prior to preparing any SAM solutions. Piranha solution was prepared with sulfuric acid and hydrogen peroxide with a 3:1 ratio, respectively. The preparation of the biosensor was only possible if there is an intermediate layer between the gold layer and the biotinylated-probe to prevent biological material from denaturing and losing their functionality.

CHAPTER 7. ZNO NANOWIRE-ARRAY BIOSENSOR CONSTRUCTION FOR THE DETECTION AND QUANTIFICATION OF TUBERCULOSIS **92**

The Biotin SAMs were prepared using the Biotin-SAM Formation reagent purchased from Sigma Aldrich. The preparation of the biotinSAMs is easy and straight forward. The following steps detail the protocol used for the formation of biotin-SAMs on the nanosensor[81]:

- 1 ml of ethanol was added to a 1  $\mu$ mol biotin -SAM formation reagent tube, pipetted and ultrasonicated at 25 °C to dissolve the reagent to make a solution of 1 mmol/L Biotin-SAM.
- Then the solution was diluted 10-fold with ethanol. This means that 9 parts of ethanol were dissolved in 1 part of the solution.
- The nanosensor with a 40 nm thin layer of gold was then immersed in the solution for 2 hours.
- After 2 hour2, the nanosensor was cleaned 4 times with ethanol and DI-water respectively.
- Then the Biotin-SAM-coated nanosensor was stored under nitrogen gas in a tightly sealed glass container at 5°C.
- Then the nanosensor with biotin-SAMs was characterised using FTIR spectroscopy..

Figure 7.1 show the FTIR spectrometer for the solution of biotin. Since Biotin-SAMs were prepared with ethanol as a solvent, the spectrometer also shows peaks for the OH group found in alcohol (blue area). The spectrometer also shows the peaks for Biotin (orange area). This means that the spectrophotometer peaks can easily be identified and verified as that of the OH and biotin.

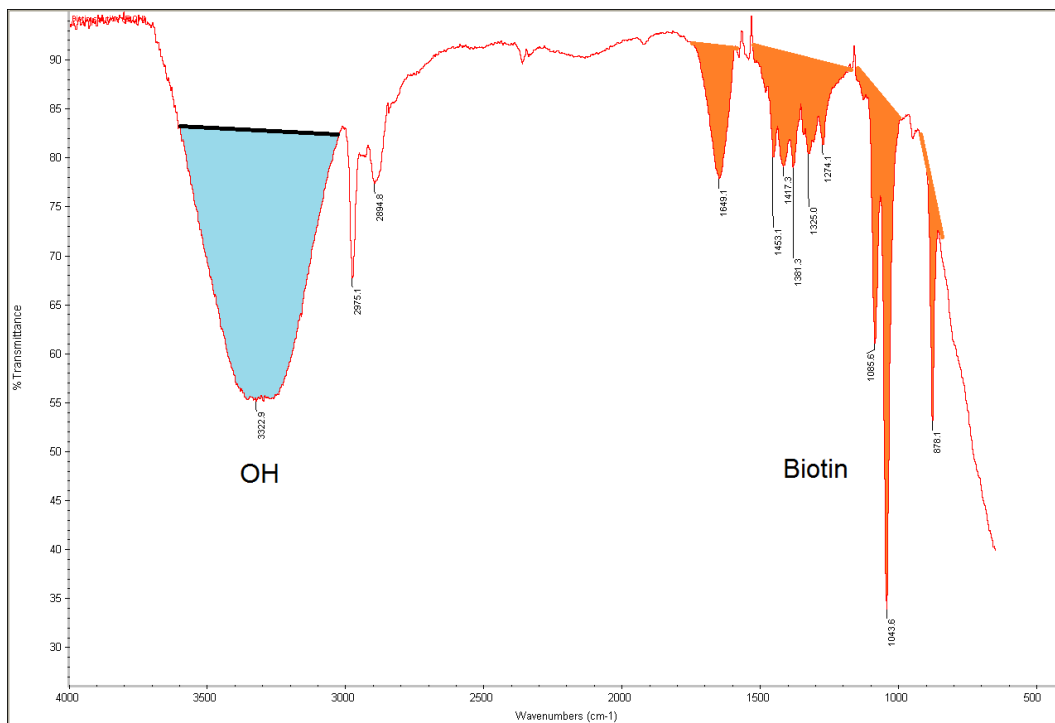


Figure 7.1: An FTIR spectrometer for biotin-SAMs solution. The SAMs solution is not yet immobilised onto the nanosensor gold surface. Since the Biotin -SAMs were prepared with ethanol as a solvent, the spectrometer also shows the OH group (blue) and the biotin (orange).

After reviewing and studying the biotin- SAM solution spectrophotometer, the gold surface was also studied with the FTIR and used as a reference point and as a results Figure 7.2 shows the spectrophotometer. There was a huge difference on the peaks between the spectrometer for biotin solution and the gold thin film. After the confirmation of the biotin-SAM solution and gold spectrophotometers, the next step was to immobilise the biotin-SAM onto the substrates.

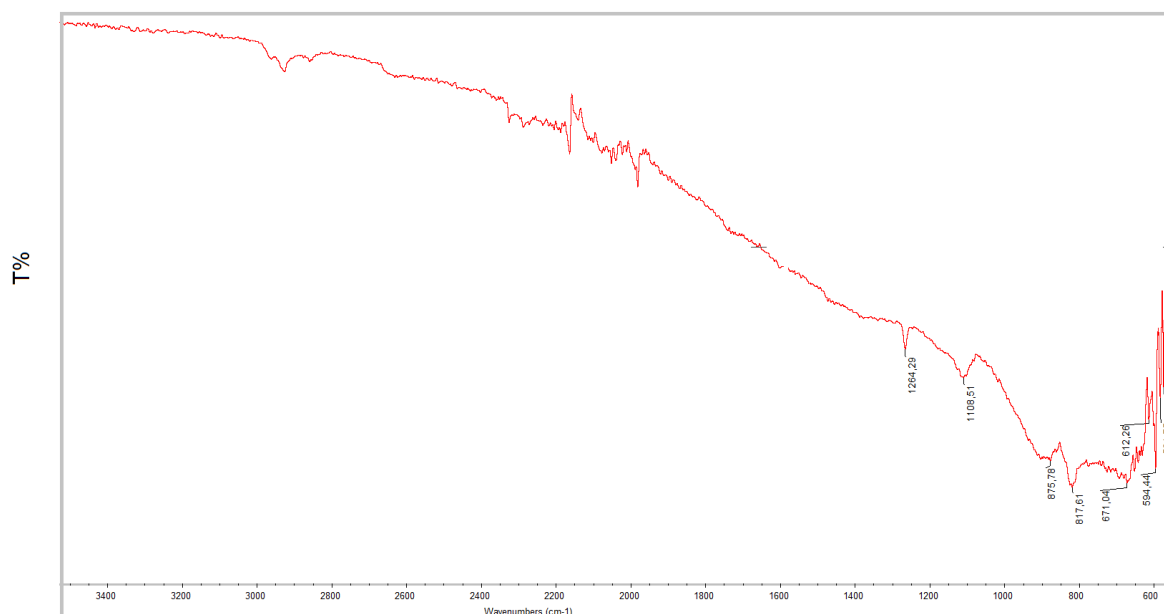


Figure 7.2: An FTIR spectrophotometer for a gold thin layer. This is included just for reference. The gold layer has not yet been immersed into the SAM solution for biotin immobilization.

After the gold-plated-substrates were immersed in the biotin SAMs as described above. They were also studied using an FTIR unit at Chemistry department. Figure 7.3 shows the spectrometer for biotin-SAMs bound to a thin gold layer. The major spectrometer peaks can be easily identified and verified. This confirms that biotin was bound to the gold surface, as the FTIR unit could pick it up and analyse it from the substrates. The FTIR analysis was used repeatedly and extensively to verify these results. And they were all the same results, the major spectrometer peaks for NH, OH, H-C=O and C-H are  $1646.16\text{ cm}^{-1}$ ,  $3326.79\text{ cm}^{-1}$ ,  $2323.82\text{ cm}^{-1}$  and  $821.84\text{ cm}^{-1}$ , respectively.



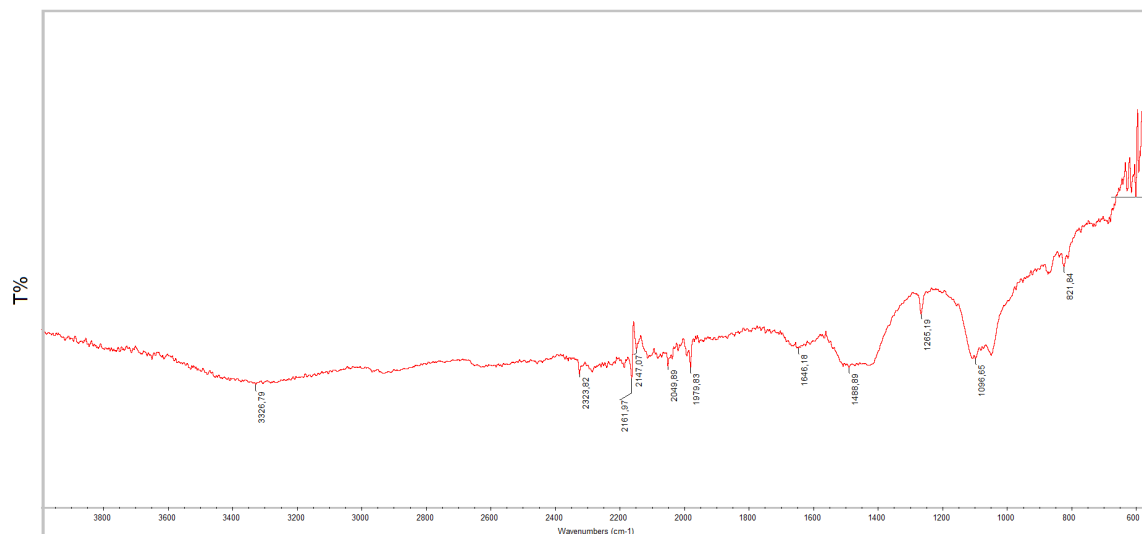


Figure 7.3: An FTIR spectrometer showing the immobilization of Biotin-SAMs on the gold surface of the nanosensor. The major spectrometer peaks can be easily identified and verified. The major spectrometer peaks for NH, OH, H-C=O and C-H are 1646.16  $\text{cm}^{-1}$ , 3326.79  $\text{cm}^{-1}$ , 2323.82  $\text{cm}^{-1}$  and 821.84  $\text{cm}^{-1}$ , respectively.

The biotin-SAM formation reagent is specifically designed to prepare streptavidin-coated biosensors. The biotinylated SAM reagent used for this project proves that it can hold more streptavidin than normally used biotin-SAMs. Now that the immobilization of biotin-SAMs was successful, the coating procedures were applied to the nanosensor itself. The next step was to coat a layer of streptavidin onto the biotin-SAMs.

The nanosensor is a piezoelectric transducer, meaning that the increase in mass of the biomaterial will induce a piezoelectric voltage, known as the direct piezoelectric effect, which can be measured across the full bridge rectifier without connecting a load resistance. The load will be removed because the capacitor will discharge through it. Before the measurements a pre-amplifier (not shown) was built to amplify the nanosensor pulse-like signals by orders of 1000  $\left[\frac{V}{V}\right]$ .

### 7.2.2 Immobilisation of Streptavidin on Biotin-SAMs

After the biotin-SAMs were immobilised onto the nanosensor, a streptavidin solution was prepared by adding 10 mg of streptavidin powder into a tube containing 1 ml of PBS (Phosphate Buffered Saline). Streptavidin was purchased from Sigma Aldrich. The nanosensors with biotin-SAMs were then immersed

in the solution and left overnight at 4 °C for a successful immobilization of streptavidin. After time had elapsed the surface modified nanosensor was removed and cleaned with PBS pH 7.4, DI water and blow dried with nitrogen gas, respectively. The immobilization of streptavidin was studied using the piezoelectric effect of the nanosensor itself and the results are shown in Figures 7.4 and 7.5. This type study will only be successfully confirmed if the pH levels of the solutions are constantly kept as the same as the physiological pH (7.4 pH). The addition of the biotinnylated-antibody onto the nanosensor induced a voltage which can be measured and analysed.

Now that the biological surface modification has been successfully achieved, the next step was to immobilise the biotinylated probe on top of the interface layer (biotin-streptavidin). Biological surface modification, such as biotin-streptavidin biological layer, helps to prevent the probe from denaturing, hence losing its biological properties and functionality.

### 7.2.3 Immobilisation of Biotinylated Probe on Biotin-Streptavidin Layer

The biotinylated probe was changed from DNA to an antibody due to unforeseen circumstances. The manufactured biotinylated-DNA came in very small amounts and were only used for the Bioanalyzer results. To acquire the DNA probes it takes about 7-8 weeks from manufacturing to delivery. A substitution biotinylated probe was used as a proof of concept, which is the biotinylated-anti-Luteinizing Hormone  $\beta$  capture probe. It was used to show whether the biosensor works or not. The biotinylated antibody, with a concentration of 0.65 mg/mL, was purchased from Novus Biologicals and was readily available in our nanolab for instant use.

After streptavidin was immobilised onto the sensor surface the next step was to immobilise the biotin-anti-Luteinizing Hormone  $\beta$  probe. The biotinylated-antibody solution was further diluted with PBS to make concentration of 15  $\mu\text{g/mL}$  before immobilization. Then 15  $\mu\text{g/mL}$  the biotinylated-antibody solution was pipetted onto the nanosensors with a layer of biotin-streptavidin. This was left in a desiccator for 3-5 hours for a successful immobilization. After the time had elapsed the surface modified nanosensor was removed and cleaned with PBS (pH 7.4), DI water and gently blow dried with nitrogen gas, respectively. The immobilization of the probe was studied using the piezoelectric effect of the nanosensor itself and results are shown in Figures 7.4 and 7.5. The addition of the biotinylated-antibody onto the nanosensor induced a voltage which can be measured and analysed. With emphasis, this type study will only be successfully confirmed if and only if the pH levels of the solutions are kept the same as the physiological pH (7.4 pH). Immobilisation of the probe is the final step and it concludes the manufacturing of the biosensor.

During immobilization of streptavidin and biotin-anti-Luteinizing Hormone

$\beta$  (capture antibody), the nanosensor piezoelectric voltage was measured to record the changes from one stage to the next. Secondly, the voltage was also measured across the full bridge rectifier to verify the voltage changes. Figures 7.4 and 7.5 show the resulting voltages due to immobilization of streptavidin and biotinylated-probe onto the nanosensor.

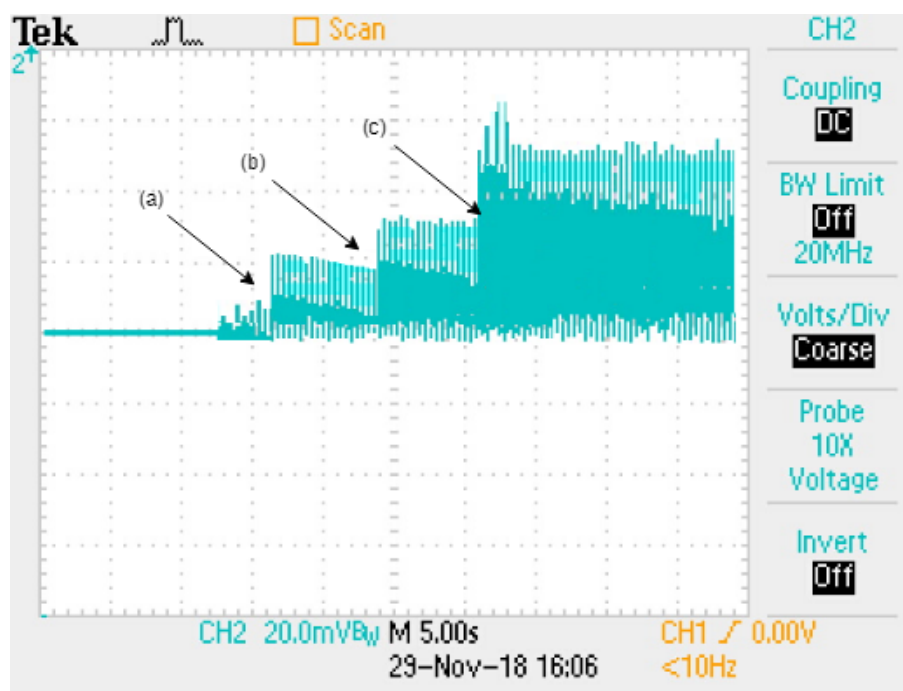


Figure 7.4: A measured piezoelectric voltage responses during the immobilization of streptavidin and biotinylated-probe. The increase in mass bends the nanowires and induce a piezoelectric voltage. During the immobilization step, PBS was first introduced as a control(a), then a solution of streptavidin was introduced (b) and lastly the biotinylated probe(c) was introduced. The voltage spikes before the incubation of PBS are due to the immobilised Biotin-SAMs.

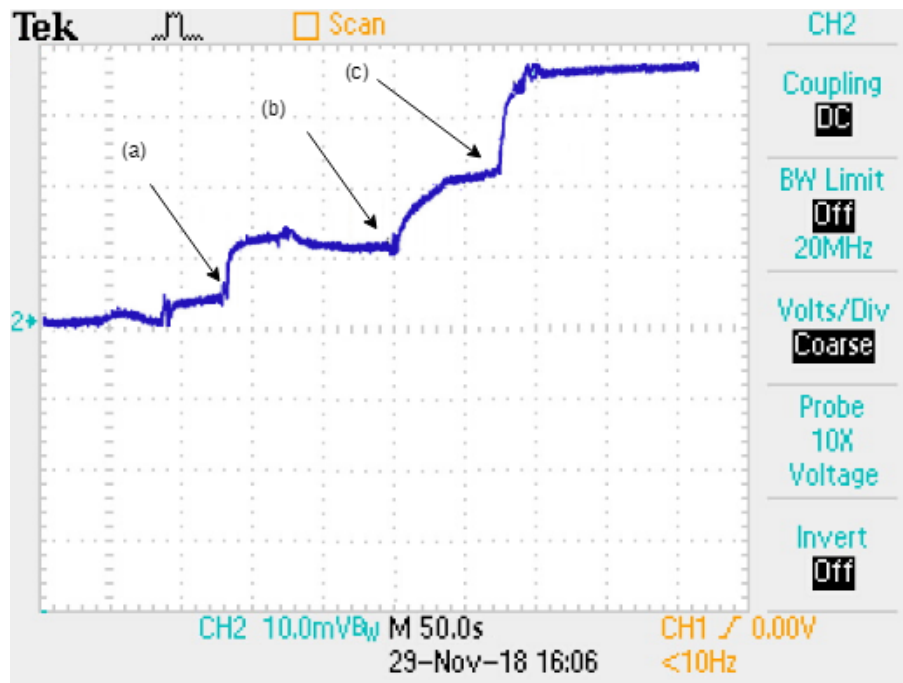


Figure 7.5: A measured output voltage of the full-bridge rectifier during the immobilization of streptavidin and biotinylated-probe. The increase in mass bends the nanowires and induce a piezoelectric voltage. During the immobilization step, PBS was first introduced as a control(a), then a solution of streptavidin was introduced (b) and lastly the biotinylated probe(c) was introduced. The small DC voltage spikes before the incubation of PBS are due to the immobilised Biotin-SAMs.

### 7.3 Biosensor Testing as a Proof Of Concept

Testing a biosensor takes longer than anticipated, the setup, shown in figure 7.6, was used to test the biosensor. The setup consist of three components: a three electrode sensor holder, a digital multimeter and a PC. The setup works in such a way that the sensor holder houses the biosensor and reads the data from the biosensor, then digital multimeter, agilent 34401a, records the data from the biosensor in real time and then the PC displays the information, using Keysight BenchVue software, in real time. The practical setup is also shown in Appendix H.

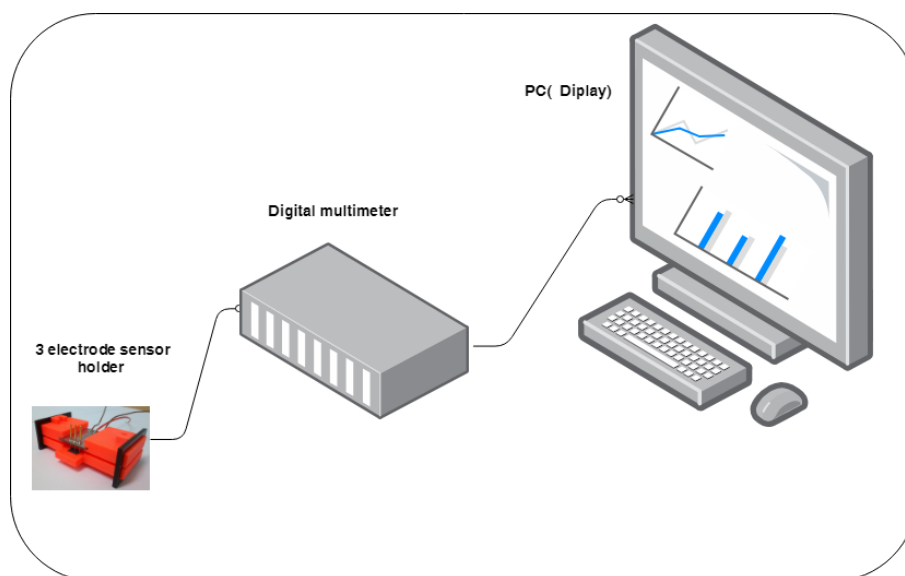


Figure 7.6: A schematic setup used for the testing of the piezoelectric biosensor. The schematic shows the 3 probe sensor holder, a digital multimeter and a PC for displaying and logging data.

Few in vitro tests were carried out using an anti-luteinizing hormone  $\beta$  antibody that is only specific to the luteinizing hormone, which can be found in our blood stream. Luteinizing hormone (LH) is produce by the gonadotropic cells situated near the pituitary gland. LH is responsible for two hormonal mechanisms: it is responsible for testosterone production in males and it triggers ovulation and corpus luteum development in females. Different analyte concentrations were pipetted onto the surface of the biosensors and were incubated in a desiccator for 1 h for successful recognition of the antigens. After an hour, the biosensors were rinsed with DI-water and gently blow dried in a desiccator. PBS was used a control buffer. During the recognition event, there is a change in the overall mass on the biosensor, hence the generated voltage increased. The measurements of the piezoelectric voltage were taken before

CHAPTER 7. ZNO NANOWIRE-ARRAY BIOSENSOR CONSTRUCTION FOR THE DETECTION AND QUANTIFICATION OF TUBERCULOSIS **100**

and after the analyte was introduced to show a piezoelectric voltage change. Figures 7.7, 7.8 and 7.9 show the piezoelectric response from the biosensor due to incubation with different analyte concentrations.

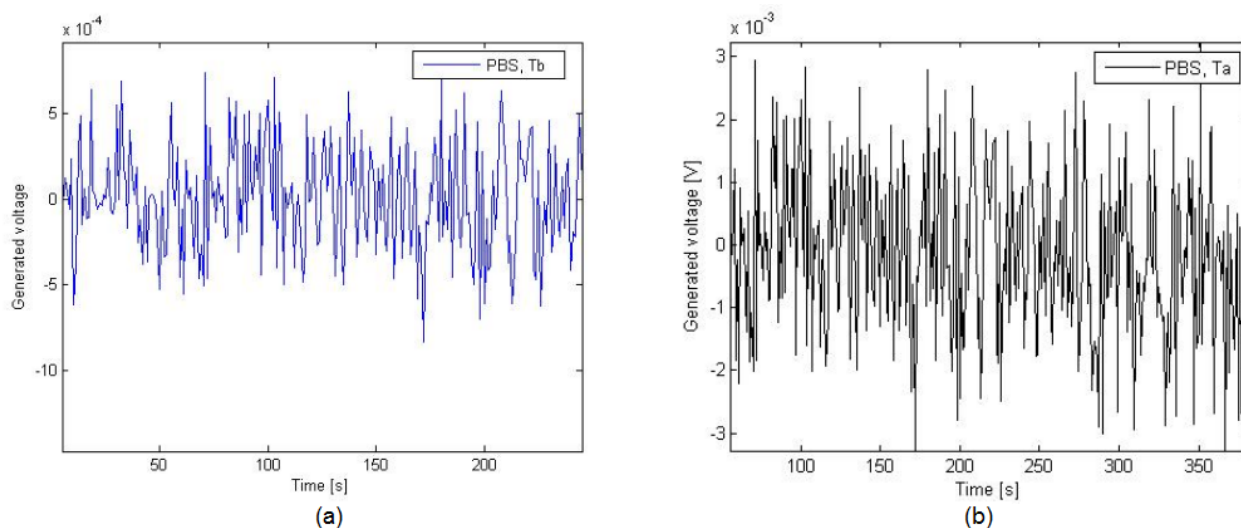


Figure 7.7: Measured output voltage of the biosensor before and after incubation of PBS as a control buffer. Figures 7.7(a) and (b) show the measured piezoelectric voltage before and after the addition of the control buffer, respectively

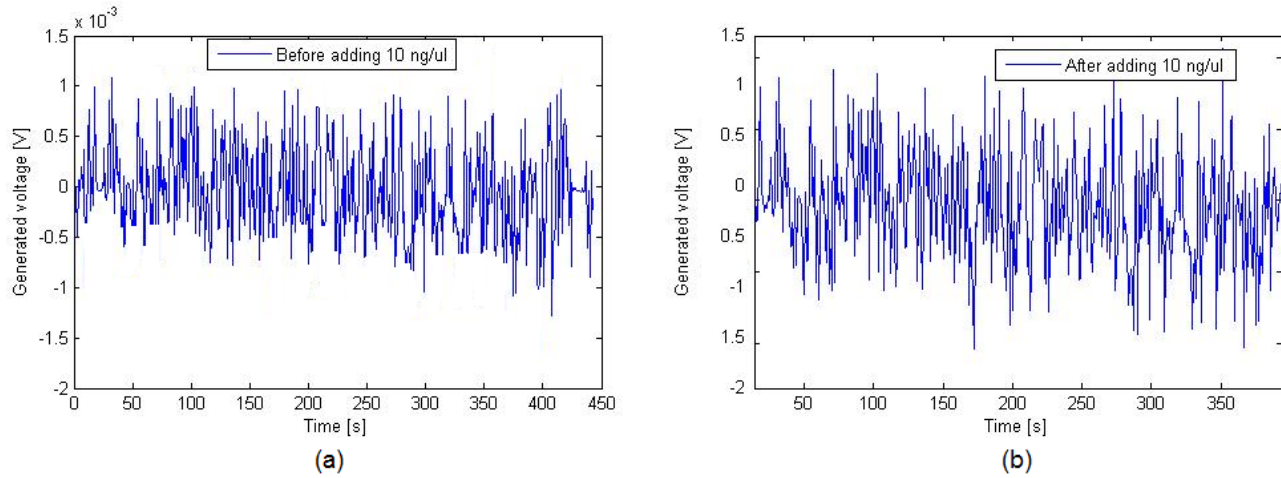


Figure 7.8: Measured output voltage of the biosensors before and after incubation of LH hormone. Figures 7.8(a) and (b) show the measured piezoelectric voltage before and after the addition of 10 ng/ $\mu$ l of LH hormone, respectively.

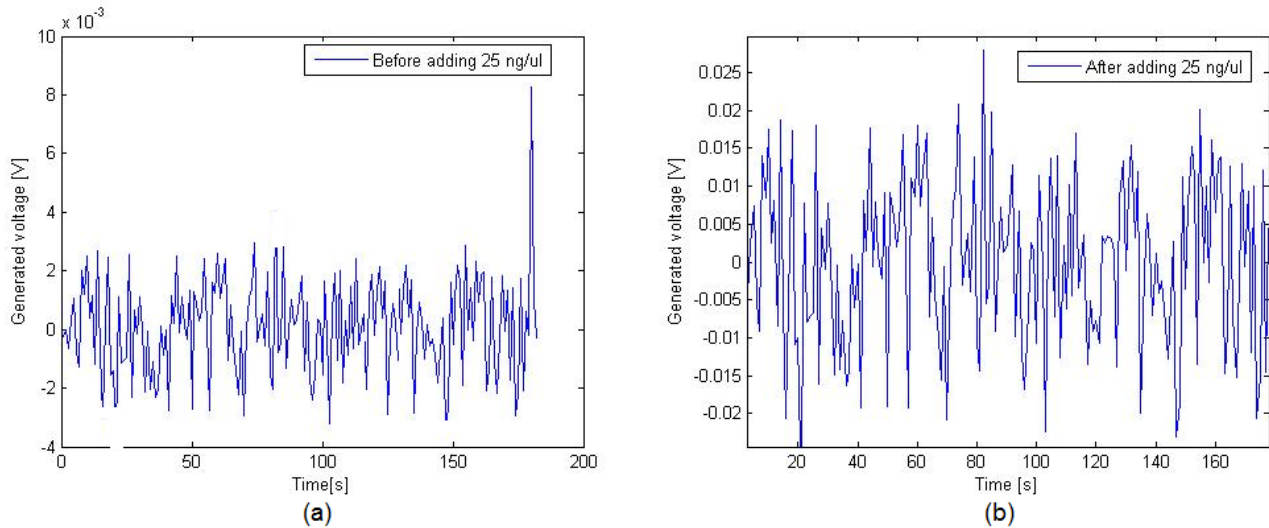


Figure 7.9: Measured output voltage of the biosensors before and after incubation of LH hormone. Figures 7.8(a) and (b) show the measured piezoelectric voltage before and after the addition of 25 ng/ $\mu$ l of LH hormone, respectively.

## 7.4 Results and Discussions

The Fourier Transform Infrared studies were conducted to study the immobilization of biotin-SAMs on surface of gold plated piezoelectric transducer. However, the studies were not conducted directly on the transducer, because the FTIR unit uses a vigorous force on samples under study, this can actually destroy the nanowires. Hence, a separate substrate sputtered with a thin layer of gold, about 5-10 nm, was used to conduct the studies. These substrates were used to confirm whether Biotin-SAMs did immobilise onto the thin layer of gold. And this was done through the use of FTIR analysis to confirm changes in the surface chemistry occurring after the modification step. Due to time constraints, FTIR analysis was only used to investigate gold thin layer, biotin solution and biotin-SAMs forming on the surface of gold.

The biotin-self-assembled monolayers were formed on the gold thin films. This was confirmed with the FTIR, that the biotin-SAMs were immobilised onto the gold layer. The formation of biotin-SAMs is one of the important steps in manufacturing a biosensor. Since the affinity of streptavidin for biotin is one of the strongest non-covalent bonds known in all of biochemistry. Hence, the binding of streptavidin to biotin was not fully investigated. The nanosensor is a piezoelectric transducer, meaning that the increase in mass of the biomaterial induced a piezoelectric voltage which can be measured across the full bridge rectifier without connecting a load resistor. Before the measurements a pre-amplifier was built to amplify the nanosensor pulse-like signals.

Immobilisation studies were conducted using the piezoelectric transducer. This is because there are many piezoelectric transducers used to monitor immobilization, one example is the vibrating QCM, which monitors mass change through frequency. It was an advantage that the ZnO transducer can react to change in mass.

During the immobilization steps there was noticeable change in both the measured piezoelectric voltage, shown in Figure. 7.4, and the rectified voltage as shown in Figure. 7.5. The increase in binding of biological material caused a change in the overall mass on the biosensor, and as results that caused strain on the nanowires which in turn produced more voltage. The addition of 200  $\mu\text{L}$  of PBS produced a voltage of 22 mV, while a 20  $\mu\text{L}$  of Streptavidin solution produced an average voltage of 30 mV and then voltage increased to an average voltage of 60 mV when 15  $\mu\text{g}/\text{mL}$  of biotinylated-probe was added.

Similarly, the rectifying circuit shows the same voltage trend. A DC voltage increased to a maximum voltage of 14 mV when 200  $\mu\text{l}$  of PBS was added onto to the biosensor, then the voltage went up to 22 mV when 20  $\mu\text{l}/\text{ml}$  of streptavidin was immobilised onto the sensor and lastly the voltage reached a steady state of 48 mV when 15  $\text{ng}/\text{ml}$  of biotinylated-probe was incubated. The voltage spikes before the the edition of PBS are due to the immobilised Biotin-SAMs on surface of the nanosensor.



*CHAPTER 7. ZNO NANOWIRE-ARRAY BIOSENSOR CONSTRUCTION FOR THE DETECTION AND QUANTIFICATION OF TUBERCULOSIS* **103**

for the in vitro testing of the piezo-biosensor: there was a gradual increase in the measured output voltage due to the increase in the biomolecules binding on the surface of biosensor. The incubation of PBS resulted in an increase in voltage from around 0.5 mV to about 3 mV. And after the incubation of 10 - 25 ng/ $\mu$ l LH hormone concentrations, the voltage increased more gradually. This proves that the piezoelectric mechanism does work.

## Chapter 8

# Conclusions

The main aim of this project was to design and manufacture a piezoelectric biosensor for the detection of biomarkers. The piezoelectric biosensor fabrication was achieved through many steps: firstly, the thorough understanding and investigation of literature. Secondly, the simulation of ZnO nanowires for parameter optimisation. ZnO nanowires were successfully modelled and simulated using Comsol multiphasic. After that, two different growth methods were studied and used to grow the piezoelectric nanowires. The Zinc oxide nanowires were successfully grown using the electrochemical deposition method and characterised using SEM and AFM. Growth along the c-axis (meaning perpendicular to the substrates), length and diameter were the most important aspects for the manufacturing of the piezoelectric transducer. Optimum conditions for growing the Zinc Oxide nanowires by the electrochemical deposition technique were also determined. The project also highlighted the manufacturing of the piezoelectric transducer. The piezoelectric transducer was successfully manufactured and characterised using SEM. Moreover, the project also focused on the design of the biotinylated probe, as a capture probe. The biotinylated cDNA was successfully designed, fabricated and studied using a bioanalyzer and a nanodrop to assess optimum hybridisation conditions with the total RNA, which was extracted from the mycobacterium tuberculosis. The study also assessed the immobilization of the capture probe onto the Au thin film layers. The immobilisation of a biotinylated-probe using streptavidin-biotin SAMs interaction.

The developed piezoelectric ZnO biosensor was tested in vitro as a proof of concept to determine whether the presented biomolecules do interact and bind to one another. The piezoelectric biosensor worked transduction principle proved to hold because the disturbance of the nanowires or array of nanowires induced a measurable piezoelectric voltage across the nanowires. The ZnO piezoelectric biosensor was successfully tested to determine whether it could recognise the interaction between probe and target analyte biomolecules. The binding of the LH  $\beta$  antibodies to the biosensor surface would cause the ZnO

nanowire array to bend , resulting in a small measurable piezoelectric potential. Increasing the antibody concentrations resulted in increased piezoelectric voltage production. This means that the increase in binding biomolecules on the surface of the biosensor, the greater the external applied force, leading to higher degree of bending in the ZnO nanowire arrays and increased piezoelectric voltage.

ZnO nanowire arrays hold a promising future as a piezoelectric transducer in the biosensor field. However, it is not an easy transducer to manufacture.

# List of References

- [1] W. T. R. 2016, *TB REPORT 2016*. [Online]. Available: <http://apps.who.int/medicinedocs/documents/s23098en/s23098en.pdf>
- [2] WHO, 2017, *TB FACTS 2017*. [Online]. Available: <https://www.who.int/news-room/fact-sheets/detail/tuberculosis>
- [3] Bhutta, Zulfiqar A and Sommerfeld, Johannes and Lassi, Zohra S and Salam, Rehana A and Das, Jai K, "Global burden, distribution, and interventions for infectious diseases of poverty", *Infectious diseases of poverty*, vol. 3, no. 1, p. 21, 2014
- [4] L. Esfandiari, S. Wang, S. Wang, A. Banda, M. Lorenzini, G. Kocharyan, H. G. Monbouquette, and J. J. Schmidt, "Pcr-independent detection of bacterial species-specific 16s rRNA at 10 fm by a pore-blockage sensor," *Biosensors*, vol. 6, no. 3, p. 37, 2016.
- [5] M. Altamirano, M. T. Kelly, A. Wong, E. T. Bessuille, W. A. Black, and J. A. Smith, "Characterization of a DNA probe for detection of Mycobacterium tuberculosis complex in clinical samples by polymerase chain reaction," *J Clin Microbiol*, vol. 30, no. 8, pp. 2173–2176, 1992.
- [6] A. L. S. Amand, A. L. S. Amand, D. N. Frank, D. N. Frank, M. A. D. Groote, M. A. D. Groote, R. J. Basaraba, R. J. Basaraba, I. M. Orme, I. M. Orme, N. R. Pace, and N. R. Pace, "Use of Specific rRNA Oligonucleotide Probes for Microscopic Detection of," *Society*, vol. 43, no. 10, pp. 5369–5371, 2005.
- [7] K. Dheda, M. Ruhwald, G. Theron, J. Peter, and W. C. Yam, "Point-of-care diagnosis of tuberculosis: Past, present and future," *Respirology*, vol. 18, no. 2, pp. 217–232, 2013.
- [8] S. R. Torati, V. Reddy, S. S. Yoon, and C. Kim, "Electrochemical biosensor for mycobacterium tuberculosis dna detection based on gold nanotubes array electrode platform," *Biosensors and Bioelectronics*, vol. 78, pp. 483–488, 2016.

- [9] B. Journal, "RAPID IDENTIFICATION OF MYCOBACTERIUM TUBERCULOSIS COMPLEX BY A NOVEL HYBRIDIZATION," pp. 964–972, 2011.
- [10] J. Vidic, M. Manzano, C.-M. Chang, and N. Jaffrezic-Renault, "Advanced biosensors for detection of pathogens related to livestock and poultry," *Veterinary Research*, vol. 48, no. 1, p. 11, 2018. [Online]. Available: <http://veterinaryresearch.biomedcentral.com/articles/10.1186/s13567-017-0418-5>
- [11] WHO. 2016, *Chest X-ray for detecting TB*. [Online]. Available: <https://apps.who.int/iris/bitstream/handle/10665/252424/9789241511506-eng.pdf?sequence=1>
- [12] J. Mairhofer, K. Roppert, and P. Ertl, "Microfluidic systems for pathogen sensing: A review," *Sensors (Switzerland)*, vol. 9, no. 6, pp. 4804–4823, 2009.
- [13] D. P. Neveling, "Development of a ZnO nanowire-array biosensor for the detection and quantification of immunoglobulins," no. December, 2013.
- [14] J. P. Chambers, B. P. Arulanandam, L. L. Matta, A. Weis, and J. J. Valdes, "Biosensor Recognition Elements," pp. 1–12, 2002.
- [15] Z. Iuni-Iui, C. Hong, and Y. Ruifu, "DNA BASED BIOSENSORS," *Biotechnology Advances Cotwicht*, vol. 15, no. 8, pp. 43–58, 1997.
- [16] D. P. Neveling, T. S. V. D. Heever, W. J. Perold, and L. M. T. Dicks, "Sensors and Actuators B : Chemical A nanoforce ZnO nanowire-array biosensor for the detection and quantification of immunoglobulins," *Sensors & Actuators: B. Chemical*, vol. 203, pp. 102–110, 2014. [Online]. Available: <http://dx.doi.org/10.1016/j.snb.2014.06.076>
- [17] T. Stanley, "Development and optimisation of a zinc oxide nanowire nanogenerator and gas sensor," no. December, 2013.
- [18] Massyn N, Peer N, English R, Padarath A, Barron P, Day C, "National TB statistics for South Africa," *District Health Barometer 2015/16*, 2017.[Online]. Available: <http://dx.doi.org/10.1016/j.snb.2014.06.076>
- [19] T. Brief, "Glossary of Drug Nanotechnology," *Particle Sciences Drug Development Services*, vol. 9, no. Technical Brief, pp. 1–4, 2012. [Online]. Available: [http://www.particlesciences.com/docs/technical\\_briefs/TB\\_2012\\_9-Nanotechnology.pdf](http://www.particlesciences.com/docs/technical_briefs/TB_2012_9-Nanotechnology.pdf)

- [20] J. N. Tiwari, R. N. Tiwari, and K. S. Kim, “Zero-dimensional, one-dimensional, two-dimensional and three-dimensional nanostructured materials for advanced electrochemical energy devices,” *Progress in Materials Science*, vol. 57, no. 4, pp. 724–803, 2012.
- [21] National Research Council, “Responsible Development of Nanotechnology,” in *A Matter of Size*, 2006, pp. 73–97. [Online]. Available: <http://www.nap.edu/catalog/11752>
- [22] N. Tolochko, “History of nanotechnology,” *Nanoscience and nanotechnology. Encyclopaedia of life Support Systems (EOLSS), Developed under the auspices of the UNESCO, SEolss Published, oxford*, 2009.
- [23] Examples of nanotechnology. [Online]. Available: <https://www.nano.gov/timeline>
- [24] D. R. Forrest, “Molecular nanotechnology,” *IEEE Instrumentation & Measurement Magazine*, vol. 4, no. 3, pp. 11–20, 2001.
- [25] N. P. Present and Future. (2002) MS Windows NT kernel description. [Online]. Available: <http://www.gaeu.com/item/this-is-nanotechnology-one-of-the-fastest-growing-markets-in-the-world>
- [26] C. Jianrong, M. Yuqing, H. Nongyue, W. Xiaohua, and L. Sijiao, “Nanotechnology and biosensors,” pp. 505–518, 2004.
- [27] R. Siegel, “Nanostructured materials-mind over matter,” *Nanostructured Materials*, vol. 4, no. 1, pp. 121–138, 1994.
- [28] G. A. I. (1999) nanostructured material. [Online]. Available: <http://eng.thesaurus.rusnano.com/wiki/article1371>
- [29] He, Jingjing and Qi, Xiaoxue and Miao, Yuqing and Wu, Hai-Long and He, Nongyue and Zhu, Jun-Jie, “Application of smart nanostructures in medicine,” *Nanomedicine*, vol. 5, no. 7, pp. 1129–1138, 2010.
- [30] Mathuria, Jitendra Prasad, “NANOPARTICLES IN TUBERCULOSIS DIAGNOSIS, TREATMENT AND PREVENTION: A HOPE FOR FUTURE.,” *Digest Journal of Nanomaterials & Biostructures (DJNB)*, vol. 4, no. 2, 2009.
- [31] MCornejo-Monroya, Delfino and Acosta-Torresb, Laura S and Moreno-Vegac, Aura I and Saldanad, Carlos and Morales-Tlalpan, Veronica and Castanoc, Victor M, “Gold nanostructures in medicine: past, present and future,” *Journal of Nanoscience Letters J. Nanosci. Lett*, vol. 3, p. 25, 2013.

- [32] Zhang, Yangyang and Ram, Manoj K and Stefanakos, Elias K and Goswami, D Yogi, "Synthesis, characterization, and applications of ZnO nanowires," *Journal of Nanomaterials*, vol. 2012, p. 20, 2012.
- [33] Choi, Ahmi and Kim, Kyoungwon and Jung, Hyo-Il and Lee, Sang Yeol, "ZnO nanowire biosensors for detection of biomolecular interactions in enhancement mode," *Sensors and Actuators B: Chemical*, vol. 148, no.2 p. 577–582, 2010.
- [34] J. Wang, S. Li, and Y. Zhang, "A sensitive dna biosensor fabricated from gold nanoparticles, carbon nanotubes, and zinc oxide nanowires on a glassy carbon electrode," *Electrochimica Acta*, vol. 55, no. 15, pp. 4436–4440, 2010.
- [35] I. Dakua and N. Afzulpurkar, "Piezoelectric energy generation and harvesting at the nano-scale: Materials and devices," *Nanomaterials and Nanotechnology*, vol. 3, p. 21, 2013.
- [36] P. Dineva, D. Gross, R. Müller, and T. Rangelov, "Dynamic fracture of piezoelectric materials," *AMC*, vol. 10, p. 12, 2014.
- [37] L. Schmidt-Mende and J. L. MacManus-Driscoll, "Zno-nanostructures, defects, and devices," *Materials today*, vol. 10, no. 5, pp. 40–48, 2007.
- [38] Z. L. Wang, "Piezopotential gated nanowire devices: Piezotronics and piezo-phototronics," *Nano Today*, vol. 5, no. 6, pp. 540–552, 2010.
- [39] T. S. van den Heever, W. Perold, and U. Büttner, "A zinc oxide nanowire pressure sensor," *Nanoscience and Nanotechnology Letters*, vol. 2, no. 3, pp. 203–207, 2010.
- [40] Z. L. Wang, "Nanogenerators for self-powered devices and systems," 2011.
- [41] H.-J. Choi, "Vapor liquid solid growth of semiconductor nanowires," in *Semiconductor Nanostructures for Optoelectronic Devices*. Springer, 2012, pp. 1–36.
- [42] K. Yoha, D. Yu, and C. Miller, "Manganese doping in lead sulfide nanowires," *Bulletin of the American Physical Society*, vol. 55, 2010.
- [43] Z. Sun, T. Liao, and L. Kou, "Strategies for designing metal oxide nanostructures," *Science China Materials*, pp. 1–24, 2017.
- [44] K. Miura, K. Hirao, and Y. Shimotsuma, "Nanowire formation under femtosecond laser radiation in liquid," in *Nanowires-Fundamental Research*. InTech, 2011.

- [45] Z. L. Wang, “Towards self-powered nanosystems: From nanogenerators to nanopiezotronics,” *Advanced Functional Materials*, vol. 18, no. 22, pp. 3553–3567, 2008.
- [46] ———, “Nanopiezotronics,” *Advanced Materials*, vol. 19, no. 6, pp. 889–892, 2007.
- [47] S. B. Nimse, K. Song, M. D. Sonawane, D. R. Sayyed, and T. Kim, “Immobilization techniques for microarray: challenges and applications,” *Sensors*, vol. 14, no. 12, pp. 22 208–22 229, 2014.
- [48] J. Cazes, *Analytical instrumentation handbook*. CRC Press, 2004.
- [49] T. Bhardwaj, “A review on immobilization techniques of biosensors,” *International Journal of Engineering*, vol. 3, no. 5, 2014.
- [50] S. D. Keighley, P. Li, P. Estrela, and P. Migliorato, “Optimization of dna immobilization on gold electrodes for label-free detection by electrochemical impedance spectroscopy,” *Biosensors and Bioelectronics*, vol. 23, no. 8, pp. 1291–1297, 2008.
- [51] C. Heise and F. F. Bier, “Immobilization of dna on microarrays,” in *Immobilisation of DNA on Chips II*. Springer, 2005, pp. 1–25.
- [52] J. C. Love, L. A. Estroff, J. K. Kriebel, R. G. Nuzzo, and G. M. Whitesides, “Self-assembled monolayers of thiolates on metals as a form of nanotechnology,” *Chemical reviews*, vol. 105, no. 4, pp. 1103–1170, 2005.
- [53] V. Perumal and U. Hashim, “Advances in biosensors: Principle, architecture and applications,” *Journal of Applied Biomedicine*, vol. 12, no. 1, pp. 1–15, 2014.
- [54] K. Kiilerich-Pedersen and N. Rozlosnik, “Cell-Based Biosensors: Electrical Sensing in Microfluidic Devices,” *Diagnostics*, vol. 2, no. 4, pp. 83–96, 2012. [Online]. Available: <http://www.mdpi.com/2075-4418/2/4/83/>
- [55] P. Banerjee and A. K. Bhunia, “Mammalian cell-based biosensors for pathogens and toxins,” *Trends in Biotechnology*, vol. 27, no. 3, pp. 179–188, 2009.
- [56] M. M. F. C. ˆA, “Fundamental Review Progress in Enzyme-Based Biosensors Using Optical Transducers,” vol. 132, pp. 107–132, 2004.
- [57] C. R. Ispas, G. Crivat, S. Andreescu, C. R. Ispas, G. Crivat, and S. A. Review, “Review : Recent Developments in Enzyme-Based Biosensors for Biomedical Analysis,” vol. 2719, no. July, 2017.



- [58] E. Katz, A. F. Bu, and M. Weg, "Self-Powered Enzyme-Based Biosensors," pp. 10 752–10 753, 2001.
- [59] A. Amine, H. Mohammadi, I. Bourais, and G. Palleschi, "Enzyme inhibition-based biosensors for food safety and environmental monitoring," vol. 21, pp. 1405–1423, 2006.
- [60] S. Sharma, H. Byrne, and R. J. O. Kennedy, "Antibodies and antibody-derived analytical biosensors," no. June, pp. 9–18, 2016.
- [61] K. R. Rogers, "Recent advances in biosensor techniques for environmental monitoring," vol. 568, pp. 222–231, 2006.
- [62] A. Sassolas, D. Leca-bouvier, J. Blum, D. Lyon, L. F, L. F, I. National, V. F, and Ä. Supe, "DNA Biosensors and Microarrays," 2008.
- [63] U. Bora, A. Sett, and D. Singh, "Nucleic Acid Based Biosensors for Clinical Applications," *Biosensors Journal*, vol. 1, no. 1, pp. 1–8, 2013.
- [64] Y. Du and S. Dong, "Nucleic Acid Biosensors: Recent Advances and Perspectives," 2017.
- [65] D. R. The, "ELECTROCHEMICAL BIOSENSORS : RECOMMENDED Electrochemical biosensors : Recommended de (®) nitions and classi (®) cation ( Technical Report )," vol. 71, no. 12, pp. 2333–2348, 1999.
- [66] K. Rathee, V. Dhull, R. Dhull, and S. Singh, "Biosensors based on electrochemical lactate detection : A comprehensive review," *Biochemistry and Biophysics Reports*, vol. 5, pp. 35–54, 2016. [Online]. Available: <http://dx.doi.org/10.1016/j.bbrep.2015.11.010>
- [67] N. J. Ronkainen, H. Brian, and W. R. Heineman, "Electrochemical biosensors," pp. 1747–1763, 2010.
- [68] J. Tkac and G. Svitel, "Monitoring of the bioconversion of glycerol to dihydroxyacetone with immobilized Gluconobacter oxydans cell using ... with immobilized Gluconobacter oxydans cell using thermometric," vol. 19, no. 5, 2001.
- [69] "Why we ' re here today ?"
- [70] D. Dey and T. Goswami, "Optical Biosensors : A Revolution Towards Quantum Nanoscale Electronics Device Fabrication," vol. 2011, 2011.
- [71] J. Svitel and J. Katrl, "Optical biosensors Pavel Damborsk y," no. June, pp. 91–100, 2016.
- [72] C. K. O. Sullivan and G. G. Guilbault, "Commercial quartz crystal microbalances - theory and applications," vol. 14, pp. 663–670, 1999.

- [73] C. Yao, T. Zhu, Y. Qi, Y. Zhao, H. Xia, and W. Fu, "Development of a Quartz Crystal Microbalance Biosensor with Aptamers as Bio-recognition Element," pp. 5859–5871, 2010.
- [74] A. Boisen and T. Thundat, "Design & fabrication of cantilever array biosensors Surface immobilization of functional receptors on microfabricated," *Materials Today*, vol. 12, no. 9, pp. 32–38, 2009. [Online]. Available: [http://dx.doi.org/10.1016/S1369-7021\(09\)70249-4](http://dx.doi.org/10.1016/S1369-7021(09)70249-4)
- [75] M. I. Friswell and S. Adhikari, "Sensor shape design for piezoelectric cantilever beams to harvest vibration energy," pp. 1–6, 2010.
- [76] Wang, Xudong and Zhou, Jun and Song, Jinhui and Liu, Jin and Xu, Ningsheng and Wang, Zhong L, "Piezoelectric field effect transistor and nanoforce sensor based on a single ZnO nanowire," vol. 6, no. 12, pp. 2768–2772, 2006.
- [77] Comsol inc., "Multiphysics simulation just got better, faster and more accessible ", [Online]. Available: <https://www.comsol.com/>
- [78] National Center for Biotechnology Information, "Standard Nucleotide BLAST", [Online]. Available: [https://blast.ncbi.nlm.nih.gov/Blast.cgi?PAGE\\_TYPE=BlastSearch](https://blast.ncbi.nlm.nih.gov/Blast.cgi?PAGE_TYPE=BlastSearch)
- [79] Agilent Technologies, "Bioanalyzer general protocol", [Online]. Available: [https://www.agilent.com/cs/library/usermanuals/Public/G2938-90321\\_SensitivityDNA\\_KG\\_EN.pdf](https://www.agilent.com/cs/library/usermanuals/Public/G2938-90321_SensitivityDNA_KG_EN.pdf)
- [80] Radovan Faltus, Miroslav Jane, Tomas Zednicek, "Storage Capacitor Properties and Their Effect on Energy Harvester Performance", [Online]. Available: [https://www.avx.com/docs/techinfo/Storage Capacitor Properties Effect Energy Harvester Performance.pdf](https://www.avx.com/docs/techinfo/Storage_Capacitor_Properties_Effect_Energy_Harvester_Performance.pdf)
- [81] Sigma Aldrich, "Biotin-SAM General Protoco", [Online]. Available: [https://www.sigmaaldrich.com/content/dam/sigma-aldrich/docs/Sigma/Product Information Sheet/1/biotin sam formation reagent-746622.pd](https://www.sigmaaldrich.com/content/dam/sigma-aldrich/docs/Sigma/Product_Information_Sheet/1/biotin_sam_formation_reagent-746622.pd)

# Appendices

# RNA extraction protocol

This section gives the full detailed extraction protocol which is summarized in Chapter 5. The extraction protocol was obtained from Stellenbosch University at the department of Biomedical Sciences by Dr. Melanie Grobbelaar.

## Total RNA isolation

### Isolation of Total RNA

1. Add 10 mL of culture to a 50 mL conical tube and pellet the cells by centrifuging at 3,000 rpm for 10 minutes at 4°C
2. Discard the supernatant , add 1/10 RNAProtect, centrifuge and discard supernatant
3. Add 1 mL of RNAPro solution to the pellet and resuspend by pipetting

**INFO:** RNAPro solution contains phenol, Guanidine Thiocyanate (GITC), water and glycerol. GITC is a strong detergent which denatures any RNases.

**CAUTION:** Phenol and GITC is very harmful and toxic – avoid exposure



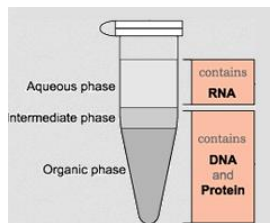
4. Transfer 1 mL of the solution to a blue-cap tube containing Lysing Matrix B

**INFO:** Lysing Matrix B 2 mL tubes containing 0.1mm silica beads are used primarily for lysis of gram positive and gram negative bacteria

5. Process the tubes in the FastPrep instrument for 25 seconds at a setting of 4.5
6. Place the tubes on ice for 1 minute and repeat step 5 three times
7. Centrifuge the tubes at 12,000 rpm for 5 minutes at 4°C

**TIP:** Orient the hinge of the micro-centrifuge tube outward to assist in locating the nucleic acid pellet, which will then be located on the same side of the hinge. Do not centrifuge at speeds higher than 12 000rpm – this will shear the RNA and cause degradation of the sample. Chilled temperatures prevent the RNA for heating - which causes shearing and degradation of the sample.

8. Transfer the liquid into a new tube (avoid transferring the cell debris and silica beads)



9. Add 300 µL of chloroform to the same tube, vortex for 10 seconds and incubate at room temperature for 5 minutes

**INFO:** Chloroform causes proteins to become denatured and become soluble in the organic phase or interphase, while nucleic acids remain in the aqueous phase/upper phase. Removes phenol from the RNA sample

## Total RNA isolation

10. Centrifuge the tube at 12,000 rpm for 10 minutes at 4°C
11. Transfer the upper phase to a new tube (do not disturb the interphase)
12. Add 500 µL of cold 100% ethanol to the tubes and vortex for 5 seconds
13. Incubate the tubes at -20°C for 1 hour
14. Centrifuge the tubes at 12,000 rpm for 20 minutes at 4°C
15. Remove the supernatant
16. Add 500 µL of cooled 75% ethanol and invert tube to wash pellet

**INFO:** When isolating and purifying RNA, 75% ethanol is used as a wash solution because RNA is precipitated at that percentage of ethanol, while most proteins and salts remain in solution. At a lower % ethanol, both the RNA and the proteins would be soluble, so you would not be able to separate them. At a higher % ethanol, both the RNA and salts would remain in the pellet, so you would not be able to separate the salts from your RNA.

17. Centrifuge at 12,000 rpm for 1 minute at room temperature
18. Discard the ethanol and air dry the pellet on a paper towel for 5 – 10 minutes
19. Resuspend the pellet in 30 µL of RNase-free water

**INFO:** Nuclease contamination in reagents used for nucleic acid isolation and analysis can contribute to experimental inconsistency and sometimes even experimental failure. Even purified water can have a high pH and minerals that can interfere with reactions that require specific salt and pH conditions. Always use nuclease-free water—diethylpyrocarbonate (DEPC)-treated water, nuclease-free water (not DEPC-treated), and RT-PCR-grade water—that all have been rigorously tested for contaminating nonspecific endonuclease, exonuclease, and RNase activity.

20. Incubate tube for 5 – 15 minutes at room temperature
21. Continue to DNase treatment step of store RNA at -80°C

## Total RNA isolation

### DNase Treatment

1. Add 10  $\mu\text{L}$  of RNase-free water, 10  $\mu\text{L}$  of RNA, 4  $\mu\text{L}$  of DNase Buffer and 4  $\mu\text{L}$  of DNase to a new tube

**TIP:** Thaw all DNase items on ice 20 minutes before use. Never place the items at room temperature and keep at  $-20^{\circ}\text{C}$  if not in use. Immediately place items back at  $-20^{\circ}\text{C}$  after use.

2. Vortex for 2 seconds and centrifuge for 5 seconds at 12,000 rpm at room temperature
3. Incubate for 30 minutes at  $37^{\circ}\text{C}$

**TIP:** Set the heating block to the correct temperature 30 minutes before use. If a manual heating block is used, make sure the correct temperature is set by using an accurate thermostat.

4. Add 172  $\mu\text{L}$  of RNase-free water and 200  $\mu\text{L}$  of cooled phenol-chloroform (4:1) to the tube

**INFO:** Acid phenol specifically leaves RNA in the aqueous phase. DNA carries a negative charge because of its phosphate backbone, which is neutralized in acid by protonation. DNA dissolves in the organic phase. RNA is not neutralized in acid because it has exposed nitrogenous bases (it is single-stranded), which can form hydrogen bonds with water, keeping it in the aqueous phase. Chloroform mixed with phenol is more efficient at denaturing proteins than either reagent is alone. The phenol-chloroform combination reduces the partitioning of poly(A)+ mRNA into the organic phase and reduces the formation of insoluble RNA-protein complexes at the interphase. Moreover, phenol retains about 10-15% of the aqueous phase, which results in a similar loss of RNA; chloroform prevents this retention of water and thus improves RNA yield.

**CAUTION:** Phenol:chloroform is very toxic and can cause chemical burns. It is also a systemic poison which can be rapidly absorbed through the skin. Inhalation of phenol fumes is dangerous and can result in permanent loss of smell. It is one of the most dangerous chemicals in a typical biochemistry laboratory.



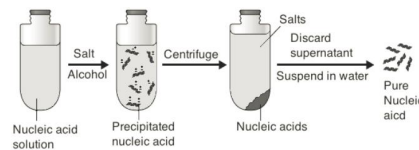
5. Mix for 2 seconds on vortex and place on ice for 10 minutes, mixing by vortex for every 2 minutes
6. Centrifuge tubes at 12,000 rpm for 10 minutes at room temperature
7. Transfer the upper phase to a new tube

**CAUTION:** This is the most important step. If the inter phase is disrupted, DNA will contaminate the RNA sample and the entire DNase treatment will have to be repeated. Never touch the sides of the tube of the interphase with the pipette tip. Always pipette from the top of the liquid layer.

## Total RNA isolation

8. Add 20  $\mu$ L cooled sodium acetate and 500  $\mu$ L cooled 100% ethanol to the tube

**INFO:** In the presence of salt (in particular, monovalent cations such as sodium ions ( $\text{Na}^+$ )), ethanol efficiently precipitates nucleic acids. The role of the salt in the protocol is to neutralize the charges on the sugar phosphate backbone. The positively charged sodium ions neutralize the negative charge on the  $\text{PO}_3^-$  groups on the nucleic acids, making the molecule less hydrophilic, and therefore much less soluble in water. The electrostatic attraction between the  $\text{Na}^+$  ions in solution and the  $\text{PO}_3^-$  ions are dictated by Coulomb's Law, which is affected by the dielectric constant of the solution. Water has a high dielectric constant, which makes it difficult for the  $\text{Na}^+$  and  $\text{PO}_3^-$  to come together. Ethanol has a much lower dielectric constant, making it much easier for  $\text{Na}^+$  to interact with the  $\text{PO}_3^-$ , shield its charge and make the nucleic acid less hydrophilic, causing it to drop out of solution.



9. Vortex for 2 seconds and incubate at 4°C overnight

**INFO:** As the temperature of an alcohol-aqueous solution decreases, its dielectric constant increases. Therefore, in principle, at increasingly chilled temperatures, precipitation efficiency should diminish. Moreover, as the temperature decreases, the viscosity of the solution increases, which retards the movement of the nucleic acid aggregate, especially if the aggregate is small (Zeugin and Hartley 1985). In addition, since solubility decreases at lower temperatures, more salts will begin to co-precipitate with the nucleic acids at lower temperatures. Therefore, incubation at temperatures below 0°C is counter-productive and not recommended.

10. Centrifuge the tubes at 12,000 rpm for 20 minutes at 4°C
11. Remove supernatant and wash pellet with 500  $\mu$ L of cooled 75% ethanol
12. Vortex for 2 seconds and centrifuge at 12,000 rpm for 2 minutes at room temperature
13. Discard the ethanol and dry the tube on a paper towel for 5 – 10 minutes
14. Add 10  $\mu$ L of RNase-free water to each tube
15. Dissolve pellet for 5 – 15 minutes
16. Assess quality and quantity
  - RNA gel (2% agarose gel, run at 150V for 1 hour)
  - PCR to determine if samples are contaminated with DNA
  - Nanodrop/Experion/BioAnalyzer to check RNA quality and concentration
17. Store RNA at -80°C



## Total RNA isolation

### Important

To prevent RNA degradation during the RNA isolation and purification steps, the following methods are used to maintain an RNase-free environment:

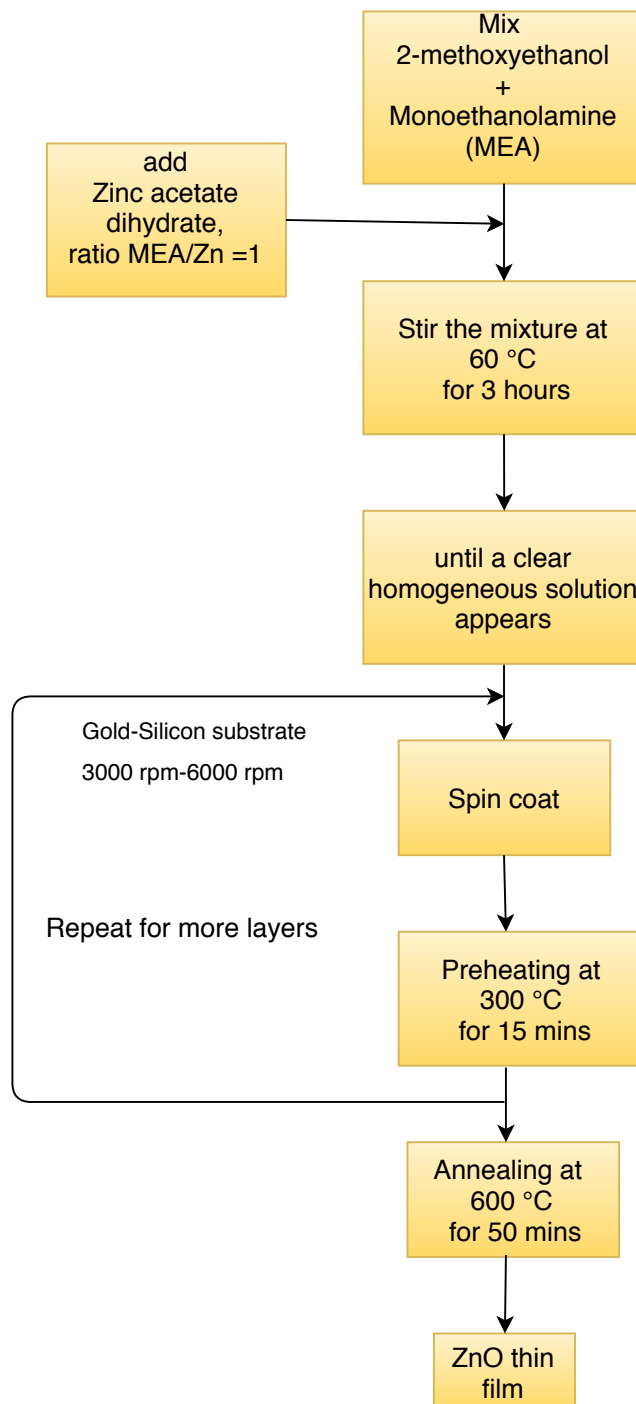
- A designated RNase-free workspace is used when working with RNA.
- RNaseZap and 70% ethanol are used to clean all equipment and work surfaces before and after use.
- Powder-free nitrile gloves are used at all times and changed frequently to prevent RNase contamination.
- RNase-free pipette tips, Eppendorf tubes and reagents are used and 75% ethanol is made with DEPC-treated water.
- All glassware should be treated with 1% SDS for 2 hours and rinsed with DEPC-treated water followed by 100% ethanol. The glassware should then be baked at 180°C for 4 hours.
- DEPC-treated water is prepared by adding 1 mL of DEPC (diethylpyrocarbonate) per litre of water to make a 1% solution. Shake overnight and autoclave before use.

**REMEMBER...** The most common sources of RNase contamination are your skin and bacteria/mold that may be present on airborne dust particles or laboratory glassware. So remember not to touch anything with your bare hands and to keep sample tubes closed whenever possible!

# Flow chart for spin coating Zinc Oxide thin films

This section shows the flow diagram for obtaining thin zinc oxide films for the growth of Zinc Oxide nanowires. The ZnO layer serves as seed to initiate growth of the nanowires. Properly spun seed layers lead more aligned vertical nanowires.

## ZnO seed layer flow diagram



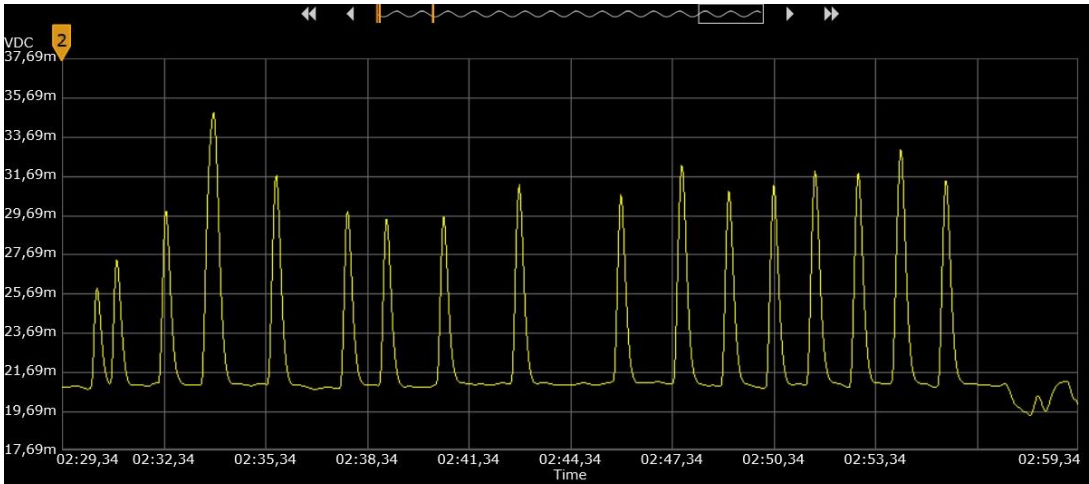
# Piezoelectric voltage curves from nanosensors

This section shows the piezoelectric voltage signals obtained from different nanosensors. A few tests were conducted to check and validate piezoelectricity of the nanogenerators.

Piezoelectric voltages generated by the

Summary	
Model:	DMM 34401A
Serial Number:	Sensor 1
Address:	ASRL11::INSTR
Acquisition Date:	2018-11-20 13:23:56
Sample Count:	4725

Chart Image:

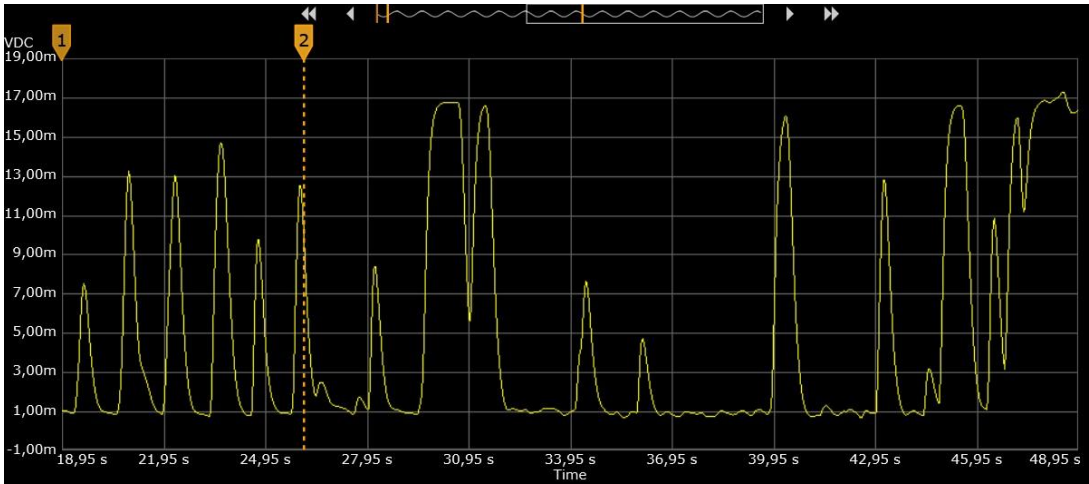


Setup Information	
Auto Range:	On
Auto Zero:	On
Input Impedance:	10 MΩ
Measurement:	DC Voltage
NPLC:	10
Range(VDC):	0,1

Piezoelectric voltages generated by the

Summary	
Model:	DMM 34401A
Serial Number:	Sensor 2
Address:	ASRL11::INSTR
Acquisition Date:	2018-11-20 13:14:19
Sample Count:	1290

Chart Image:

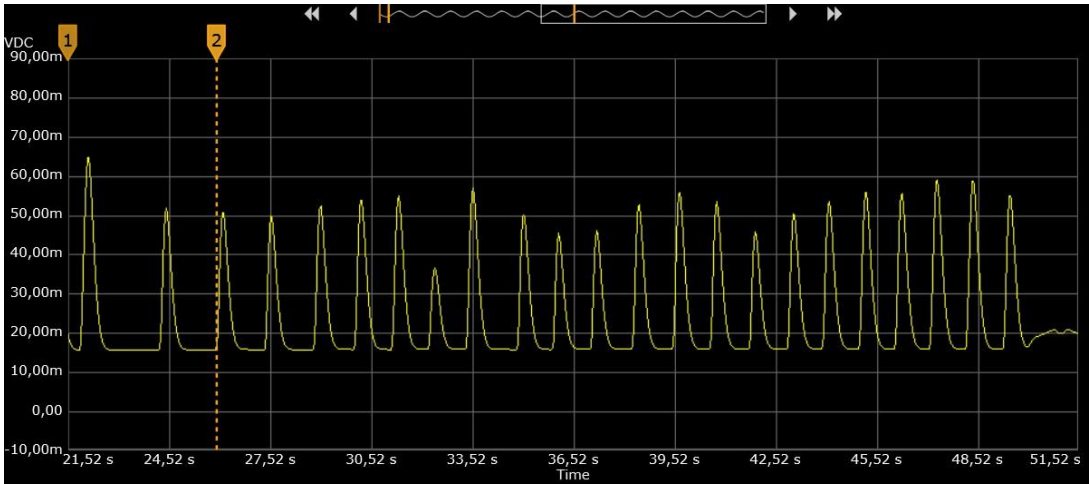


Setup Information	
Auto Range:	On
Auto Zero:	On
Input Impedance:	10 MΩ
Measurement:	DC Voltage
NPLC:	10
Range(VDC):	0,1

Piezoelectric voltages generated by the

Summary	
Model:	DMM 34401A
Serial Number:	Sensor 3
Address:	ASRL11::INSTR
Acquisition Date:	2018-11-20 13:40:05
Sample Count:	1357

Chart Image:

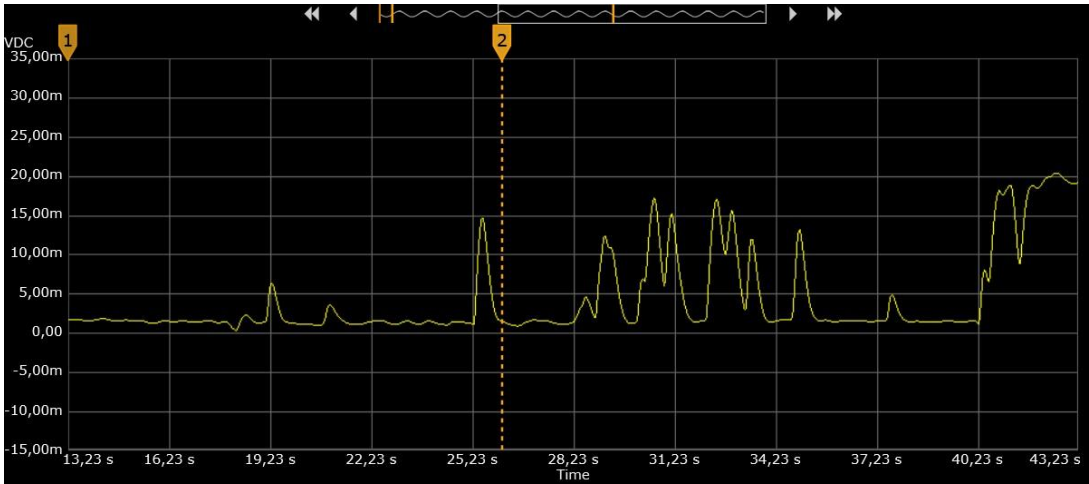


Setup Information	
Auto Range:	On
Auto Zero:	On
Input Impedance:	10 MΩ
Measurement:	DC Voltage
NPLC:	10
Range(VDC):	0,1

Piezoelectric voltages generated by the

Summary	
Model:	DMM 34401A
Serial Number:	Sensor 4
Address:	ASRL11::INSTR
Acquisition Date:	2018-11-20 13:09:35
Sample Count:	1140

Chart Image:



Setup Information	
Auto Range:	On
Auto Zero:	On
Input Impedance:	10 MΩ
Measurement:	DC Voltage
NPLC:	10
Range(VDC):	0,1



## Schematic and PCB board

This section shows the PCB board design and its schematic diagram. In the schematic, the blank rectangle represent the microcontroller which receives two inputs from ports "out1" and "Vref1". Then it will process the data and send it to the driving transistor circuit.

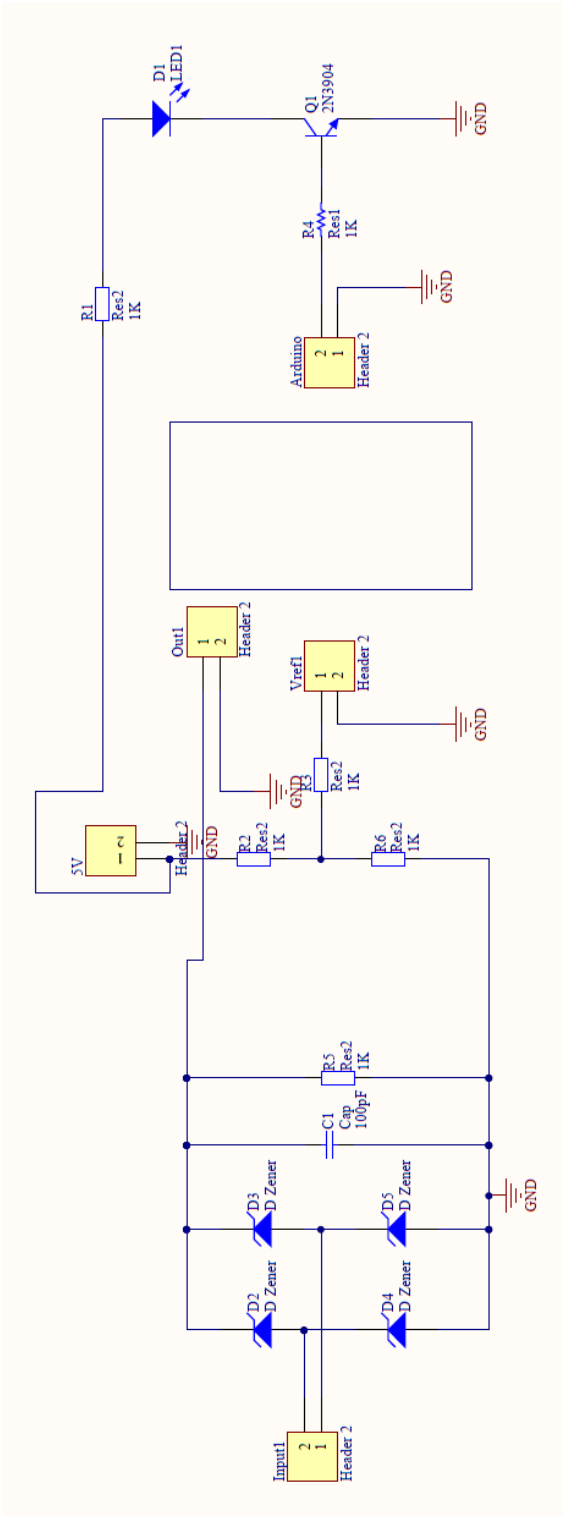


Figure 1: PCB board designed with Altium.

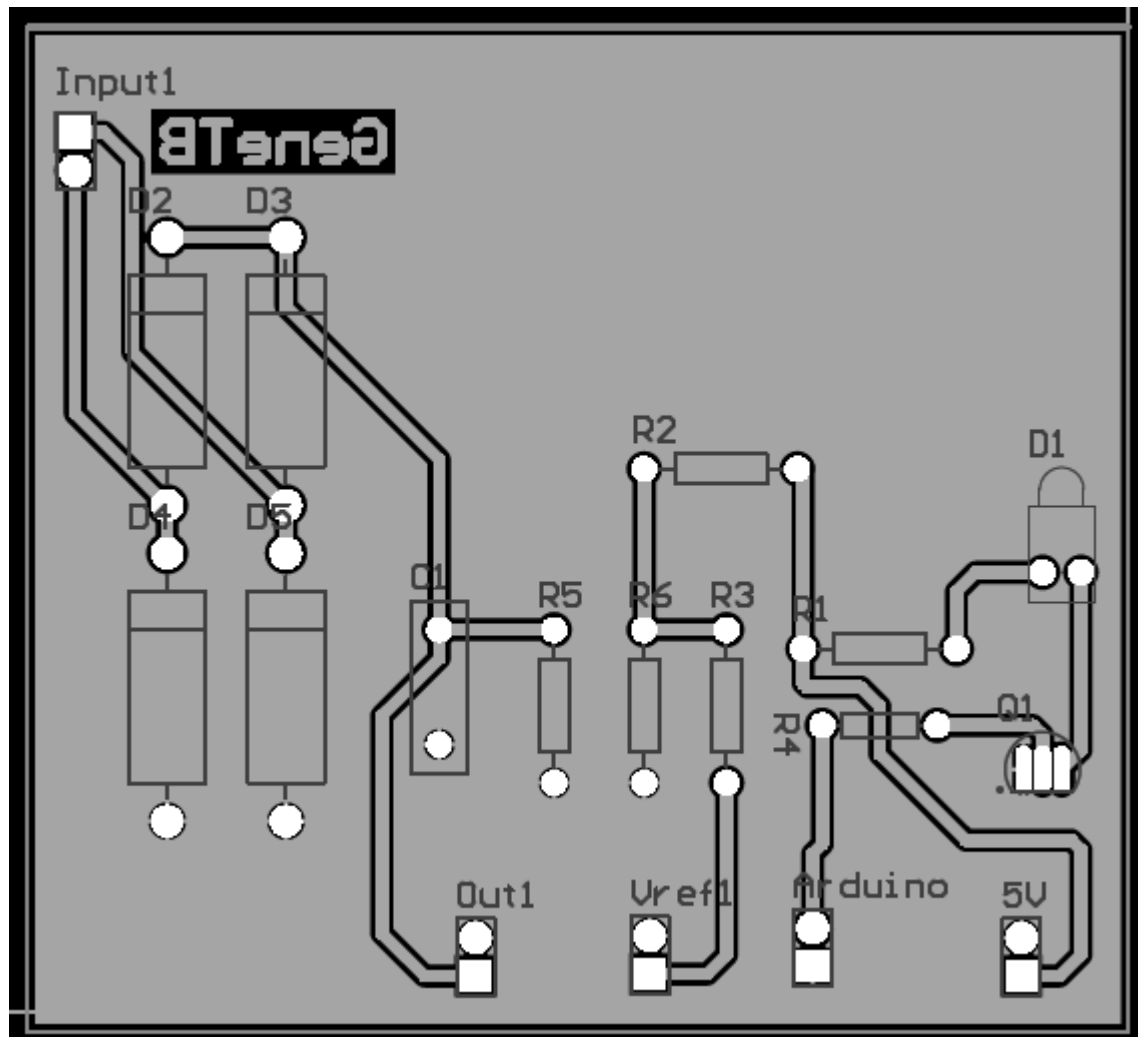


Figure 2: PCB board designed with Altium.

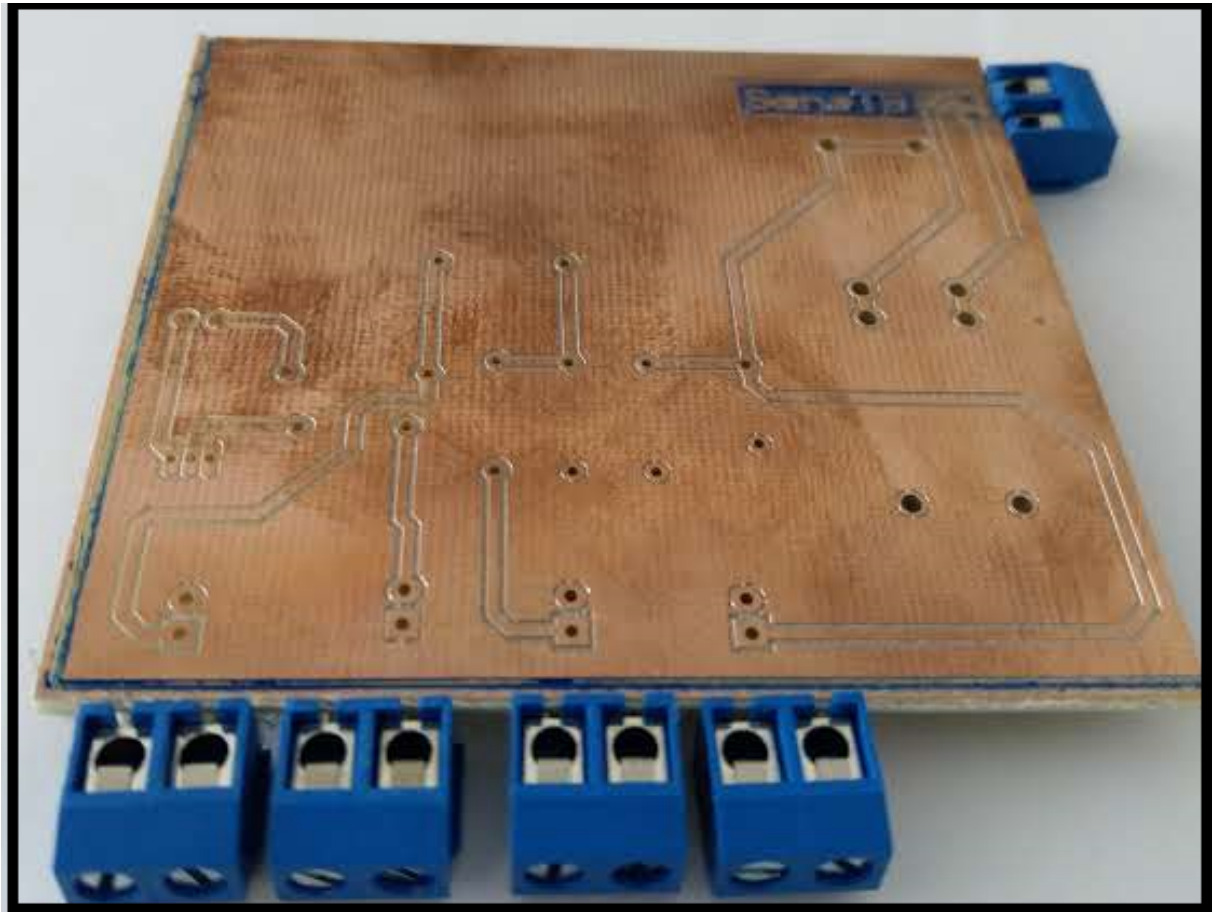


Figure 3: A manufactured GeneTB PCB board designed with Altium designer.

# Bioanalyzer Experiments

A bioanalyzer is an electrophoresis machine that incorporates microchips used to analyse total RNA, DNA, and protein. It performs high quality digital data logging such as RIN for RNA samples, DNA and protein sample quality control. This section shows the experiments and results that were obtained from the mycobacterium tuberculosis total RNA samples.

## Bioanalyzer Experiments

Analytical Report	1215BIO_A_WAR_RNA		Confidential 21 November 2018
Document number	19112018-001_BIO	Version	1

### 1. Background and samples submitted

This report provides the quality control results for thirty-two (32) Bacterial (*Mycobacterium tuberculosis*) RNA samples analysed using the Agilent Bioanalyzer Prokaryote Total RNA Nano Assay and Nanodrop 8000 Spectrophotometer.

The samples were received on the 16th of November 2018 and the tubes were labelled 1 to 32. Sample IDs are shown in Tables 1 and 2 below.

An internal quality control sample (80ng/μl) was included as an internal reference.

### 2. Abbreviations and keywords

RIN: RNA Integrity Number

rRNA ratio

Manual integration: manually adjusting the prerequisite threshold

### 3. Analysis synopsis

The NanoDrop 8000 Spectrophotometer and the Agilent Bioanalyzer RNA Nano Assay kit were used to assess the quality and integrity of the bacterial RNA samples.

### 4. Detailed analysis

#### 4.1. NanoDrop Results

The NanoDrop 8000 was used to determine the sample concentration and the presence of possible contaminants and/or inhibitors. Following the Nanodrop measurements most of the samples except for the six (6) highlighted samples underwent a 1:5 dilution as the measured concentrations for most samples were above the Agilent Bioanalyzer's maximum quantitative range of 500ng/μl. To reduce sample variability, all samples with concentrations above 200ng/μl were diluted in the same way. The expected concentrations these dilutions are expressed in column 5 of Table 1 below.

For RNA samples to be considered free of contaminants and salts the  $A_{260/280}$  ratio should be between 1.7 and 2.0 and  $A_{260/230}$  ratios between 1.5 and 3. **All samples met these criteria.**

**The  $A_{260/280}$  and  $A_{260/230}$  ratios for the control sample were 2.0 and 1.9 respectively. These ratios indicate that the process and the equipment are within bounds.**

# Bioanalyzer Experiments

Analytical Report	1215BIO_A_WAR_RNA		Confidential 21 November 2018
Document number	19112018-001_BIO	Version	1

**Table 1: Nanodrop results**

Sample ID	Conc.(ng/μl)	A <sub>260/280</sub>	A <sub>260/230</sub>	Expected conc. Post dilution (ng/μl)
Control RNA	82,29	2,0	1,9	
R721 #1 Cont	704	1,9	2,0	140,8
R721 #1 Rif	717,5	1,8	2,0	143,5
R721 #2 Cont	928,9	1,8	2,0	185,78
R721 #2 Rif	646,3	1,9	2,0	129,26
R721 #3 Cont	674,7	1,9	1,9	134,94
R721 #3 Rif	665,1	1,9	2,0	133,02
R721/C6 #1 Cont	364,7	1,9	1,9	72,94
R721/C6 #1 Rif	491,7	1,9	1,8	98,34
R721/C6 #2 Cont	389,8	1,9	2,0	77,96
R721/C6 #2 Rif	409,5	1,9	1,9	81,9
R721/C6 #3 Cont	376,9	1,9	1,9	75,38
R721/C6 #3 Rif	408,2	1,9	1,9	81,64
R721/C5.5 #1 Cont	425,6	1,9	2,0	85,12
R721/C5.5 #1 Rif	326,5	1,9	2,0	65,3
R721/C5.5 #2 Cont	320,1	1,9	2,0	64,02
R721/C5.5 #2 Rif	365,8	2,0	2,0	73,16
R721/C5.5 #3 Cont	312,4	1,9	1,9	62,48
R721/C5.5 #3 Rif	284,4	1,9	1,9	56,88
R4370 #1 Cont	98,26	1,9	1,5	
R4370 #1 Rif	379,1	1,9	2,0	75,82
R4370 #2 Cont	436,1	1,9	2,0	87,22
R4370 #2 Rif	397,2	1,8	2,0	79,44
R4370 #3 Cont	368,2	1,9	2,0	73,64
R4370 #3 Rif	443,3	1,9	2,0	88,66
WT #1	429,9	1,8	2,0	85,98
WT #2	577,1	1,7	1,9	115,42
WT #3	597,4	1,8	2,0	119,48
Tom 250ug (water)	19,1	1,9	2,0	
Tom 300ug (water)	21,59	1,8	2,0	
Tom 350ug (water)	24	1,7	1,9	
Tom 300ug (TE)	24,49	1,9	1,0	
Tom 350ug (TE)	28,07	2,0	1,1	

## Bioanalyzer Experiments

Analytical Report	1215BIO_A_WAR_RNA		Confidential 21 November 2018
Document number	19112018-001_BIO	Version	1

### 4.2. Bioanalyzer Results – Summary

The assay details are provided as a pdf attachment

#### RIN Applicability:

- Good RIN between 7 and 10

#### rRNA Ratio [16s / 23s]:

- Good ratio between 1.0 and 2.6

#### Quantitative Range:

- 25-500ng/μl

#### Other:

- Data Algorithm set to nucleotides (nt)
- Flat Baseline

Table 2: Bioanalyzer results

Sample ID	RIN	Comment
Control RNA	7.9	Passed
R721 #1 Cont	8.6	Passed
R721 #1 Rif	8.5	Passed
R721 #2 Cont	8.3	Passed
R721 #2 Rif	8.6	Passed
R721 #3 Cont	7.7	Passed
R721 #3 Rif	7.8	Passed
R721/C6 #1 Cont	6.3	Failed
R721/C6 #1 Rif	6.2	Failed
R721/C6 #2 Cont	7	Passed
R721/C6 #2 Rif	7	Passed
R721/C6 #3 Cont	5.2	Failed
R721/C6 #3 Rif	7.6	Passed
R721/C5.5 #1 Cont	8.2	Passed
R721/C5.5 #1 Rif	6.8	Failed
R721/C5.5 #2 Cont	6.5	Failed
R721/C5.5 #2 Rif	6	Failed
R721/C5.5 #3 Cont	7.1	Passed
R721/C5.5 #3 Rif	6	Failed



## Bioanalyzer Experiments

Analytical Report	1215BIO_A_WAR_RNA		Confidential 21 November 2018
Document number	19112018-001_BIO	Version	1

R4370 #1 Cont	5.9	Failed
R4370 #1 Rif	6.5	Failed
R4370 #2 Cont	7.3	Passed
R4370 #2 Rif	5.7	Failed
R4370 #3 Cont	6.7	Failed
R4370 #3 Rif	8.3	Passed
WT #1	6.8	Failed
WT #2	6.8	Failed
WT #3	7.2	Passed
Tom 250ug (water)	9.6	Passed
Tom 300ug (water)	9.0	Passed
Tom 350ug (water)	9.8	Passed
Tom 300ug (TE)	7.9	Passed
Tom 350ug (TE)	7.9	Passed

The Bioanalyzer QC results were as follows:

- Nineteen (19) samples passed QC checks with RIN values ranging from 7 to 9.8.
- Thirteen (13) samples (highlighted in red) failed QC checks with RINs lower than 7. Their RIN values ranged between 5.2 and 6.8. **These failures ranged from samples with low ribosomal ratios to raised baselines.**

The control RNA sample passed QC with a RIN of 7.9. This RIN indicates that the process and the equipment are within bounds.

### 5. Experimental procedures

#### 5.1. NanoDrop

RNA concentration and quality were determined using the NanoDrop 8000. Concentration of each sample was measured after blanking with 1.2µl of water. Both pedestals were wiped with a lint free paper and 1.2µl of sample was placed and measured. This was repeated until all samples had been measured.

#### 5.2. Bioanalyzer

RNA samples, control RNA and the Agilent RNA Nano Ladder were heat denatured at 70°C for 2 minutes in a thermal cycler. These were then placed immediately on ice after a brief spin. After priming the chip on the chip priming station with Agilent RNA Nano gel-dye mix,

## Bioanalyzer Experiments

Analytical Report	1215BIO_A_WAR_RNA		Confidential 21 November 2018
Document number	19112018-001_BIO	Version	1

5µl Agilent RNA Nano Marker was added to all wells including the ladder well. 1µl of sample was then added to respective wells and the ladder (1µl) to the ladder well. The chip was vortexed with the IKA vortexer for 1minute at 2400rpm and run in the Agilent 2100 Bioanalyzer.

### 6. Deviations

---

No deviations were observed during the processing of these samples.

### 7. Enquiries

---

Your application specialists on this project was Lebo Seutloali. Please do not hesitate to contact her on 021 447 5669 or [lebo.seutloali@cpgr.org.za](mailto:lebo.seutloali@cpgr.org.za) for additional discussion or information on this report.

### 8. Appendices

---

2100 expert\_Prokaryote Total RNA Nano\_DE72901831\_2018-11-16\_17-04-05.pdf

2100 expert\_Prokaryote Total RNA Nano\_DE72901831\_2018-11-16\_17-35-44.pdf

2100 expert\_Prokaryote Total RNA Nano\_DE72901831\_2018-11-16\_18-00-46.pdf

# Final representation of the biosensor

This section shows a schematic representation of the finished biosensor.

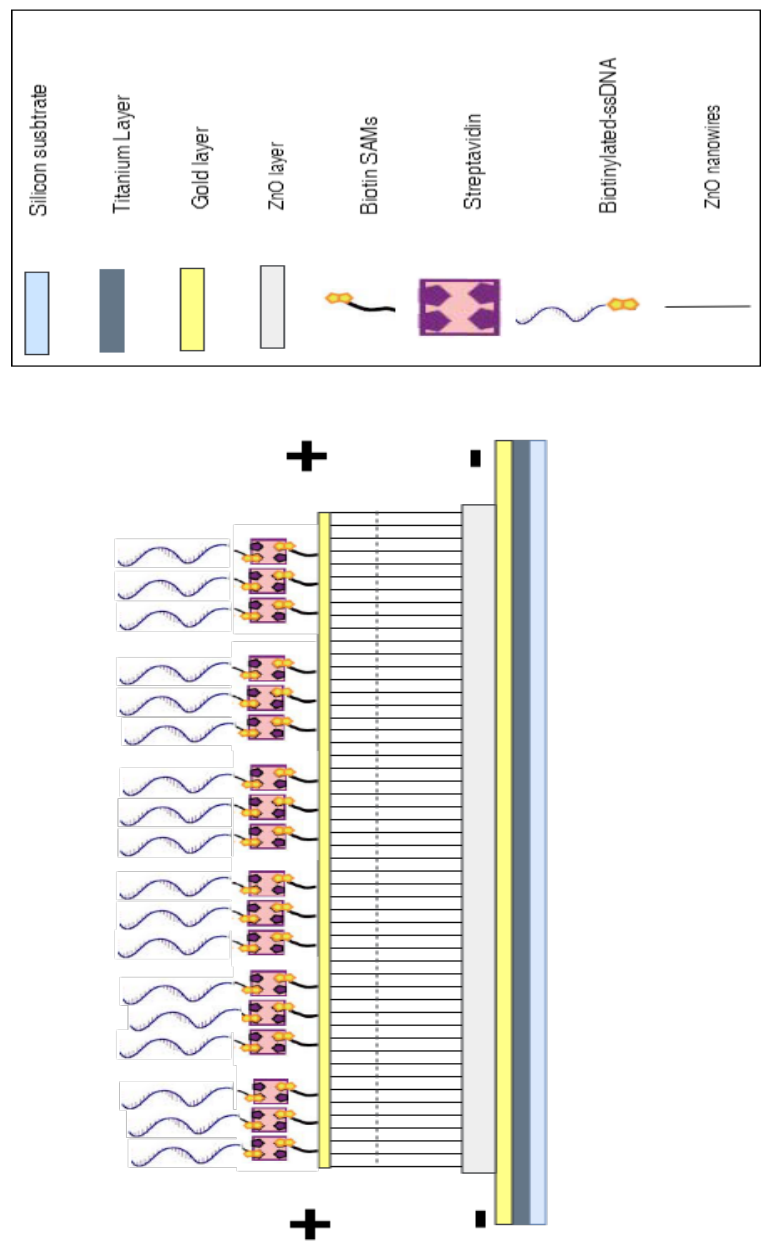


Figure 4: A schematic representation of the final working biosensor.

## FTIR Chart

This section shows a Fourier Transform InfraRed (FTIR) spectroscopy correspondence table list of absorption or transmittance of peaks, denoted as wavenumber, for common types of molecular bonds and functional groups analysed and found in a sample. The table shows the stretch of the wave of a specific functional group and its peak bends.

## Fourier Transform Infrared Chart

## CHARACTERISTIC INFRARED ABSORPTION BANDS OF FUNCTIONAL GROUPS

Class of Compounds	Absorption, cm <sup>-1</sup>	Intensity	Assignment	Class of Compounds	Absorption, cm <sup>-1</sup>	Intensity	Assignment
<b>Alkanes and Alkyls</b>	2850-3000 1450-1470 1370-1390 1365 + 1395 (two bands) 715-725	s s m m w	C-H stretch C-H bend CH <sub>3</sub> C-H bend -CH(CH <sub>3</sub> ) <sub>2</sub> or -(CH <sub>3</sub> ) <sub>3</sub> bend -(CH <sub>2</sub> ) <sub>n</sub> bend	<b>Carboxylic Acids</b>	2500-3500 R-C(O)-OH 1710-1715 C=C-C(O)-OH or Ar-C(O)-OH 1680-1710	s, broad s, broad s	O-H stretch C=O stretch C=O stretch
<b>Alkenes</b>	3020-3140 1640-1670 RCH=CH <sub>2</sub> 910 + 990 (two bands) RR'C=CH <sub>2</sub> 885-895 <i>cis</i> -RCH=CHR' 665-730 <i>trans</i> -RCH=CHR' 960-980 RCH=CR'R'' 790-840	w-m vw-m m + s s m-s, broad s s	=C-H stretch C=C stretch =C-H bend =C-H bend =C-H bend =C-H bend	<b>Esters</b>	aliphatic 1160-1210 acetates ~1240 aromatic 1250-1310 R-C(O)-O-R 1735-1750 C=C-C(O)-O-R or Ar-C(O)-O-R 1715-1730 R-C(O)-O-Ar 1760-1790	s-vs s s s	O=C-O-C stretch C=O stretch C=O stretch C=O stretch
<b>Alkynes</b>	R-C≡C-H 3265-3335 2100-2140 610-700 R-C≡C-R' 2190-2260	s, sharp m s, broad vw-w	≡C-H stretch C≡C stretch ≡C-H bend C≡C stretch	<b>Acyl Chlorides</b>	R-C(O)-Cl 1785-1815 Ar-C(O)-Cl 1770-1800	s s	C=O stretch C=O stretch
<b>Alkyl halides</b>	R-F 1000-1350 R-Cl 750-850 R-Br 500-680 R-I 200-500	vs s s s	C-F stretch C-Cl stretch C-Br stretch C-I stretch	<b>Anhydrides</b>	R-C(O)-O-C(O)-R ~1750 + ~1815 Ar-C(O)-O-C(O)-Ar ~1720 + ~1775 (both two bands)	s,s s,s	C=O symmetric & asym. stretch
<b>Alcohols</b>	3300-3400 C=C-CH <sub>2</sub> -OH 1035-1050 R-CH <sub>2</sub> -OH (1°) or C=C-CH(R)-OH 1050-1085 RR'CH-OH (2°) or C=C-CRR'-OH 1085-1125 RR'R''C-OH (3°) 1125-1205 Ar-O-H 1180-1260	s, broad m-s m-s m-s m-s m-s	O-H stretch C-O stretch C-O stretch C-O stretch C-O stretch C-O stretch	<b>Nitriles</b>	R-C≡N 2240-2260 C=C-C≡N or Ar-C≡N 2220-2240	m-s s	C≡N stretch C≡N stretch
<b>Ethers</b>	R-O-R' 1085-1150 Ar-O-R 1020-1075 and 1200-1275 (two band)	s m-s	C-O-C stretch =C-O-C sym. & asym. stretch	<b>Amines</b>	R-NH <sub>2</sub> ~3400 + ~3500 (two bands) 1580-1650 RR'N-H 3310-33350	w w-m w	N-H symmetric & asym. stretch N-H bend N-H stretch
<b>Aldehydes</b>	2700-2725 R-CH=O 1720-1740 C=C-CH=O or Ar-CH=O 1685-1710	m s s	H-C=O stretch C=O stretch C=O stretch	<b>Amides</b>	R-C(O)-NH <sub>2</sub> 3200-3400 and 3400-3500 (two bands) 1650-1690 1590-1655 R-C(O)-NH-R 3400-3500 1640-1690 1510-1560 R-C(O)-NR'R'' 1630-1680	w-m s, broad m-s w-m s, broad m-s m-s	N-H symmetric & asym. stretch C=O stretch N-H bend N-H stretch C=O stretch N-H bend C=O stretch
<b>Ketones</b>	RR'C=O 1710-1720 C=C-C(O)-R 1665-1685 Ar-C(O)-R 1675-1695 four member 1770-1780 cyclic five member 1740-1755 cyclic six member 1710-1720 cyclic	s s s s s s	C=O stretch C=O stretch C=O stretch C=O stretch C=O stretch C=O stretch	<b>Nitro Compounds</b>	R-NO <sub>2</sub> ~1550 and ~1370 C=C-NO <sub>2</sub> or Ar-NO <sub>2</sub> ~1525 and ~1335 (both two bands)	s s s s	N-O symmetric & asym. stretch N-O symmetric & asym. stretch
				<b>Aromatic Compounds</b>	3010-3100 1450-1600 (two to four bands) monosubstituted 730-770 and 690-710 (two bands) <i>o</i> -disubstituted 735-770 <i>m</i> -disubstituted 750-810 and 690-710 <i>p</i> -disubstituted 810-840	m m-s sharp s s s s	Ar C-H stretch ring C=C stretch C-H bend C-H bend C-H bend C-H bend C-H bend

Intensity abbreviations: vw = very weak, w = weak, m = medium, s = strong, vs = very strong

# Biosensor Testing Setup

This section shows the setup of the equipment used to test the biosensor. Shown in Figure 5 are parts that make up the biosensor holder, how the biosensor fits in its housing, the three electrode for conduction, the assembled biosensor holder and the setup used in during the the testing of the biosensor.

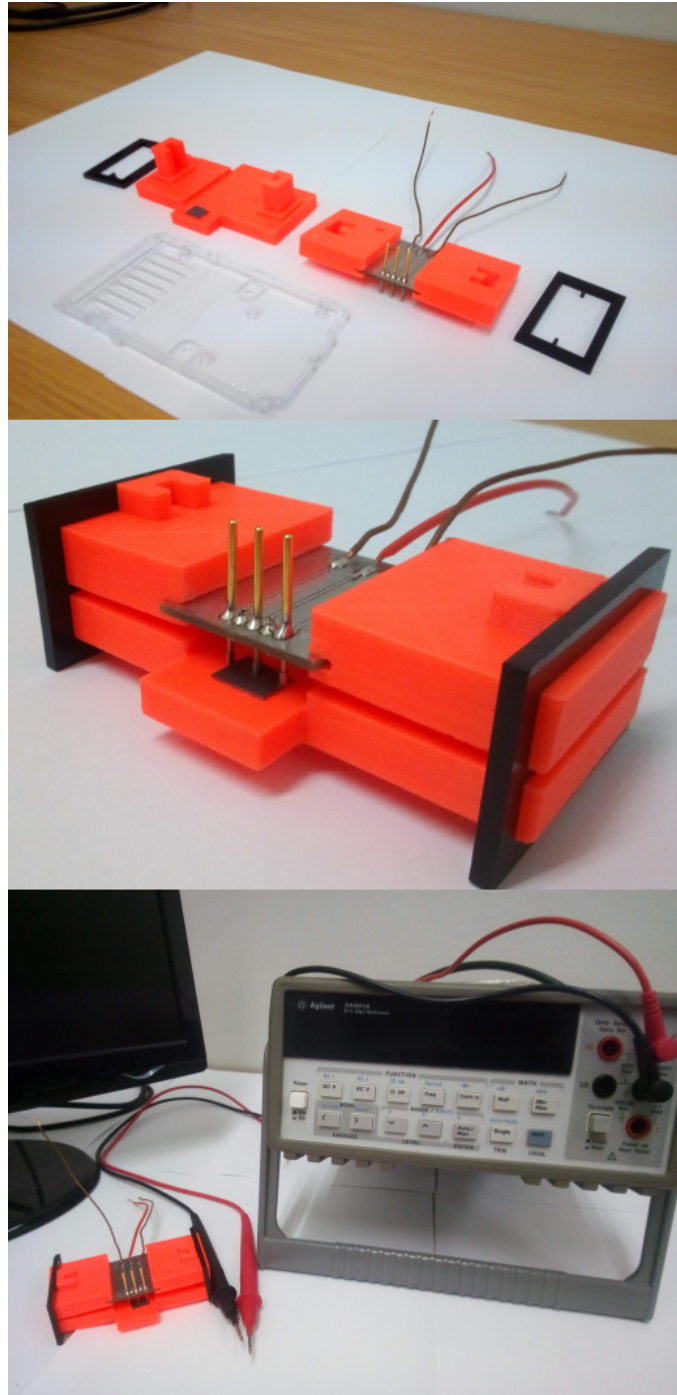


Figure 5: The setup of the equipment used to test the biosensor.



## Arduino code

This section shows the code used to test the LED driving circuit. Shown in Figure 6 is the working code. The code compares the reference voltage and the sensor voltage and decide wheter to switch the LED On or Off



```

Piezoelectric_sensor | Arduino 1.8.5
File Edit Sketch Tools Help

Piezoelectric_sensor$

#define led 13 //output LED
#define Vref A0 // assigning Vref to pin A0
#define Vsensor A1// assigning Vrsensor to pin A1

void setup()//setting up the pin configuration of the microprocessor
{
  pinMode (Vref,INPUT); //Reference voltage
  pinMode (Vsensor,INPUT); // sensor voltage
  pinMode (led,OUTPUT); // LED connection
}

void loop()
{
  float val1 = analogRead(Vsensor);
  float val2 = analogRead(Vref);

  if (val1 > val2) // if the sensor voltage is greater than the reference voltage
  {
    digitalWrite(led,HIGH); //switch LED on
    delay(3000); //for 3 sec
  }
  else if (val2 > val1) // or else if the reference voltage is greater than the sensor voltage
  {
    digitalWrite(led,LOW); //switch LED off
    delay(3000); //for 3 sec
  }

  else if (val1 == val2) //else if the sensor voltage is equal to the reference voltage
    digitalWrite(led,HIGH); //switch LED on
  }
}

Done compiling.
Sketch uses 1372 bytes (4%) of program storage space. Maximum is 32256 bytes.
Global variables use 9 bytes (0%) of dynamic memory, leaving 2039 bytes for local variables. Maximum is 2048 bytes.

4 Arduino/Genuino Uno on COM3

```

Figure 6: The code used to test the LED driving circuit.